Experimental Methods of Measuring Energy Dissipation in Acoustic Resonators

by

Andrew M. Fusco

Submitted to the Department of Mechanical Engineering
in partial fulfillment of the requirements for the degrees of

Master of Science

and

Bachelor of Science

at the

MASSACHUSETTS INSTITUTE OF TECHNOLOGY

June 1991

Signature of Author .....
Department of Mechanical Engineering
May 10, 1991

Certified by .....
C. Forbes Dewey
Professor of Mechanical Engineering
Thesis Supervisor

Accepted by .....
Ain A. Sonin
Chairman, Departmental Committee on Graduate Students

Experimental Methods of Measuring Energy Dissipation in Acoustic Resonators

by

Andrew M. Fusco

Submitted to the Department of Mechanical Engineering
on May 10, 1991, in partial fulfillment of the
requirements for the degrees of
Master of Science
and
Bachelor of Science

Abstract

This study examines a method of measuring energy dissipation in acoustic resonators. The method, known as the two microphone method, accounts for both internal and external energy losses in acoustic resonators. Viscous and thermal losses within the boundary layer of the working fluid contribute to most of the internal losses, while external loads were modeled by empty volumes at the nondriven ends of the resonators.

The two microphone method of measuring energy losses requires the measurement of the acoustic pressure amplitude at different points along the length of the resonator. The quantities required to determine energy losses are the pressure magnitudes at the two points of measurement and the phase difference between the complex pressures at these points. As will be shown, the pressure magnitudes combine to form the auto spectra of the acoustic wave and the magnitudes and the phase angle determines the cross spectra. The calculation of these quantities account for viscous and thermal wall losses as well as tube attenuation.

Energy dissipation measurements using the two microphone method were conducted on two half wavelength standing wave acoustic resonators. The first resonator had a diameter of 1 in. and was driven by a loudspeaker. The pressure amplitudes in the 1 in. diameter resonator ranged from 0.01 psi to 0.9 psi. The second resonator had a diameter of 5 in. and was driven by either a loudspeaker or a thermoacoustic driver, TAD[1]. When the TAD was used, measured energy dissipation got as high as 116.1 W with an acoustic pressure amplitude of about 8 psi. In most cases, the two microphone method measured the energy dissipation to within 10% of the predicted values.

Thesis Supervisor: C. Forbes Dewey
Title: Professor of Mechanical Engineering

Contents

List of Figures

List of Tables

Acknowledgements

I would like to thank the Division of Energy Conversion and Utilizing Technologies at the U.S. Department of Energy who sponsored the research conducted in this study at Los Alamos National Laboratory.

I owe an immeasurable amount of gratitude to Dr. Gregory Swift. Greg provided invaluable advice, guidance, and patience while his love of science and companionship made my research at Los Alamos absolutely enjoyable. I also owe a great debt of gratitude to Prof. C. Forbes Dewey, who made extremely useful contributions of advice and time concerning the experimental procedures and the overall composition of this report.

Dr. William Ward deserves special thanks for his efforts in helping me understand some of the background theory and machines that seem to have minds of their own. I also want to recognize and appreciate the ideas provided to me by Dr. Vincent Kotsubo, who inspired ways of looking at problems from different perspectives. Special appreciation goes out to Chris Espinoza and Jack Dyson who helped repair and build countless parts which were used in the laboratory. Also, several people participated in the proof reading of this document that I would like to thank. They are Audrey Fusco, Lois Irvin, Kristin Slanina, and Penny Plummer.

Finally, I would like to thank my parents, Alfred and Audrey Fusco, and my sister and brother-in-law, Christine and Michael Kiely, who made my stay in Los Alamos and at MIT much better through visits and moral and financial support.

Chapter 1

Introduction

With the need for economical, reliable, and environmentally safe power sources, thermoacoustic engines may be prudent alternatives to more conventional means of power. These engines, which use a temperature gradient to induce a standing acoustic wave, have no moving parts and require no exotic materials, close tolerances, or critical dimensions, which provide for a longer engine lifetime and minimal construction costs. The working fluids used in the engines are low Prandtl Number fluids, which can be gaseous, like helium, or liquids like liquid metals, or even water. Recently, thermoacoustic engines have been studied using liquid sodium as a working fluid[2] in an electric generator, as underwater sound sources for sonar detection, and as drivers for orifice pulse tube refrigerators.

Like all thermodynamic processes, thermoacoustic engines can act as prime movers by producing mechanical work from a temperature gradient or act as refrigerators by using mechanical work to produce a temperature gradient. When the engines are used as prime movers, the thermodynamic process begins by introducing a temperature gradient across a stack of closely spaced thermally conductive plates which are held in an acoustic resonator. The resonator is simply a narrow tube, which is designed to 1/4 or 1/2 of a given acoustic wavelength, λ (based on thermodynamic conditions of the working fluid), shown in Figure 1.1. At a large enough temperature gradient across the stack of plates

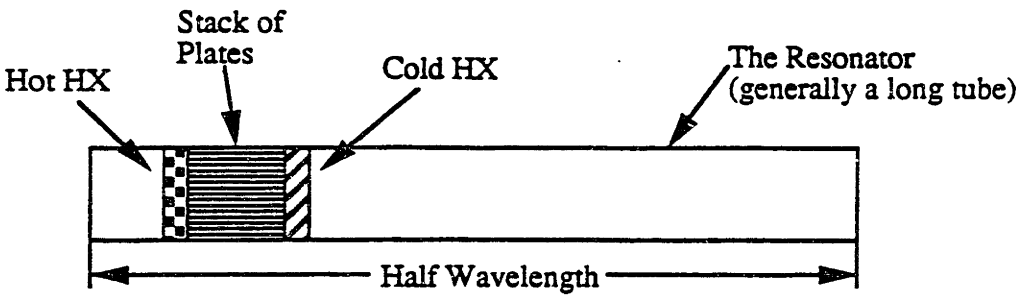

Figure 1-1: A thermoacoustic engine.

an acoustic standing wave will spontaneously occur in the working fluid in the resonator. The motion of the fluid transfers the heat from the hot side of the stack of plates to the cold side, introducing mechanical work in the form of an acoustic standing wave.

Energy can be tapped from the engine in several ways. One way involves using the acoustic pressure swings to perform some type of reciprocating work. Another interesting way of converting the acoustic energy involves using liquid sodium as a working fluid. An electric generator can be made by placing the resonator so that the sodium oscillates through a magnetic field. A refrigerator can be produced by simply reversing the process by introducing an acoustic standing wave in a resonator holding a stack of plates and heat exchangers.

Since the physics behind thermoacoustic engines is fairly well established, more effort is needed in the optimization of these engines and making these engines suitable for various applications, such as electric generators or reciprocating pressure sources. In most cases concerning the study of the performance of these engines, a key measurement that will be made is the measurement of energy dissipation. Energy can be dissipated

by internal loss mechanisms, such as viscous and thermal effects. Energy can also be dissipated externally by whatever loads the user decides to put on the engine. A simple and reliable method of measuring this dissipation in acoustic engines must be developed to aid in future studies of thermoacoustic engines and their loads.

This thesis describes a study of the two microphone method, which is a method of determining energy dissipation in acoustic resonators by measuring the acoustic pressure amplitudes at two points along the resonators. By measuring the complex acoustic pressures at two points along the resonator, the magnitudes and the phase between the two points can be determined. The phase and magnitudes determine the auto and cross spectra of the wave in the resonator, which describe how the intensity of the wave diminishes due to losses at the walls of the resonator and losses incurred as the acoustic wave reflects off of the end caps.

With the advent of digital equipment, the two microphone method became a reasonable technique in measuring energy dissipation. Methods of using only the cross spectrum to determine acoustic intensity were developed by Chung[3]. Chu[4] suggested that the effects of attenuation should be accounted for, and he corrected the theory by including the auto spectra at the points of measurement. Studying sound propagation in ducts, Seybert[5] unified the calculation of sound intensity and measurement of acoustic properties in ducts, by a general decomposition theory.

This study begins with a review of the acoustic theory needed to calculate the energy dissipation. In Chapter 2, the relevant acoustic and thermodynamic parameters are approximated by using linear expansions. These linear parameters are used to derive the energy flux through a resonator. The energy flux is then reduced to a function of only the acoustic pressure by relating the pressure to the particle velocity of the working fluid and determining an expression for the wave number pertaining to the first harmonic of the resonator. Viscous and thermal losses at the resonator walls are incorporated into the reduction of the energy flux.

Chapters 4 and 5 describe two known techniques of determining energy dissipation

in acoustic resonators, which are compared to the results given by the two microphone method. Chapter 4 describes how the quality factor, Q, and the stored energy in a resonator, E_{st}, are measured. This technique of measuring energy dissipation accounts for internal energy losses (i.e. losses due to viscous or thermal effects at the walls of the resonator or losses caused by geometric imperfections within the resonator), and external energy dissipation (i.e. losses caused by attaching some load that converts acoustic energy into another form of energy). Chapter 5 describes how internal energy dissipation and external energy dissipation are measured separately. The internal energy dissipation is measured using the same method discussed in Chapter 4, which uses a quality factor that assumes there is no external load on the resonator. Chapter 5 explains how modeled loads, called 'dummy loads', dissipate energy. These loads are simply empty volumes connected to the resonator by a small pipe. The resistance to the fluid flow through an orifice to the volume causes energy dissipation by lowering the acoustic pressure amplitude in the resonator. External energy dissipation is determined by measuring the pressure drop between the acoustic pressure amplitude in the resonator and the pressure amplitude in the dummy load. The internal and external energy dissipation measurements are then added, giving the total energy dissipation.

Chapter 6 explains the two microphone method of measuring energy dissipation in detail. An expression for determining the energy dissipation using the complex pressures measured by the microphones is derived first, using the background theory provided in Chapter 2. The experimental procedures for using the two microphone method are explained next. Results from tests using the two microphone method under various conditions are then compared to the results yielded from the techniques described in Chapters 4 and 5.

Although the two microphone method applies to resonators or ducts in many shapes and sizes, the resonators used in this investigation are exclusively closed, one half wavelength resonators that support standing acoustic waves, since many thermoacoustic engines use such resonators. Also, the working fluid in all these tests of the two microphone

method was helium, because of its low Prandtl Number (Pr=0.7).

Considering other methods for measuring energy dissipation, measuring the acoustic pressure amplitude was easiest and most reliable. The method of using hot wire anemometry to measure the fluid velocity was ruled out since the hot wire probe would disturb the flow of the working fluid. Also, Laser Doppler Velocimetry was considered but not used because such measurements require more instrumentation that was more expensive than that of the two microphone method. Measuring the pressure allowed for minimal profile defects inside of the resonator and required less instrumentation, thus keeping the measurement process simple and inexpensive.

Chapter 2

Theoretical Background

To show how the pressures measured by the two microphone method are needed to calculate the energy dissipation in acoustic resonators, an expression for the energy flux in terms of the acoustic pressure must be derived. The energy dissipation is calculated in this chapter using a fundamental theory for damped oscillations in tubes, developed by Rott[6]. The derivation of the energy flux begins with an expansion of the thermodynamic and acoustic variables of temperature, density, pressure, and velocity. The expansions are then simplified to the first order. Also, a general expression for the energy dissipation is derived. The energy dissipation is then manipulated to be a function of only the measurable quantity of pressure, using the Navier-Stokes Equation, the continuity equation, and the general equation of heat transfer.

2.1 The Acoustic Approximation

To begin the derivation of the energy dissipation, the parameters p, pressure; $\mathbf{v}$, velocity; T, temperature; and ρ, density need to be clearly defined. For a simple point source in free space (shown in Figure 2.1) the parameters depend on time and position

$$p = p_o + p_1(x,y,z,t) + p_2(x,y,z,t) + p_3(x,y,z,t) + ..., \tag{2.1}$$

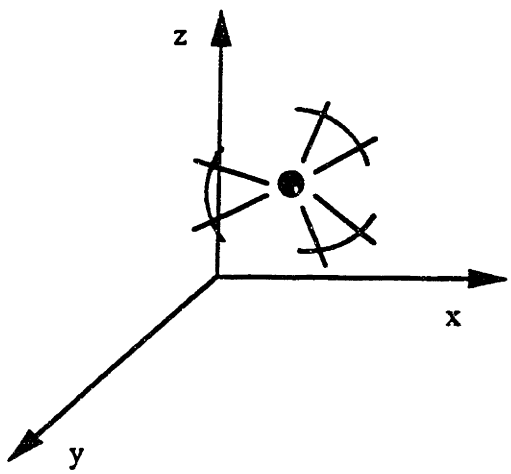

Figure 2-1: Propagation of an acoustic wave from a simple point source.

$$\mathbf{v} = v_o + v_1(x,y,z,t) + v_2(x,y,z,t) + v_3(x,y,z,t) + ..., \tag{2.2}$$

$$T = T_o + T_1(x,y,z,t) + T_2(x,y,z,t) + T_3(x,y,z,t) + ..., \tag{2.3}$$

$$\rho = \rho_o + \rho_1(x,y,z,t) + \rho_2(x,y,z,t) + \rho_3(x,y,z,t) + ..., \tag{2.4}$$

using cartesian coordinates (x,y,z), where t is time, and the numerical subscripts denote the order.

The three dimensional case can be simplified to a one dimensional case for the remainder of this study because this thesis is only concerned with long, thin resonators. The resulting waveform is a plane wave that oscillates along the longitudinal axis of the resonators. Also, since this thesis deals with only cylindrically shaped resonators, a cylindrical coordinate system (shown in Figure 2.2) will be used, simplifying the following

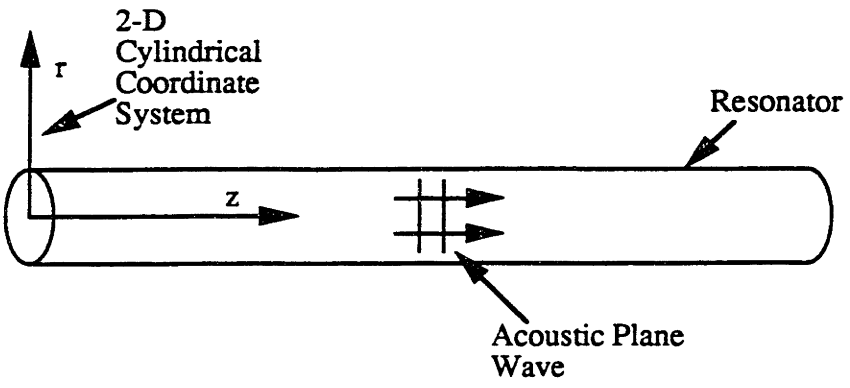

Figure 2-2: The coordinate system of a cylindrical resonator.

calculations. The acoustic standing wave oscillates along the z-axis.

Using the one dimensional simplification, the thermodynamic and acoustic parameters can be examined more closely. Using the following Fourier expansions, these parameters become

$$p = \sum_{n=-\infty}^{\infty} p_n e^{i|n|\omega t} e^{ink z} = p_o + p_1 e^{i(\omega t + kz)} + p_{-1} e^{i(\omega t - kz)} + p_2 e^{2i(\omega t + kz)} + p_{-2} e^{2i(\omega t - kz)} + \ldots, \tag{2.5}$$

$$\mathbf{v} = \sum_{n=-\infty}^{\infty} v_n e^{i|n|\omega t} e^{ink z} = v_o + v_1 e^{i(\omega t + kz)} + v_{-1} e^{i(\omega t - kz)} + v_2 e^{2i(\omega t + kz)} + v_{-2} e^{2i(\omega t - kz)} + \ldots, \tag{2.6}$$

$$T = \sum_{n=-\infty}^{\infty} T_n e^{i|n|\omega t} e^{in\mathbf{k}z} = T_o + T_1 e^{i(\omega t+\mathbf{k}z)} + T_{-1} e^{i(\omega t-\mathbf{k}z)} + T_2 e^{2i(\omega t+\mathbf{k}z)} + T_{-2} e^{2i(\omega t-\mathbf{k}z)} + ..., \tag{2.7}$$

$$\rho = \sum_{n=-\infty}^{\infty} \rho_n e^{i|n|\omega t} e^{in\mathbf{k}z} = \rho_o + \rho_1 e^{i(\omega t+\mathbf{k}z)} + \rho_{-1} e^{i(\omega t-\mathbf{k}z)} + \rho_2 e^{2i(\omega t+\mathbf{k}z)} + \rho_{-2} e^{2i(\omega t-\mathbf{k}z)} + ..., \tag{2.8}$$

where ω is the resonant frequency and $\mathbf{k}$ is the complex acoustic wave number, which will be derived later. These expansions describe an acoustic wave that propagates in the positive and negative directions along the z-axis, starting at time $t = 0$.

When dealing with acoustic waves, several assumptions can be made to make the calculations manageable. For all of the calculations in this thesis only the steady state and first order terms of the expansions will be kept. The higher order terms can be considered to be insignificant by comparison to the lower order terms[1]. The resulting expressions for the expanded parameters are

$$p = p_o + p_1 e^{i(\omega t+\mathbf{k}z)} + p_{-1} e^{i(\omega t-\mathbf{k}z)}, \tag{2.9}$$

$$\mathbf{v} = v_o + v_1 e^{i(\omega t+\mathbf{k}z)} + v_{-1} e^{i(\omega t-\mathbf{k}z)}, \tag{2.10}$$

$$T = T_o + T_1 e^{i(\omega t+\mathbf{k}z)} + T_{-1} e^{i(\omega t-\mathbf{k}z)}, \tag{2.11}$$

$$\rho = \rho_o + \rho_1 e^{i(\omega t+\mathbf{k}z)} + \rho_{-1} e^{i(\omega t-\mathbf{k}z)}. \tag{2.12}$$

The velocity can be simplified to

$$\mathbf{v} = v_1 e^{i(\omega t + \mathbf{k}z)} + v_{-1} e^{i(\omega t - \mathbf{k}z)}, \tag{2.13}$$

because there is no net velocity in a closed resonator.

2.2 Acoustic Energy

The energy flux in an acoustic flow is defined as the energy contained in an acoustic wave that flows through a given cross sectional area. As was discussed qualitatively in Chapter 1, the two microphone method can aid in determining the energy flux in a resonator by measuring the pressures at two points along the length of the resonator. A general energy flux equation needs to be derived for acoustic waves in resonators. For the derivation conducted in this section the working fluid will be treated as an ideal fluid, meaning viscous effects will be neglected[7, pp. 9–10].

To simplify the notation a bit, the first order expansions of pressure and density will be abbreviated as follows

$$p = p_o + p', \tag{2.14}$$

$$\rho = \rho_o + \rho', \tag{2.15}$$

where p' and ρ' represent the first order terms in the expansions.

The energy flux, $\dot{E}$, can be derived by integrating the energy flux density, Φ, over the area through which the acoustic wave flows. To determine the energy flux density the energy density, e, of the wave must be combined with the continuity equation and Euler's Equation. The energy density is the sum of the kinetic energy per unit volume plus the potential energy per unit volume,

$$e = \frac{1}{2}\rho v_z^2 + \rho\epsilon, \tag{2.16}$$

where v_z is the particle velocity along the longitudinal axis of the resonator and ϵ is the internal energy per unit mass of the fluid. The continuity equation is

$$\frac{\partial \rho}{\partial t} + \nabla \cdot (\rho \mathbf{v}) = 0, \tag{2.17}$$

and Euler's Equation is

$$\frac{\partial \mathbf{v}}{\partial t} + (\mathbf{v} \cdot \nabla)\mathbf{v} = -\frac{1}{\rho}\nabla p. \tag{2.18}$$

In Euler's Equation, the density is treated as a constant since the acoustic oscillations are small compared to the mean density, ρ_o.

The time derivative of the energy density should be taken so equations (2.17) and (2.18) can be used. The time derivative of the energy density is

$$\frac{\partial e}{\partial t} = \frac{\partial}{\partial t}(\frac{1}{2}\rho v_z^2 + \rho\epsilon). \tag{2.19}$$

Now the kinetic and the potential parts of the right hand side of equation (2.19) need to be examined separately. The time derivative of the kinetic energy density is

$$\frac{\partial}{\partial t}(\frac{1}{2}\rho v_z^2) = \frac{1}{2}v_z^2\frac{\partial \rho}{\partial t} + \rho \mathbf{v} \cdot \frac{\partial \mathbf{v}}{\partial t}. \tag{2.20}$$

Substituting equations (2.17) and (2.18) into equation (2.20) for $\frac{\partial \rho}{\partial t}$ and $\frac{\partial \mathbf{v}}{\partial t}$, respectively, the expression becomes

$$\frac{\partial}{\partial t}(\frac{1}{2}\rho v_z^2) = -\frac{1}{2}v_z^2\nabla \cdot (\rho \mathbf{v}) - \mathbf{v} \cdot \nabla p - \rho \mathbf{v} \cdot (\mathbf{v} \cdot \nabla)\mathbf{v}. \tag{2.21}$$

The term ∇p is replaced using the thermodynamic expression

$$dp = \rho dw - \rho T ds, \tag{2.22}$$

which becomes

$$\nabla p = \rho \nabla w - \rho T \nabla s, \tag{2.23}$$

where w is the enthalpy per unit mass of the fluid, and s is the entropy per unit mass of the fluid. Also, $\mathbf{v} \cdot (\mathbf{v} \cdot \nabla)\mathbf{v}$ can be replaced by

$$\mathbf{v} \cdot (\mathbf{v} \cdot \nabla)\mathbf{v} = \frac{1}{2}\mathbf{v} \cdot \nabla v_z^2, \tag{2.24}$$

making equation (2.21)

$$\frac{\partial}{\partial t}(\frac{1}{2}\rho v_z^2) = -\frac{1}{2}v_z^2 \nabla \cdot (\rho \mathbf{v}) - \rho \mathbf{v} \cdot \nabla(\frac{1}{2}v_z^2 + w) + \rho T \mathbf{v} \cdot \nabla s. \tag{2.25}$$

The thermodynamic relation for the potential energy part of the energy density is

$$d\epsilon = Tds - pdV_m = Tds + (\frac{p}{\rho^2})d\rho, \tag{2.26}$$

where V_m is the specific volume. Performing the expansion of the term $d(\rho\epsilon)$ and substituting the identity $\epsilon = w - p/\rho$, the potential energy term becomes

$$d(\rho\epsilon) = \epsilon d\rho + \rho d\epsilon = w d\rho + \rho T ds, \tag{2.27}$$

making the time derivative

$$\frac{\partial(\rho\epsilon)}{\partial t} = -w \nabla \cdot (\rho \mathbf{v}) - \rho T \mathbf{v} \cdot \nabla s. \tag{2.28}$$

Combining the kinetic and the potential terms the resulting expression is

$$\frac{\partial}{\partial t}(\frac{1}{2}\rho v_z^2 + \rho\epsilon) = -(\frac{1}{2}v_z^2 + w)\nabla \cdot (\rho \mathbf{v}) - \rho \mathbf{v} \cdot \nabla(\frac{1}{2}v_z^2 + w), \tag{2.29}$$

or

$$\frac{\partial}{\partial t}(\frac{1}{2}\rho v_z^2 + \rho\epsilon) = -\nabla \cdot [\rho \mathbf{v}(\frac{1}{2}v_z^2 + w)], \tag{2.30}$$

where the energy flux density is

$$\Phi = \rho \mathbf{v}(\frac{1}{2}v_z^2 + w). \tag{2.31}$$

To determine the given amount of energy flow, equation (2.30) must be integrated over some volume

$$\frac{\partial}{\partial t}\int(\frac{1}{2}\rho v_z^2 + \rho\epsilon)dV = -\int\nabla\cdot[\rho\mathbf{v}(\frac{1}{2}v_z^2 + w)]dV. \tag{2.32}$$

By changing the right hand term to a surface integral, the energy flux through a given cross section can be determined

$$\frac{\partial}{\partial t}\int(\frac{1}{2}\rho v_z^2 + \rho\epsilon)dV = -\oint\rho\mathbf{v}(\frac{1}{2}v_z^2 + w)\cdot dA. \tag{2.33}$$

Looking at equation (2.33) from an acoustic standpoint, some terms can be considered insignificant, making the expression simpler. Considering the energy flux density, the $\frac{1}{2}\rho\mathbf{v}v_z^2$ term can be neglected, since it is a third order term. The fluctuating quantity $w = w_o + w'$ should be substituted for the specific enthalpy (as was done in equations (2.14) and (2.15) for pressure and density). For small changes in w', the relation $w' = (\partial w/\partial p)_s p' = p'/\rho$ can be assumed (with the subscript s denoting constant entropy), making the energy flux

$$\dot{E} = \oint(w_o\rho\mathbf{v} + p'\mathbf{v})\cdot dA. \tag{2.34}$$

By substituting equation (2.15) for ρ in the first term, some more simplifications can be made. The first term will look like $w_o\rho_o\mathbf{v} + w_o\rho'\mathbf{v}$. The $w_o\rho_o\mathbf{v}$ term deals with a steady state situation and does not relate to sound waves. The second term, $w_o\rho'\mathbf{v}$, relates to the energy flux due to the change in mass of the fluid, and is zero in a closed volume situation, like that in closed acoustic resonators. The resulting energy flux becomes

$$\dot{E} = \oint p' \mathbf{v} \cdot dA. \tag{2.35}$$

Since the energy flux over a long period of time is desired rather than the instantaneous energy flux, the time averaged value of the energy flux must be determined for more meaningful results. Also, by applying equation (2.35) to cylindrical resonators, a more specific expression would be

$$\dot{E} = \int_0^{r_o} 2\pi r \overline{p' v_z} dr, \tag{2.36}$$

where r_o is the radius of the resonator, and the overbar denotes the time average. Using equation (2.36), the time averaged energy flux in the resonator can be solved.

2.3 Resonator Losses

Now that a simple equation for the energy flux in a resonator has been derived, the energy flux equation must be reduced to an expression that is only a function of the measured parameter, pressure, and other known quantities. The two quantities that are related to pressure in this section are the longitudinal velocity, v_z, and the complex wave number, $\mathbf{k}$ (which is shown in the expansions of p and $\mathbf{v}$). The derivations carried out in this section take into account the losses in the resonator.

The three equations used to simplify equation (2.36) are the Navier-Stokes Equation, the continuity equation, and the general equation of heat transfer[7, pg. 194]. The Navier-Stokes Equation is

$$\frac{\partial(\rho \mathbf{v})}{\partial t} + (\mathbf{v} \cdot \nabla)(\rho \mathbf{v}) = -\nabla p + \nabla^2(\mu \mathbf{v}) + \nabla \left(\nabla \cdot \left((\zeta + \frac{\mu}{3}) \mathbf{v} \right) \right), \tag{2.37}$$

where μ is the dynamic viscosity, and ζ is the second viscosity. The continuity equation is given in equation (2.17). The general equation of heat transfer is

$$\frac{\partial(\rho Ts)}{\partial t} + \mathbf{v} \cdot \nabla(\rho \mathrm{Ts}) = \nabla \cdot (\mathrm{K} \nabla \mathrm{T}), \tag{2.38}$$

given that K is the thermal conductivity of the fluid.

The fluid velocity will first be related to the acoustic pressure, using the Navier-Stokes Equation. The Navier-Stokes Equation can be simplified by assuming that the density and the temperature of the fluid are constant, since the fluctuating terms ρ' and T' are much smaller than the mean values of ρ_o and T_o, respectively. With this assumption, the density and the viscosities can be treated as constants, making the Navier-Stokes Equation

$$\rho \left[\frac{\partial \mathbf{v}}{\partial t} + (\mathbf{v} \cdot \nabla)\mathbf{v} \right] = -\nabla p + \mu \nabla^2 \mathbf{v} + \left(\zeta + \frac{\mu}{3} \right) \nabla (\nabla \cdot \mathbf{v}). \tag{2.39}$$

By approximating the geometric terms in equation (2.39) a simpler expression results. The viscous boundary layer thickness, δ_ν, for an acoustic flow can be calculated from the simple expression[7, pg. 306]

$$\delta_\nu = \sqrt{\frac{2\nu}{\omega}}, \tag{2.40}$$

where ν is the kinematic viscosity, and ω is the frequency of oscillation.

The boundary layer thickness can be considered much smaller than the wavelength since the resonator is a long slender tube

$$\delta_\nu \ll \frac{\lambda}{2\pi}. \tag{2.41}$$

The derivative along the z-axis is proportional to the inverse of the wavelength

$$\frac{\partial}{\partial z} \sim \frac{2\pi}{\lambda}, \tag{2.42}$$

and the radial derivative is proportional to the inverse of the viscous boundary layer thickness

$$\frac{\partial}{\partial r} \sim \frac{1}{\delta_\nu}. \tag{2.43}$$

Since the waves are considered plane waves along the longitudinal axis, any radial velocity is considered negligible, giving

$$\frac{v_z}{v_r} \geq \frac{\lambda}{2\pi\delta_\nu}. \tag{2.44}$$

Using the preceding approximations, the Navier-Stokes Equation reduces to

$$\rho_o \frac{\partial v_z}{\partial t} = \frac{-dp'}{dz} + \mu \frac{1}{r}\frac{\partial}{\partial r}\left(r\frac{\partial v_z}{\partial r}\right). \tag{2.45}$$

Finally, the time derivative of the velocity is simply $i\omega$ times the velocity, reducing equation (2.45) to

$$i\omega\rho_o v_z = \frac{-dp'}{dz} + \mu \frac{1}{r}\frac{\partial}{\partial r}\left(r\frac{\partial v_z}{\partial r}\right). \tag{2.46}$$

Solving the differential equation for v_z and using the boundary condition $v_z(r = r_o) = 0$, the velocity, v_z, is

$$v_z = \frac{i}{\omega\rho_o}\frac{dp'}{dz}\left[1 - \frac{J_o[(i-1)r/\delta_\nu]}{J_o[(i-1)r_o/\delta_\nu]}\right]. \tag{2.47}$$

Substituting equation (2.47) into equation (2.36) and solving the integral, the resulting energy flux is

$$\dot{E} = \frac{\pi r_o^2}{2\omega\rho_o}\mathrm{Re}\left[i\tilde{p}'\frac{dp'}{dz}\left(1 - \frac{2J_1[(i-1)r_o/\delta_\nu]}{[(i-1)r_o/\delta_\nu]J_o[(i-1)r_o/\delta_\nu]}\right)\right], \tag{2.48}$$

where $\tilde{p}$ is the complex conjugate of p. The function, f_ν[6], can be defined as

$$f_\nu = \frac{2J_1[(i-1)r_o/\delta_\nu]}{[(i-1)r_o/\delta_\nu]J_o[(i-1)r_o/\delta_\nu]}. \tag{2.49}$$

Now the energy flux through the resonator can be written as

$$\dot{E} = \frac{\pi r_o^2}{2\omega\rho_o}\mathrm{Re}\left[i\tilde{p}'\frac{dp'}{dz}(1-f_\nu)\right]. \tag{2.50}$$

The complex wave number, k, in the exponential terms of the pressure given in equation (2.9) must be found so that the energy flux can be solved in terms of pressure only. The wave number can be found from a second order differential equation of the pressure, called the wave equation, which takes the form

$$p' + \frac{1}{\mathbf{k}^2}\frac{d^2p'}{dz^2} = 0. \tag{2.51}$$

The wave equation can be derived using the continuity equation, equation (2.17), and the general equation of heat transfer, equation (2.38). Using the same assumptions stated in equations (2.41) through (2.44), along with assuming that the density is constant along the z-axis, the continuity equation reduces to

$$\frac{\partial\rho}{\partial t} + \frac{\partial}{\partial z}(\rho_o v_z) = 0. \tag{2.52}$$

The time derivative of the density is simply $i\omega$ times the fluctuating part of the density expansion, giving

$$i\omega\rho' + \frac{\partial}{\partial z}(\rho_o v_z) = 0. \tag{2.53}$$

Solving equation (2.46) for the mean density and substituting it into equation (2.53), the continuity equation becomes

$$i\omega\rho' - \frac{1}{i\omega}\frac{d^2p'}{dz^2} + \frac{\partial}{\partial z}\left(\frac{\mu}{i\omega r}\frac{\partial}{\partial r}\left(r\frac{\partial v_z}{\partial r}\right)\right) = 0. \tag{2.54}$$

Multiplying both sides of equation (2.54) by $i\omega$, the expression becomes

$$-\omega^2\rho' - \frac{d^2p'}{dz^2} + \frac{\partial}{\partial z}\left(\mu\frac{1}{r}\frac{\partial}{\partial r}\left(r\frac{\partial v_z}{\partial r}\right)\right) = 0. \tag{2.55}$$

The first order density, ρ', can be obtained through the equation of state

$$\rho' = -\rho_o \beta T' + (\gamma/a^2)p', \tag{2.56}$$

where β is the thermal expansion coefficient ($\beta = -(\partial\rho_o/\partial T)_p/\rho_o$), and γ is the ratio of isobaric to isochoric specific heats. By substituting equation (2.56) into equation (2.55), the expression becomes

$$\omega^2 \rho_o \beta T' - \frac{\omega^2}{a^2}\gamma p' - \frac{d^2 p'}{dz^2} + \frac{\partial}{\partial z}\left(\mu \frac{1}{r}\frac{\partial}{\partial r}\left(r\frac{\partial v_z}{\partial r}\right)\right) = 0. \tag{2.57}$$

Equation (2.57) involves three different fluctuating quantities: the particle velocity, the acoustic pressure, and the temperature. The particle velocity is given in equation (2.47). The wave equation that will be derived must be in terms of the acoustic pressure, so an expression relating the temperature to the pressure must be found and substituted into equation (2.57). The general equation of heat transfer (equation (2.38)) is used to make this relation. Looking at the left side of equation (2.38), the mean values of the density and the temperature are much larger than their fluctuating terms, allowing them to be considered constant. The general equation of heat transfer becomes

$$\rho T\left(\frac{\partial s}{\partial t} + \mathbf{v}\cdot\nabla \mathrm{s}\right) = \nabla\cdot(K\nabla T). \tag{2.58}$$

The same geometric assumptions given in equations (2.41) through (2.44) are used, with the exception of replacing the viscous boundary layer thickness with the thermal boundary layer thickness, δ_κ[7, pg. 306]. The thermal boundary layer thickness is

$$\delta_\kappa = \sqrt{\frac{2\alpha}{\omega}}, \tag{2.59}$$

where the thermal diffusivity is $\alpha = K/\rho_o c_p$, where c_p is the fluids isobaric specific heat. From thermodynamics, the entropy term in equation (2.58) is

$$ds = (c_p/T)\,dT - (\beta/\rho)\,dp. \tag{2.60}$$

Substituting equation (2.60) into the general equation of heat transfer and applying the geometric approximations, the expression reduces to

$$\rho_o c_p \left(\frac{\partial T'}{\partial t} + v_z \frac{dT_o}{dz} \right) - T_o \beta \frac{\partial p'}{\partial t} = K \frac{1}{r} \frac{\partial}{\partial r} \left(r \frac{\partial T'}{\partial r} \right). \tag{2.61}$$

Once again, the time derivatives of the fluctuating quantities T' and p' are $i\omega$ times the fluctuating quantity, giving

$$\rho_o c_p \left(i\omega T' + v_z \frac{dT_o}{dz} \right) - i\omega T_o \beta p' = K \frac{1}{r} \frac{\partial}{\partial r} \left(r \frac{\partial T'}{\partial r} \right). \tag{2.62}$$

Equation (2.62) is solved by assuming the fluctuating term of the temperature is zero at the resonator walls because of the thermal contact with the walls, $T'(r_o) = 0$, and there is no temperature gradient along the length of the resonator, since the acoustic amplitudes are low, $\frac{dT_o}{dz} = 0$. Using these assumptions the fluctuating temperature is given as

$$T' = \frac{T_o \beta}{\rho_o c_p} p' \left(1 - \frac{J_o[(i-1)r/\delta_\kappa]}{J_o[(i-1)r_o/\delta_\kappa]} \right). \tag{2.63}$$

The wave equation including losses can now be found. First, an identity can be made similar to equation (2.49), yielding the function[6]

$$f_\kappa = \frac{2J_1[(i-1)r_o/\delta_\kappa]}{[(i-1)r_o/\delta_\kappa]J_o[(i-1)r_o/\delta_\kappa]}. \tag{2.64}$$

Also, the following thermodynamic relation was used

$$\frac{\beta^2 T_o a^2}{c_p} = \gamma - 1. \tag{2.65}$$

The resulting wave equation is found by using equations (2.47) and (2.63) for v_z and T', respectively, and substituting into equation (2.57). Multiplying both sides of equation (2.57) by r and then taking the integral along the radius of the resonator from 0 to r_o, the wave equation becomes

$$(1+(\gamma-1)f_\kappa)p' + \frac{a^2}{\omega^2}\frac{d^2p'}{dz^2}(1-f_\nu) = 0. \tag{2.66}$$

By changing equation (2.66) to the form

$$p' + \frac{d^2p'}{dz^2}\frac{a^2}{\omega^2}\frac{1-f_\nu}{(1+(\gamma-1)f_\kappa)} = 0, \tag{2.67}$$

the complex wave number, $\mathbf{k}$, is found, which is simply the coefficient of the second derivative of the pressure,

$$\mathbf{k}^2 = \frac{\omega^2}{a^2}\Big(\frac{1+(\gamma-1)f_\kappa}{1-f_\nu}\Big). \tag{2.68}$$

The energy flux through the resonator can now be solved as a function of only the acoustic pressure. As will be seen in Chapter 6, the pressure will be solved by applying boundary conditions to the wave equation. The pressure will be broken into real and imaginary parts and the energy flux equation will be manipulated algebraically so that the measured complex acoustic pressures can be substituted and a value for the energy flux can be determined.

Chapter 3

Experimental Equipment and Instrumentation

The experiments conducted in this thesis required simple laboratory hardware and instrumentation. The resonator is simply a pipe with a driver connected to one end, and with mounting holes cut at various positions along the resonator for pressure transducers. For the most part, the instrumentation is very common, and can be found in almost any modern laboratory. This chapter presents a detailed description of the experimental hardware along with the instrumentation configuration.

3.1 The Resonator Assembly

There were two resonators used in the experiments. The first resonator, shown in Figure 3.1, was a seamless aluminum tube, five inches in diameter and 12 feet long. The driver on this resonator was a one inch tweeter with an electrical resistance of 7.5 ohms. Three mounting holes for pressure transducers are located on the resonator. Two holes are located between the driver and the quarter wavelength point, and the third is on the nondriven end plate (for the exact placements of the mounting holes, see Figure 3.1). To simulate external loading, a 1500 cc tank was connected to the nondriven end of the

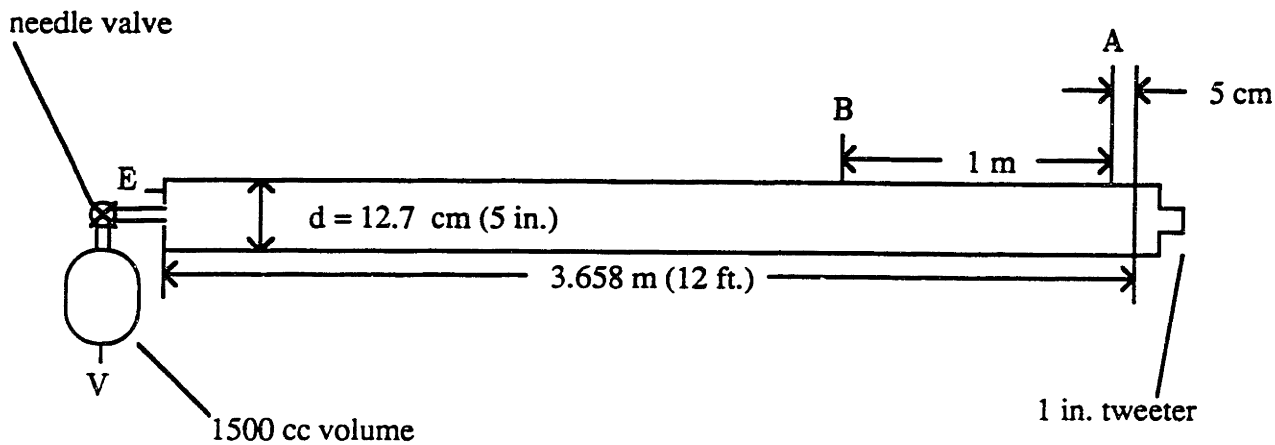

Figure 3-1: The five inch diameter resonator assembly.

resonator through a needle valve (Appendix A describes how the size of the tank was chosen). A pressure transducer was attached to the 1500 cc tank also.

The second resonator was a one inch diameter, 12 foot long seamless brass tube. The same one inch tweeter used on the five inch resonator was coupled to the one inch resonator. This resonator had a 75 cc tank coupled to the nondriven end. The one inch resonator is shown in Figure 3.2.

The working fluid used in all of the tests (except in some of the pressure transducer calibrations) was helium. To insure the purity of the helium, the system was evacuated, and then the resonator was flushed several times using helium. Since low and high pressures were used in the tests, two different pressure gauges were needed to give accurate mean pressure readings at low and high pressures. The entire plumbing system is shown in Figure 3.3.

Higher amplitude acoustic pressure swings were desired to test the limits of the two

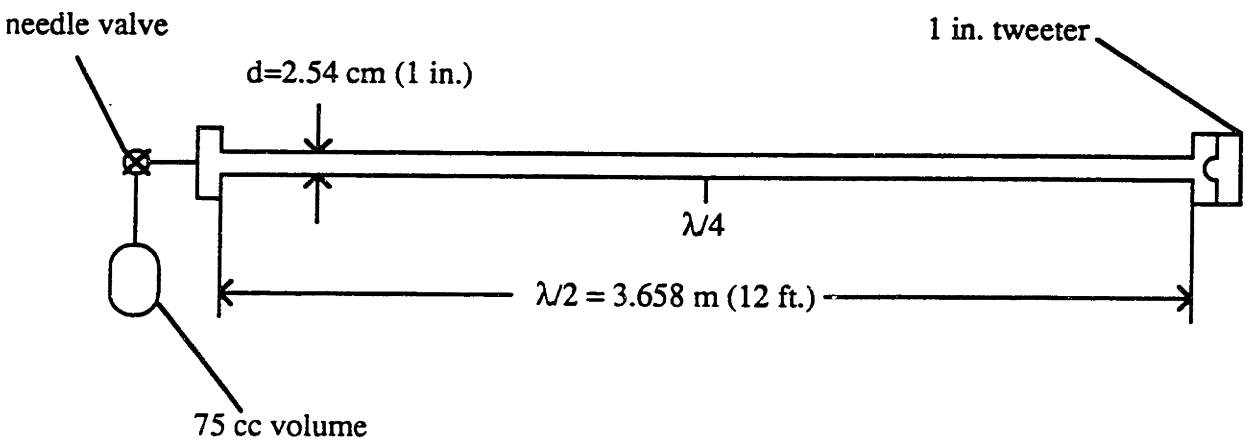

Figure 3-2: The one inch diameter resonator assembly.

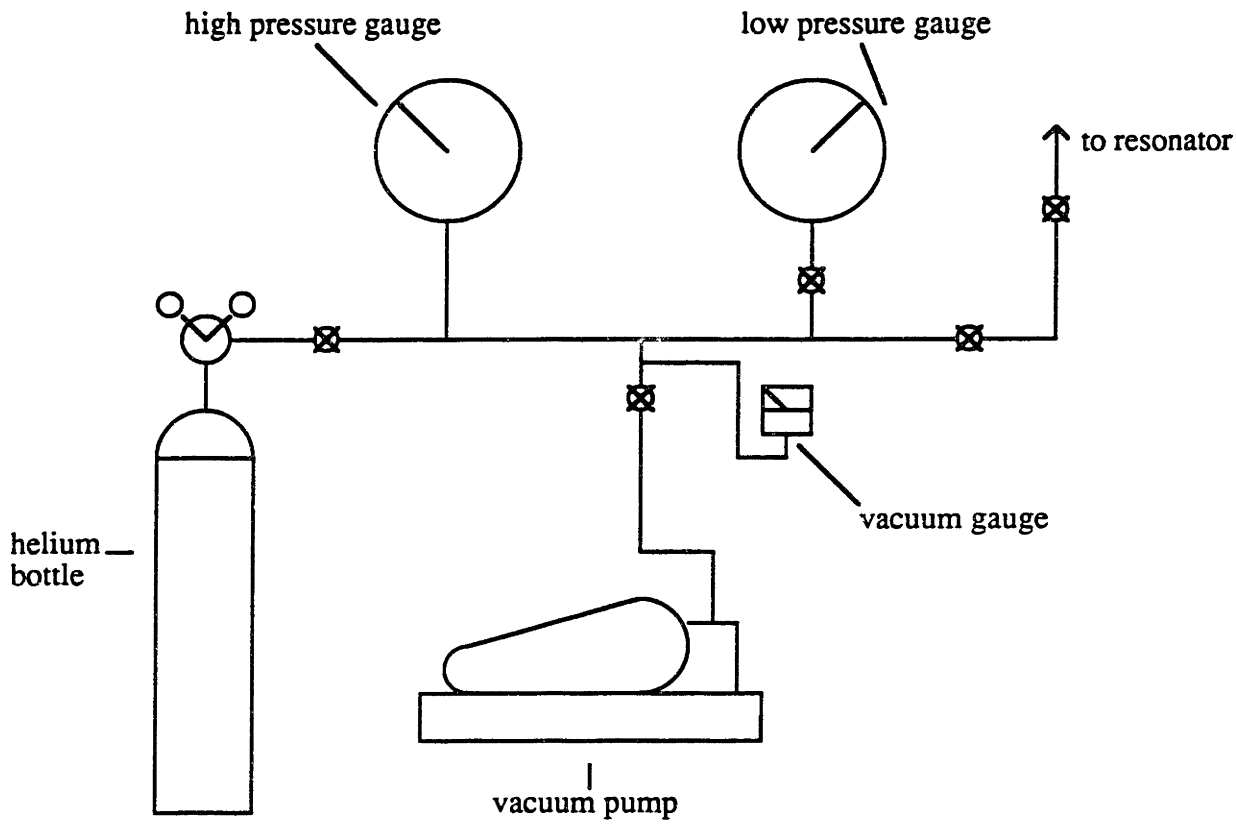

Figure 3-3: The resonator plumbing system.

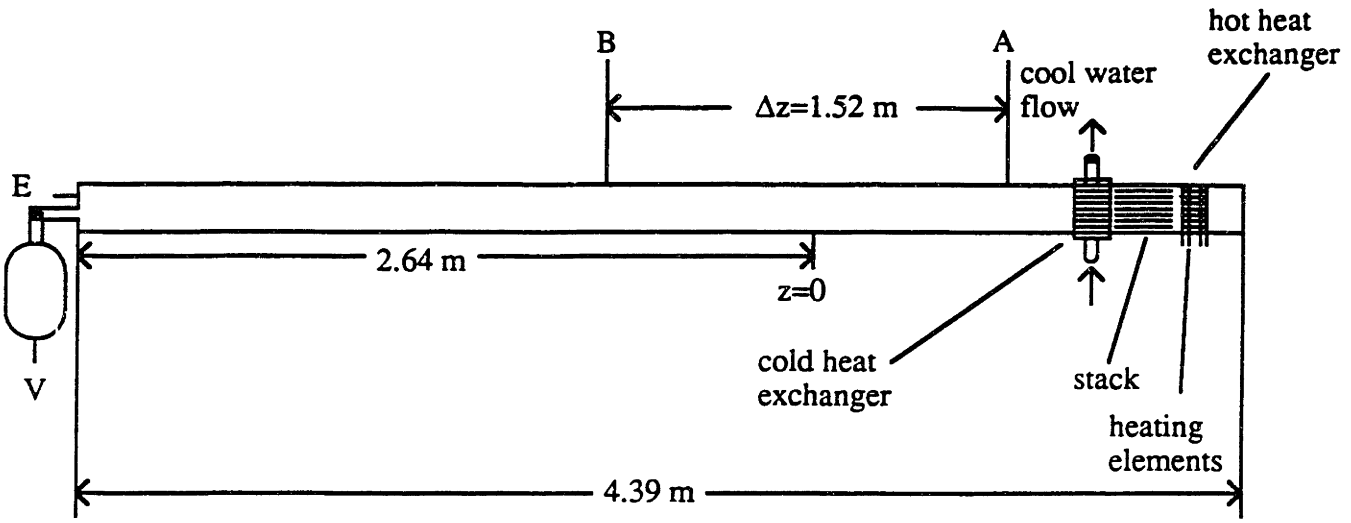

Figure 3-4: The five inch diameter resonator with the TAD connected.

microphone method. Since the one inch tweeter could only produce peak to peak pressure amplitudes of the order of 0.1 psi, more powerful drivers were needed. The next step up from the tweeter was a 4.5 inch diameter speaker, similar to ones used in fog horns. This speaker operated like a tweeter, but the diaphragm was made of hardened cloth much more rigid than that of the diaphragm on the one inch tweeter. The magnet on the 4.5 inch speaker weighed approximately 25 lbs. The high amplitude speaker produced pressure amplitudes as high as 0.9 psi.

The highest amplitude driver is a thermoacoustic driver (TAD), which is explained in Chapter 1. The TAD is held in a tube the same diameter as the five inch resonator and simply bolted onto the five inch resonator, making the total resonator length 4.39 m (173 inches). The TAD, shown in Figure 3.4, is composed of two heat exchangers, one hot (up to 480°C) and one cold (about 20°C). In between the heat exchangers sits a stack of thin steel plates, closely spaced (discussed by Swift[1]). The temperature gradient produced

by the heat exchangers induces a standing wave in the resonator. The cold heat exchanger acts like an automobile radiator, with cold water pumped through several small tubes connected to fins. The hot heat exchanger acts similarly to the cold heat exchanger, except that the tubes do not have water flowing through them, but rather the tubes act as sheaths, in which cylindrical heating elements are inserted. While the engine is operating at maximum capacity, the TAD produces peak pressure amplitudes of nearly 8 psi. Points A and B in Figure 3.4 represent pressure transducer positions for the two microphone tests.

3.2 Instrumentation

The driving tweeter was powered by two means. For experiments requiring the measurement of the quality factor, Q, of the resonator or finding the resonant frequency, a sweep was used. By using the source of a Hewlett Packard Dynamic Signal Analyzer, model #3562A, a sinusoidal signal at nearly any desired voltage could be swept through a chosen frequency range. When the driver had to be run at a given frequency a Hewlett Packard Function Generator, model #3325A, was used. Signals from both generators were run through a Hafler 500 audio amplifier before being fed to the tweeter.

The pressure transducers, or microphones, used in all of the experiments were PCB Piezotronics Inc. model #102A05 pressure transducers. These dynamic pressure transducers, with a rated sensitivity of 50 mV/psi, are prescribed for general purpose use. The calibration procedure for these transducers is rather complicated and is described in detail in Appendix B.

The signals from the pressure transducers could be interpretted in many ways. First, the signals were fed to a PCB model #482A04 voltage follower. The signals were then fed into a junction switch, and in the case of a weak signal, the signal was amplified by an amplifier with filters to improve the signal to noise ratio. In the swept sine mode, the signal was fed to the HP Dynamic Signal Analyzer where the power spectrum could

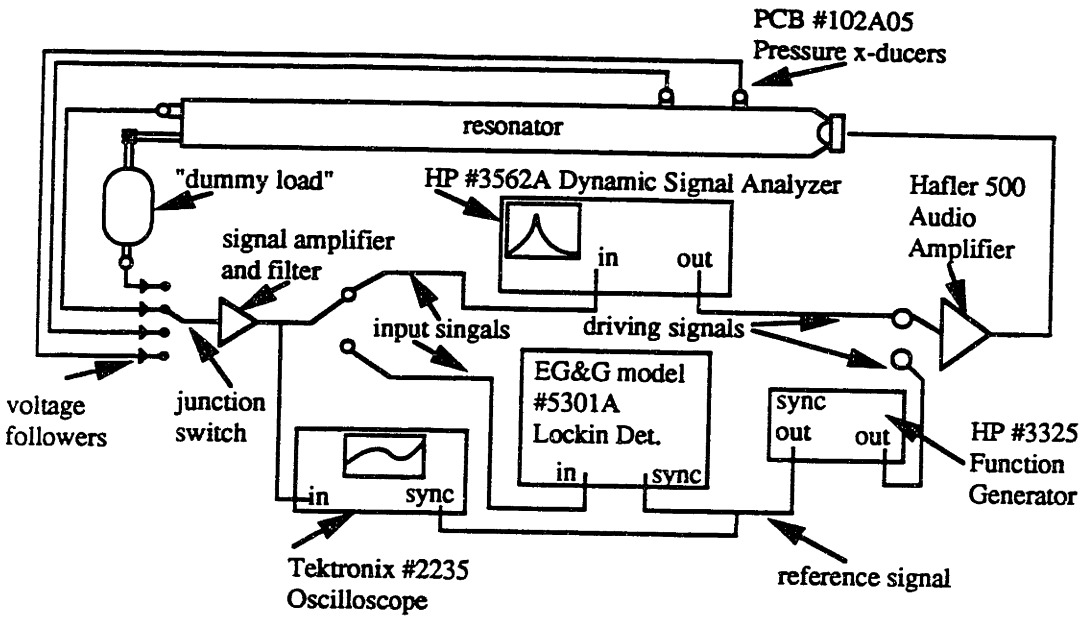

Figure 3-5: The instrumentation setup.

be displayed on the screen and stored. When the resonator was driven at a constant frequency, and numerical values of the signal were desired, the signal was fed into an EG&G Lockin Amplifier, model #5301A. The Lockin Amplifier can filter out noise and higher harmonics of the signal, and will only display the strength of the signal at the driven frequency. In these tests, the Lockin Amplifier uses a trigger input from the Function Generator to capture the signal resulting from the driven standing wave. A diagram of the entire instrumentation setup is shown in Figure 3.5.

Chapter 4

Internal Resonator Losses and the Quality Factor

An accurate method of measuring energy dissipation in an acoustic resonator must be found which can be used as a standard against which other methods can be compared. One such standard involves measuring the quality factor, Q, of the system. The quality factor is inversely proportional to the energy dissipation rate of the modeled acoustic system, and it determines what fraction of the stored energy of the system is dissipated while operating on resonance. As explained later, Q can be determined from the characteristics of the resonant peak of any damped harmonic system and can be used to determine energy dissipation quite easily. This chapter presents the theory relating the quality factor, Q, to the energy dissipation of the modeled acoustic system, outlines the procedures used in measuring Q, examines the experimental accuracy of this standard, and presents experimental energy dissipation measurements using this method. These results will be compared in Chapters 5 and 6 to the energy dissipation measurements made with the two microphone method and a second standard for measuring external energy losses.

4.1 Theoretical Analysis

An expression for the energy dissipation rate, $\dot{E}_{diss}$, must be derived, which can be compared to the two microphone results. As will be seen, $\dot{E}_{diss}$ is a function of the pressure amplitude of the standing acoustic wave, the geometric characteristics of the acoustic resonator, and known values of properties of the working fluid. The geometric characteristics are described by the quality factor of the system.

Nielsen[8] defines the theoretical quality factor as

$$Q_{theory} = \frac{\omega E_{st}}{\dot{E}_{diss}}, \tag{4.1}$$

where E_{st} is the maximum energy stored in the system, and $\dot{E}_{diss}$ is the energy lost per unit second by the system. The theoretical quality factor identifies specific geometric characteristics in the expression for $\dot{E}_{diss}$ which contribute to energy dissipation. These characteristics do not account for geometric imperfections, such as imperfect boundaries caused by drivers, joints, and protrusions in the resonator. In order to take these effects into account, Q_{theory} must be factored out of the expression for $\dot{E}_{diss}$, and replaced by an experimentally determined quality factor, Q_{meas}. The quality factor can be measured by determining the sharpness of the resonant peak of the power spectrum of the system[9, pp. 24–26], a typical peak is shown in Figure 4.1. The measured quality factor is

$$Q_{meas} = \frac{f_o}{f_1 - f_2}, \tag{4.2}$$

where f_1 and f_2 are the frequencies on the power spectrum curve at which the magnitude of the power is half of the peak value, and f_o is the resonant frequency.

The theoretical discussion starts with some assumptions about the acoustic wave in the resonator. The coordinate system in the resonator is also redefined. These assumptions are then applied to the derivations of $\dot{E}_{diss}$ and the stored energy of the system, E_{st}.

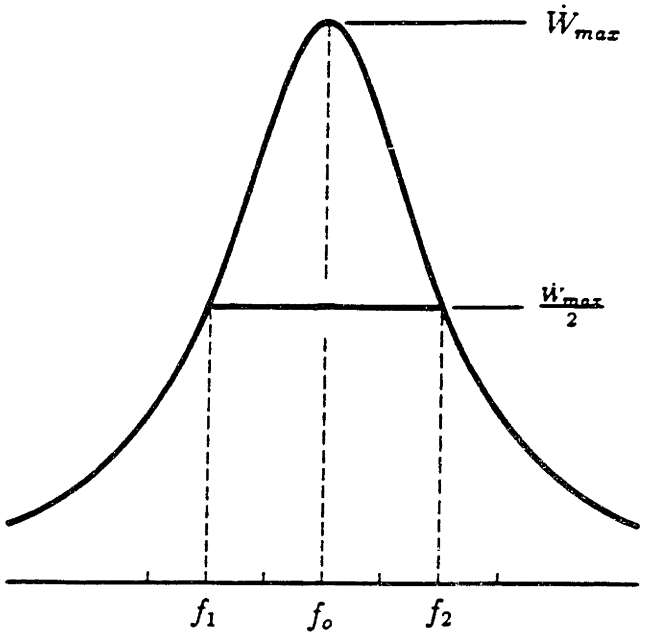

Figure 4-1: A typical resonance curve.

4.1.1 The Acoustic Standing Wave

The following derivations will be used to determine what fraction of the amplitudes of a lossless acoustic standing wave will decay due to internal losses in the system. Therefore, the acoustic wave is assumed to be wholly standing, with the peak pressure amplitude occurring at the ends of the resonator, and the peak velocity amplitude occurring in the center of the half wavelength resonator.

To make the mathematics in the following derivations simpler, the coordinate system in the resonator is redefined. Along the z-axis, zero occurs at the middle of the resonator instead of one of the ends of the resonator. Also, since the following derivations deal with the effects within the boundary layers at the walls of the resonator, the walls can be assumed to be flat plates, and a cartesian coordinate system can be used. Looking at the two dimensional picture in Figure 4.2, the r-axis will be the vertical cartesian axis (normally the y-axis) with its zero at the center of the diameter of the resonator, and the z-axis will be the horizontal cartesian axis (normally the x-axis), with its zero at the

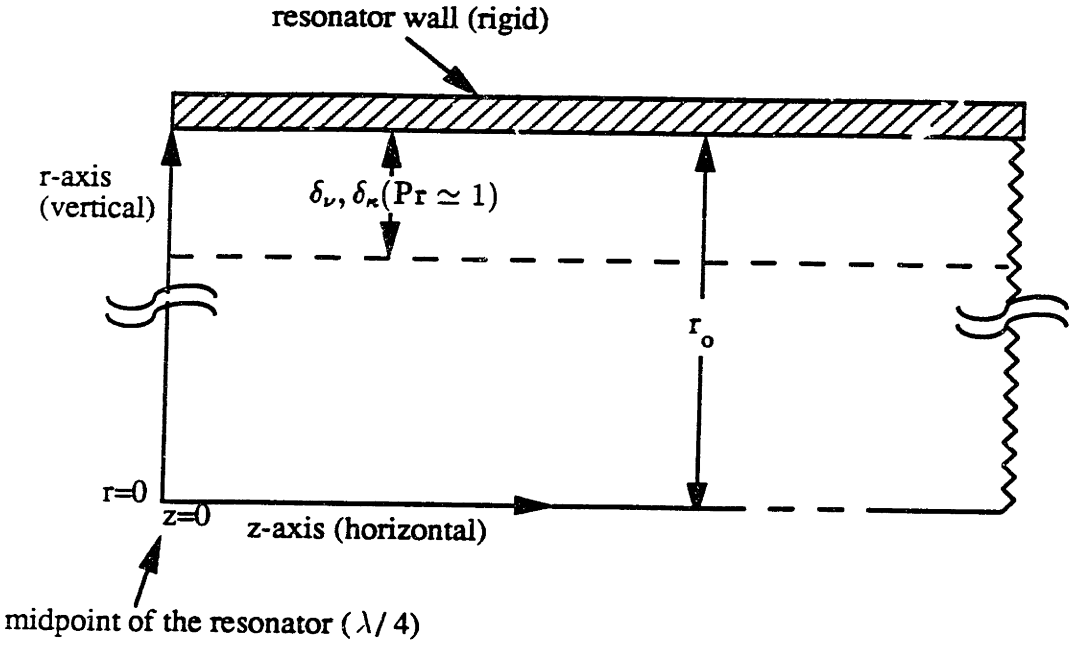

Figure 4-2: The cartesian coordinate system for the standing wave resonator.

center of the resonator.

Since the acoustic wave is assumed to be perfectly standing, the oscillating parts of the pressure and velocity are assumed to be simple trigonometric functions

$$p' = p'_E \sin(\frac{\omega}{a} z) \equiv p'^s, \tag{4.3}$$

and

$$v_z = i v_A \cos(\frac{\omega}{a} z) \equiv i v_z^s, \tag{4.4}$$

where p'_E is the pressure amplitude at the ends of the resonator, v_A is the velocity amplitude at $z = 0$, and the superscript s denotes the standing wave quantities. As before, the time derivative, $\frac{\partial}{\partial t}$, is equivalent to $i\omega$.

Since the pressure and velocity expressions do not include losses here, Euler's Equation (equation (2.18)) can be used to relate the two. Assuming the acoustic wave is a plane wave along the z-axis under lossless conditions, Euler's Equation reduces to

$$\rho_o \frac{\partial v_z}{\partial t} = -\frac{\partial p'}{\partial z}. \tag{4.5}$$

By carrying out the derivatives, substituting for the standing wave values, and solving for v_z^s, the standing wave velocity is related to the pressure amplitude

$$v_z^s = \frac{p'_E}{\rho_o a} \cos(\frac{\omega}{a} z). \tag{4.6}$$

4.1.2 Energy Dissipation

The energy dissipation rate and the stored energy of the system will now be derived. Using the approximations and coordinate system described above, each expression will reduce to a simple function of the pressure amplitude. The two expressions will be combined to identify Q_{theory}.

The energy stored in the resonator can be found from the energy density[7, pg. 9], e, in equation (2.16)

$$e = \frac{1}{2}\rho v_z^{s2} + \rho\epsilon.$$

The expressions $\rho = \rho_o + \rho'$ and $\epsilon = \epsilon_o + \epsilon'$ are substituted into the energy density equation. The term $\frac{1}{2}\rho' v_z^{s2}$ can be neglected since it is of third order. Using a second order expansion for the potential energy term, the energy density becomes

$$e = \rho_o\epsilon_o + \rho' \frac{\partial(\rho\epsilon)}{\partial\rho_o} + \frac{1}{2}\rho'^2 \frac{\partial^2(\rho\epsilon)}{\partial\rho_o^2} + \frac{1}{2}\rho_o v_z^{s2}. \tag{4.7}$$

Since the sound wave is assumed to be adiabatic, the derivatives are taken at constant entropy. Using the thermodynamic relation $d\epsilon = Tds + (p'^2/\rho^2)d\rho$, the following expression is found

$$\left(\frac{\partial(\rho\epsilon)}{\partial\rho}\right)_s = \epsilon + \frac{p'}{\rho} = w, \tag{4.8}$$

and the second derivative becomes

$$\left(\frac{\partial^2(\rho\epsilon)}{\partial\rho^2}\right)_s = \left(\frac{\partial w}{\partial\rho}\right)_s = \left(\frac{\partial w}{\partial p}\right)_\epsilon \left(\frac{\partial p}{\partial\rho}\right)_s = \frac{a^2}{\rho_o}. \tag{4.9}$$

Substituting these expressions back into the energy density equation, and keeping only the terms second order or lower, the energy density becomes

$$e = \rho_o\epsilon_o + w_o\rho' + \frac{1}{2}a^2\frac{\rho'^2}{\rho_o} + \frac{1}{2}\rho_o v_z'^2. \tag{4.10}$$

The term $\rho_o\epsilon_o$ is the energy per unit volume when the fluid is at rest, and therefore does not relate to the acoustic energy density. The second term, $w_o\rho'$, is the change in energy due to the change in mass of the fluid per unit volume. When integrating over the total volume of the fluid (the volume of the resonator) the second term becomes zero, since the system is assumed to be closed, allowing no change in mass. The energy density reduces to

$$e = \frac{1}{2}a^2\frac{\rho'^2}{\rho_o} + \frac{1}{2}\rho_o v_z'^2. \tag{4.11}$$

By taking the time average and using the thermodynamic relation $a^2 = p'^s/\rho'$, the energy density becomes

$$e = \frac{1}{4}\left(\frac{p'^{s2}}{\rho_o a^2}\right) + \frac{1}{4}\rho_o v_z'^2. \tag{4.12}$$

By integrating over the volume of the resonator, the stored energy can be found

$$E_{st} = \int_V e dV = \frac{1}{4}\frac{|p'_E|^2}{\rho_o a^2}\pi r_o^2 L. \tag{4.13}$$

To derive the energy dissipation rate of the acoustic wave in the resonator, the energy dissipation rate per unit area, $\dot{e}_{diss}$, needs to be found, which can be integrated over the surface area of the interior of the resonator. The energy dissipation rate per unit area accounts for the acoustic energy that is absorbed by the walls of the resonator due to

viscous and thermal effects within the boundary layers. To find $\dot{e}_{diss}$, the component of the acoustic velocity within the boundary layers, $\overline{v}_z^s$ (the overbar denotes a vector), normal to the walls of the resonator is simply multiplied by the acoustic pressure, p'^s. The time average of $\dot{e}_{diss}$ needs to be taken, since the instantaneous value has little meaning. The acoustic velocity within the boundary layers is found through the superpositioning of several velocity vectors within the boundary layer[10, pp. 519–529],

$$\overline{v}_{wall} = \overline{v}_z^s + \overline{v}_\nu + \overline{v}_\kappa, \tag{4.14}$$

where $\overline{v}_{wall}$ is the velocity of the resonator wall ($\overline{v}_{wall}$ is zero since the wall is assumed to be rigid and fixed to the reference frame), $\overline{v}_\nu$ is the fluid velocity due to vorticity effects near the walls, and $\overline{v}_\kappa$ is the fluid velocity due to thermal relaxation near the walls. Using superposition, the no-slip boundary conditions at the wall, $r = r_o$, will be satisfied.

To solve for $\dot{e}_{diss}$, the velocities, $\overline{v}_\nu$, and $\overline{v}_\kappa$ in equation (4.14) must be put in terms of v_z^s and p'^s. The viscous velocity is given by equation (2.47). To convert this expression to the cartesian coordinate system used in this exercise, the Bessel Functions can be replaced by hyperbolic cosines[6] as follows

$$\overline{v}_\nu = \frac{i}{\rho_o \omega}\frac{dp'^s}{dz}\Big(1 - \frac{\cosh((1+i)r/\delta_\nu)}{\cosh((1+i)r_o/\delta_\nu)}\Big). \tag{4.15}$$

The thermal velocity can be identified in the derivation carried out in Appendix E as

$$\overline{v}_\kappa = \frac{-i(\gamma-1)\delta_\kappa}{2\rho_o a^2}\frac{dp'^s}{dt}. \tag{4.16}$$

First, $\overline{v}_\nu$ will be put in terms of $\overline{v}_z^s$. By taking the horizontal divergence of equation (4.14), the thermal term will be eliminated, since $\overline{v}_\kappa$ can be assumed to be in the direction of the temperature gradient within the boundary layer normal to the wall. The horizontal divergence is

$$\nabla_T \cdot \overline{v}_{\nu T} + \nabla_T \cdot \overline{v}_{zT}^s = 0, \tag{4.17}$$

where the subscript T denotes the component tangential to the wall. The horizontal divergence reduces to $\frac{\partial}{\partial r}$ for the viscous term, using the assumptions stated in equations (2.41) through (2.44), giving

$$\frac{i}{\rho_o \omega}\frac{dp'^s}{dz}\Big(\frac{(1+i)}{\delta_\nu}\frac{\sinh((1+i)r/\delta_\nu)}{\cosh((1+i)r_o/\delta_\nu)}\Big) + \nabla_T \cdot \overline{v}^s_{zT} = 0. \tag{4.18}$$

Since this derivation satisfies the no-slip condition at the resonator walls ($r = r_o$), the hyperbolic terms reduce to a hyperbolic tangent, which is approximately 1 because r_o/δ_ν is of the order of 100. Equation (4.18) becomes

$$\frac{(i-1)}{\rho_o \omega \delta_\nu}\frac{dp'^s}{dz} + \nabla_T \cdot \overline{v}^s_{zT} = 0. \tag{4.19}$$

Very close to the resonator walls, the viscous velocity is

$$\overline{v}_\nu \cdot \mathbf{n} = \frac{1}{\rho_o \omega}\frac{dp'}{dz}, \tag{4.20}$$

which gives

$$\nabla_T \cdot \overline{v}^s_{zT} = \frac{(1-i)}{\delta_\nu}\overline{v}_\nu \cdot \mathbf{n}. \tag{4.21}$$

The normal component of equation (4.14) is taken, giving

$$\overline{v}^s_z \cdot \mathbf{n} + \overline{v}_\nu \cdot \mathbf{n} + \overline{v}_\kappa \cdot \mathbf{n} = 0. \tag{4.22}$$

The normal component of $\overline{v}_\nu$ is found from equation (4.21), and equation (4.16) is used for the thermal velocity (which is assumed to be normal to the wall). Assuming $\frac{\partial p'}{\partial t} = i\omega p'$, equation (4.22) becomes

$$\overline{v}^s_z \cdot \mathbf{n} + \frac{(1+i)}{2}\delta_\nu \nabla_T \cdot \overline{v}^s_{zT} + \frac{(\gamma-1)}{2\rho_o a^2}\omega \delta_\kappa p'^s = 0. \tag{4.23}$$

To determine $\dot{e}_{diss}$, equation (4.23) is multiplied by p'^s, and $p'^s \overline{v}^s_z \cdot \mathbf{n}$ is moved to the other side of the equation. Taking the real part of the expression and putting the viscous term

in terms of $\overline{v}_z^s$, the energy dissipation per unit area is

$$\dot{e}_{diss} = p'^s \overline{v}_z^s \cdot \mathbf{n} = \frac{\rho_o \omega}{2} \delta_\nu \overline{v}_z^{s2} + \frac{(\gamma - 1)}{2\rho_o a^2} \omega \delta_\kappa (p'^s)^2. \tag{4.24}$$

Equations (4.3) and (4.4) are substituted for $\overline{v}_z^s$ and p'^s. The time average of equation (4.24) is

$$\dot{e}_{diss} = \frac{1}{4} \frac{\omega |p'_E|^2}{\rho_o a^2} (\delta_\nu + \delta_\kappa(\gamma - 1)). \tag{4.25}$$

An expression for the time averaged energy dissipation rate can be found by integrating over the total internal surface area of the resonator,

$$\dot{E}_{diss} = \int_A \dot{e}_{diss} dA = \frac{1}{4} \frac{\omega |p'_E|^2}{\rho_o a^2} \pi r_o L \Big(\delta_\nu + \delta_\kappa(\gamma - 1) + \delta_\kappa(\gamma - 1) \frac{2r_o}{L} \Big). \tag{4.26}$$

The term $\frac{2r_o}{L}$ accounts for thermal losses at the end caps of the resonator. There is no such term for the viscous losses because $\overline{v}_\nu$ is assumed to be normal to the end caps.

Using equation (4.1), the resulting theoretical quality factor is

$$Q_{theory} = \frac{r_o}{\delta_\nu + \delta_\kappa(\gamma - 1)(1 + \frac{2r_o}{L})}. \tag{4.27}$$

Equation (4.1) can also be rearranged to give

$$\dot{E}_{diss} = \frac{\omega E_{st}}{Q_{theory}}. \tag{4.28}$$

The theoretical quality factor can be replaced by Q_{meas} to give a more accurate calculation of $\dot{E}_{diss}$, which will be discussed later in this chapter.

4.2 Experimental Procedures and Results

As can be seen from the theoretical analysis, calculating energy dissipation by measuring the quality factor can be a simple process. By measuring the pressure at the nondriven end of the resonator, both the Q and the pressure amplitude can be determined. As will be seen, the resonators have geometries that make the prediction of Q more difficult than expected.

4.2.1 Measuring Internal Losses

The Q of a resonator can be measured very simply. By measuring the acoustic pressure amplitude at the end of the resonator, p'_E, and sweeping the input signal, the HP Dynamic Signal Analyzer can create a power spectrum from which the Q can be found by using the output of the pressure transducer. From Q and p'_E, the internal losses can be calculated. The Q's of both resonators were measured at mean pressures of 12, 20, 40, 60, 80, and 100 psia. The driver was run with an input of 3.3 W, which produced a sinusoidal acoustic wave in both resonators.

4.2.2 Experimental Results

Measurements of the Q's of the five inch resonator were performed using the prescribed mean pressures at an ambient temperature of 20°C (Appendix C gives all of the necessary properties of helium under the various conditions). Table 4.1 displays the results from the experiments and shows the matching theoretical quantities explained in Section 4.1. The power spectrum curves for the tests on the five inch resonator can be seen in Figures D.1 - D.6 in Appendix D. The resulting measured and theoretical quality factors from tests run on the one inch resonator are provided in Table 4.2, along with the measured energy dissipation. Room temperature in this case was about 20°C. These power spectrum curves are given in Figures D.7 - D.12.

The results from the measurements for both resonators suggest that more energy is be-

Table 4.1: Quality Factors for the Five Inch Diameter Resonator

Mean Pressure (psia)	p'_E[Pa]	Q_{meas}	Q_{theory}	$\dot{E}_{diss}$[mW]
12	25.3	56.2	59.4	0.824
20	50.3	73.1	76.9	1.50
40	119	98.5	108.9	3.13
60	186	120.1	133.5	4.19
80	249	138.3	154.3	4.90
100	303	150.5	172.8	5.34

Table 4.2: Quality Factors for the One Inch Diameter Resonator

Mean Pressure (psia)	p'_E[Pa]	Q_{meas}	Q_{theory}	$\dot{E}_{diss}$[nW]
12	103	10.4	12.0	2.83
20	145	12.6	15.6	3.96
40	361	16.3	22.0	6.76
60	505	18.4	26.3	7.82
80	652	20.9	30.4	8.62
100	758	23.7	34.1	8.23

ing dissipated in the resonators than theory predicts, since dissipated energy is inversely proportional to Q. In the case of the one inch resonator, these losses are considerably higher than the predicted quantities. One contribution to the energy dissipation is the fact that the resonators are not perfectly smooth and rigid. Additional volume leading to inlet valves, pressure transducer mountings, and joints connecting flanges to the tube causes some additional losses. The largest contributor to the imperfections of the resonators was the driver, though. Since the tweeter had a diaphragm made of hardened cloth, the driven end of the resonators did not act like a perfectly rigid flat plate, thus lowering the Q's considerably.

4.2.3 Measurements with a Noncompliant Driver

To check if the one inch tweeter dissipates a large amount of energy, thus lowering the Q of the system, a different driver was used on the one inch resonator. The driver, commonly used as a speaker in headsets or earphones, is about a half an inch in diameter and has a steel plate on its face, making it more rigid than the one inch tweeter. The driver was glued to a brass plate (shown in Figure 4.3) and coupled to the resonator. The dissipation was measured at mean pressures of 50 and 100 psia ($T_o = 20°C$), and the speaker was driven at 4.1 V_{peak}, causing the amplitude of the acoustic pressure wave to be about 6.3 Pa at $p_o = 50$ psia and 9.3 Pa at $p_o = 100$ psia. Using such a small speaker, the pressure amplitude was hard to measure, but the signal analyzer was able to record the power spectra (shown in Figures 4.4 and 4.5) at these mean pressures, giving Q's of 23.5 and 33.0 at 50 and 100 psia respectively. These measured Q's match the calculated quantities of 24.0 and 34.1 well, and show that the geometry and construction of the one inch tweeter played a significant role in dissipating energy in the resonator, while the internal geometric imperfections played a minor role in dissipating energy.

The same experiment was not conducted on the five inch resonator because of the extremely weak acoustic wave that would result, but the effect of the tweeter on the Q of the five inch resonator could be calculated. The Q of any resonator is a combination

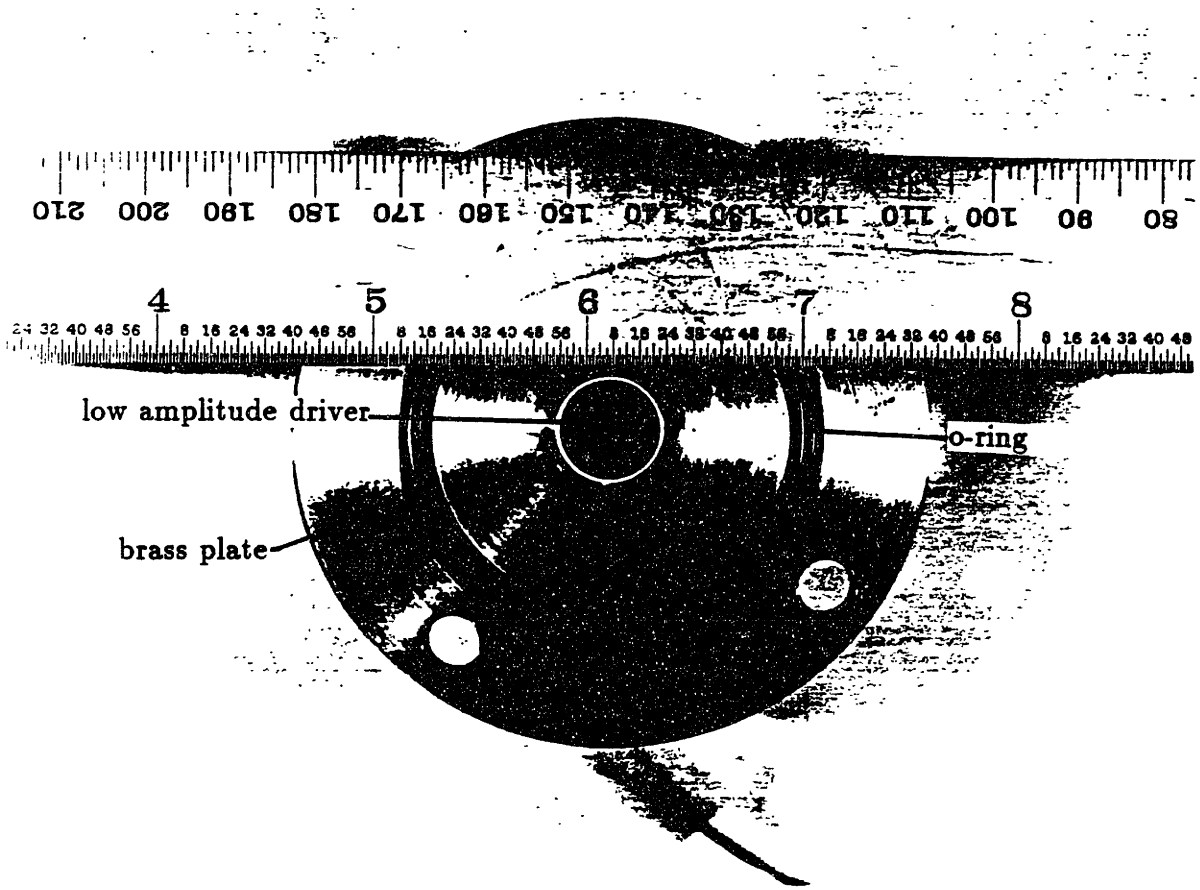

Figure 4-3: The noncompliant driver, glued to the brass coupling plate.

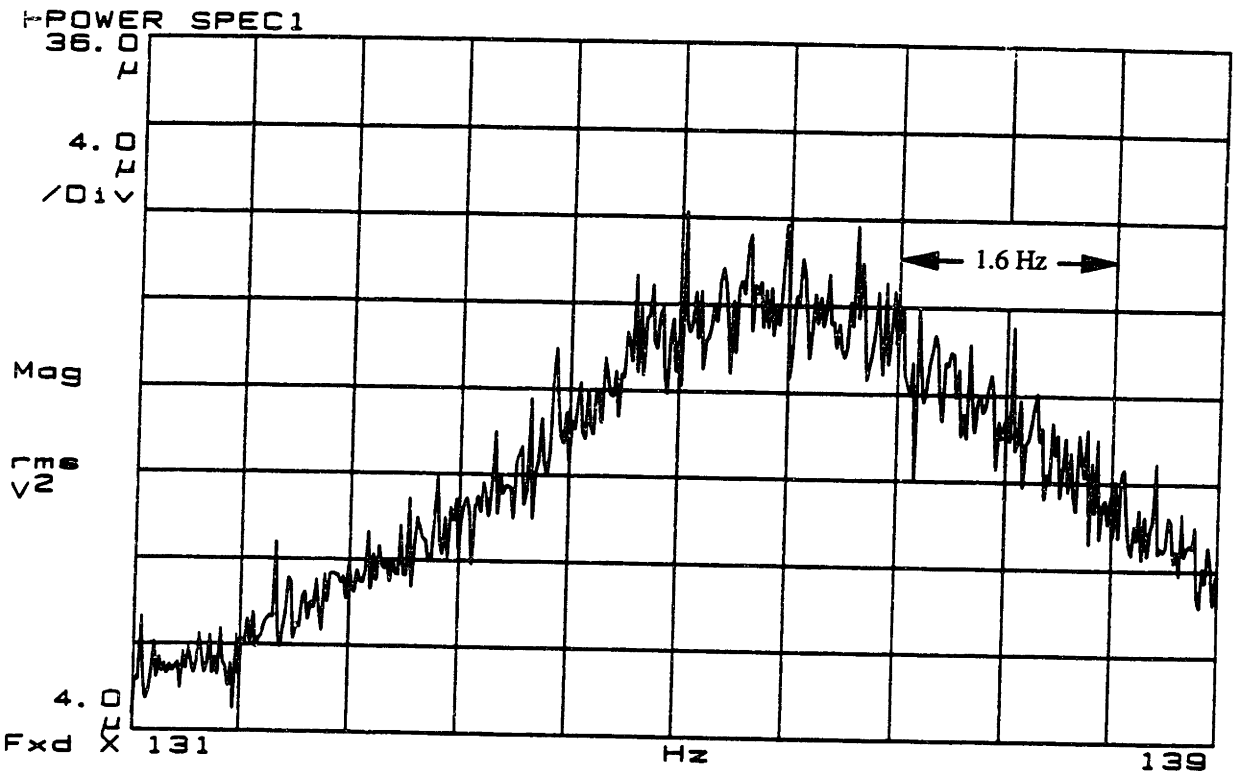

Figure 4-4: The resonance curve using the noncompliant driver on the one inch diameter resonator at 50 psia.

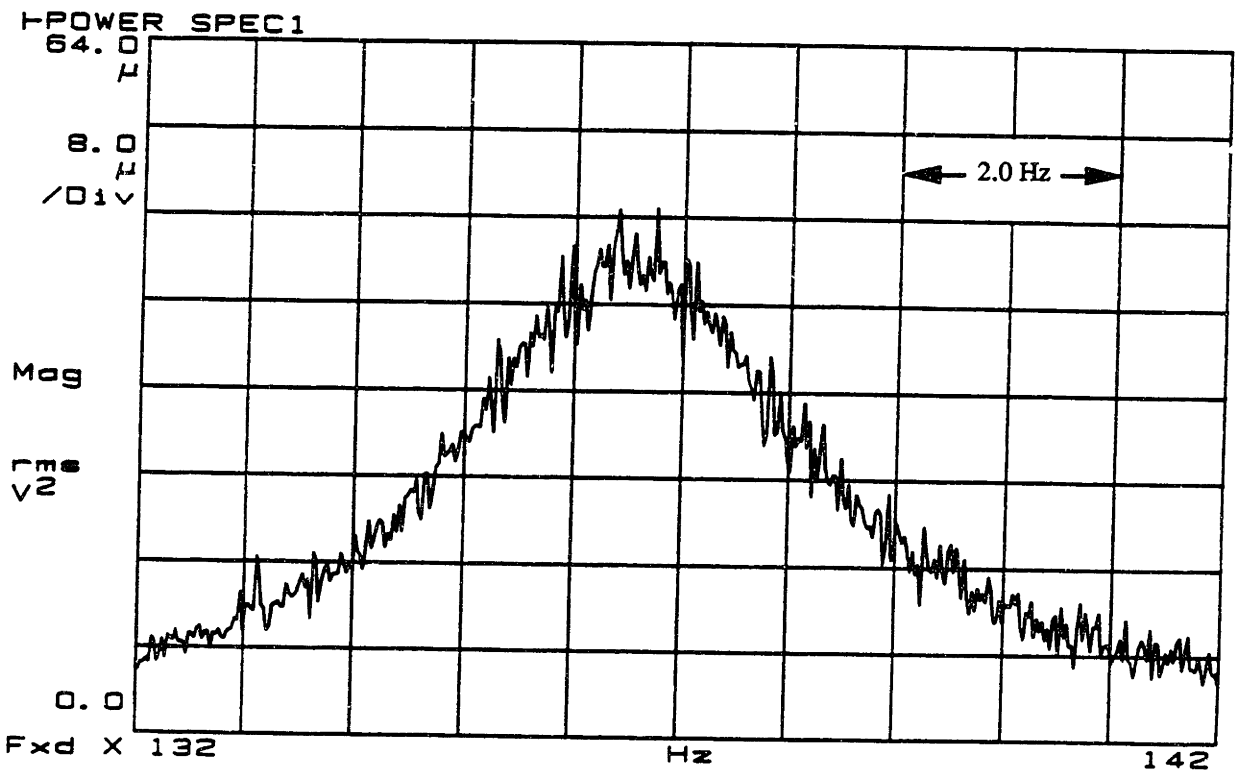

Figure 4-5: The resonance curve using the noncompliant driver on the one inch diameter resonator at 100 psia.

of several different loss mechanisms which are additive

$$\frac{1}{Q} = \frac{1}{Q_{theory}} + \frac{1}{Q_{driver}} + \frac{1}{Q_{misc}}, \tag{4.29}$$

where Q is found to be the combination of the losses produced by the driver, Q_{driver}, and other losses such as external loads or geometric irregularities, Q_{misc}, as well as Q_{theory}.

The combination of $\frac{1}{Q_{driver}}$ and $\frac{1}{Q_{misc}}$ can be found from the difference of the inverses of Q_{theory} and Q_{meas}. Looking at the case when the noncompliant driver was used, assuming $\frac{1}{Q_{driver}} = 0$ the term, Q_{misc} can be established for the one inch resonator. So Q_{driver} can be found for the one inch tweeter in the one inch resonator too. By doing these calculations, Q_{misc} for the one inch resonator was found to be about 1000 (losses this small were difficult to measure exactly), which makes $Q_{driver} \simeq 80$.

While the value of Q_{driver} changes for different resonators, the tweeter will dissipate the same amount of energy for all resonators under the same conditions. So, Q_{driver} for the five inch resonator can be found through the following relation

$$Q_{driver,5inch} = \frac{E_{st}}{\dot{E}_{1inch}}. \tag{4.30}$$

After equation (4.30) is simplified, $Q_{driver,5inch}$ is found to be

$$Q_{driver,5inch} = Q_{driver,1inch} \times \frac{r^2_{o,5inch}}{r^2_{o,1inch}}, \tag{4.31}$$

where $\frac{r^2_{o,5inch}}{r^2_{o,1inch}}$ is the ratio of the squares of the radii of both resonators, which is 25, making $Q_{driver,5inch} \simeq 2000$. With $Q_{driver,5inch}$ determined, $Q_{misc,5inch}$ can be found also. The measured and extracted values for Q_{driver} and Q_{misc} which resulted from the tests described earlier are shown in Tables 4.3 and 4.4.

Table 4.3: Tweeter and Miscellaneous Quality Factors for the One Inch Diameter - Resonator, Using $Q_{misc} = 1000$

p_o [Pa]	$\frac{1}{Q_{driver}} + \frac{1}{Q_{misc}}$	$\frac{1}{Q_{driver}}$
12	0.0128	0.0118
20	0.0125	0.0115
40	0.0159	0.0149
60	0.0164	0.0154
80	0.0149	0.0139
100	0.0128	0.0118

Table 4.4: Tweeter and Miscellaneous Quality Factors for the Five Inch Diameter - Resonator, Using $Q_{driver} = 2000$

p_o [Pa]	$\frac{1}{Q_{driver}} + \frac{1}{Q_{misc}}$	$\frac{1}{Q_{misc}}$
12	0.000959	0.000459
20	0.000859	0.000359
40	0.000970	0.000469
60	0.000835	0.000335
80	0.000749	0.000249
100	0.000858	0.000358

4.3 Summary

The internal resonator losses can now be measured accurately with a good sense of exactly where the energy within the resonators is going. The next step is to see how accurately external loads can be measured with the method described in this chapter, as well as other methods. The measured quantities found in this chapter will be used in the next chapter to determine total energy dissipation in a loaded resonator, since the method described in the next chapter accounts for all losses. Later, in Chapter 6, the theoretical quantities derived in this chapter will be used in comparison to the two microphone method. These quantities will be used because the two microphone method cannot measure losses in the driven end of the resonators. This will be described later.

Chapter 5

External Energy Dissipation

With the understanding of internal resonator losses in place, and a reliable method of measuring these losses, measurements of external acoustic energy dissipation can be examined. In practical applications, acoustic resonators may have external loads which perform some type of mechanical work. In these cases, internal and external energy dissipation may need to be measured. As described in Chapter 4, the quality factor, Q, accounts for all losses in the system, including external losses. Now, another method of measuring energy dissipation will be discussed, which is specifically used for measuring external energy dissipation.

5.1 Theoretical Analysis

In an acoustic resonator, a load can dissipate energy by using the pressure swings at the end of the resonator to perform some type of reciprocating mechanical work. For the sake of modeling such dissipation, the rigid end of a resonator should be replaced with a mechanism which converts the pressure swings into some form of work. The best way to picture an acoustic load on a resonator is by comparing the system to an electrical circuit. In an electrical circuit the power is given as $P = \overline{IV_A}$, where I is the current and V_A is the voltage of the AC source. In the simple RC circuit, shown in Figure 5.1, the

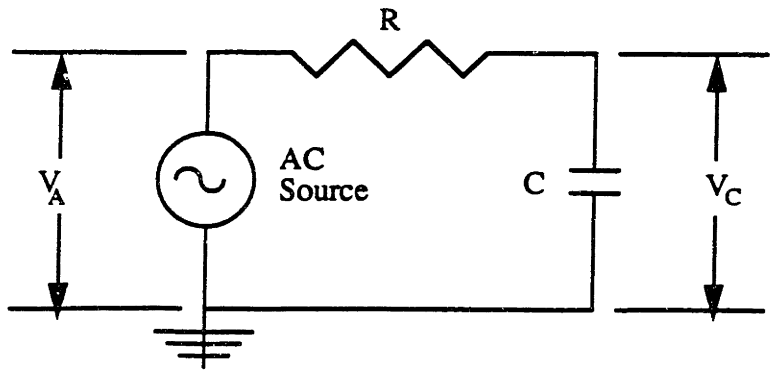

Figure 5-1: The analog electric circuit to the acoustic system.

power dissipated is

$$P = \omega C \overline{i V_A V_B}, \tag{5.1}$$

where C is the capacitance, and V_B is the voltage across the capacitor.

To make a comparison to an acoustic system, some simple analogies can be made. The resonator acts like an oscillating voltage source, with the pressure swings analogous to the voltage. The volume velocity is comparable to the current, and hence, since a capacitor is a charge storage element, a large volume is its acoustic analog. The aperture of the needle valve connecting the resonator to the volume acts like a variable resistor. With the electrical circuit analogy, the acoustic power dissipated through external loading is

$$\dot{W}_{ex} = \overline{p'_E \dot{V}}, \tag{5.2}$$

where $\dot{V}$ is the volume velocity into the load.

Some assumptions must be made about the system. For low amplitude acoustic waves, it is safe to assume that the walls of the volume and connecting pipe are isothermal (in high amplitude cases temperature gradients arise because of viscous effects so heat sinks

must be installed to maintain a constant temperature). However, the walls may not be treated as adiabatic since compressive energy in the working fluid near the walls is dissipated through thermal relaxation (see Appendix E). Remembering these assumptions, the volume velocity can be related to the pressure inside of the volume, p'_V, as

$$\dot{V} = \frac{1}{\gamma p_o}\frac{dp'_V}{dt}\left[V - i\frac{\gamma-1}{2}\delta_\kappa A\right], \tag{5.3}$$

where V is the volume of the load, and A is the surface area of the load. Combining equations (5.2) and (5.3), the power dissipated in the load is

$$\dot{W}_{ex} = \frac{\omega}{2\gamma p_o}\mathrm{Re}\left[\tilde{p}'_E p'_V\left[iV + \frac{\gamma-1}{2}\delta_\kappa A\right]\right], \tag{5.4}$$

or

$$\dot{W}_{ex} = \frac{\omega V|p'_E||p'_V|}{2\gamma p_o}\left[\sin\phi + \frac{A\delta_\kappa(\gamma-1)}{2V}\cos\phi\right], \tag{5.5}$$

where ϕ is the phase angle between p'_E and p'_V.

Now, losses measured in the resonator can be compared to losses measured in the load. By letting the resonator run without an external load, the Q of the resonator, Q_{res}, can be measured. Using equation (4.28), the power dissipated by the unloaded resonator is then

$$\dot{E}_{\mathrm{res}} = \frac{\omega E_{st}}{Q_{\mathrm{res}}}. \tag{5.6}$$

If an external load were connected to the resonator, Q_{tot} could be measured from the resonance. The quality factor, Q_{tot}, accounts for the losses in the resonator as well as the power dissipation caused by the load. So the total energy dissipated in the loaded system is similarly

$$\dot{E}_{\mathrm{tot}} = \frac{\omega E_{\mathrm{st}}}{Q_{\mathrm{tot}}}. \tag{5.7}$$

Since $\dot{E}_{tot}$ accounts for the energy dissipated in the resonator and the energy lost in any external loading, a good way to check the entire method of measuring energy dissipation is through the expression

$$\dot{E}_{\rm tot} = \dot{E}_{\rm res} + \dot{W}_{ex}. \tag{5.8}$$

5.2 Experimental Procedures and Results

Using the theoretical background from this chapter and Chapter 4, the external energy dissipation in acoustic resonators can be determined in two different ways. Since the method of measuring the Q to determine energy dissipation appears to work accurately, the technique of measuring the losses in only the load can be checked and evaluated. To measure $\dot{W}_{ex}$, the signals from pressure transducers at the end of the resonator and in the volume need to be separated into real and imaginary parts, requiring more instrumentation and effort. However, the procedure for measuring Q_{tot} is exactly the same as was outlined in Chapter 4.

5.2.1 Measuring External Losses

To perform the external load measurements, the five inch diameter resonator was used. Coupled to the resonator was the 1500 cc volume described in Chapter 3. Three sets of experiments were run at mean pressures of 12, 50, and 100 psia. At 12 psia, the aperture of the needle valve connecting the 1500 cc volume to the resonator was set to 1/3, 2/3, and the fully opened positions. At the higher mean pressures, the aperture was set to 1/12, 1/6, 1/3, and 2/3 opened positions. The input to the speaker was adjusted for each mean pressure to produce a sine wave which showed no nonlinearities. To obtain Q_{tot}, the input signal was swept in the same fashion as described in Section 4.2.1. To find ϕ and the complex quantities p'_E and p'_V, the system was driven at its resonant frequency and the signals from the nondriven end and the external load were fed into the Lockin

Amplifier, where the real and imaginary parts could be deciphered.

5.2.2 External Loss Results

The energy dissipation rate in the load, $\dot{W}_{ex}$, was found using equation (5.5). The magnitudes of the signals in the volume and at the end of the resonator provided values for $|p'_V|$ and $|p'_E|$, while the phase angle, ϕ, was found by separating the real and imaginary parts of the pressure signals as follows

$$\phi = \tan^{-1}\left(\frac{\mathrm{Im}(p'_V)}{\mathrm{Re}(p'_V)}\right) - \tan^{-1}\left(\frac{\mathrm{Im}(p'_E)}{\mathrm{Re}(p'_E)}\right). \tag{5.9}$$

The energy lost in the resonator was calculated by using the Q's measured in Section 4.2.2 and letting them equal Q_{res} in equation (5.6). Since measuring $\dot{E}_{tot}$ and $\dot{E}_{res} + \dot{W}_{ex}$ both account for all of the losses in the system, including Q_{driver}, all of the measured values of the quality factor were used in the calculations, instead of just Q_{theory} and Q_{misc}.

To get a broad range of data, the aperture to the load was opened to the various settings prescribed in Section 5.2.1. Measurements were not taken at the fully opened setting at $p_o = 50$ and 100 psia because the boundary layer thicknesses were supressed so much that the aperture was larger than the boundary layer thicknesses, causing severe nonlinear effects which distorted the measurements of the pertinent variables.

Plots of Q_{tot} are shown for the various mean pressures and aperture settings in Figures D.13 through D.23. The sum of the energy dissipation rate in the resonator and in the load matched the measurement of the total energy dissipation rate well. The measured pressures from the tests are given in Table 5.1, and the energy dissipation values are displayed in Table 5.2. Figure 5.2 shows a plot of the energy dissipation versus mean pressure. The ambient temperature during these sets of tests was 22°C.

One interesting note about these tests is that the resonant frequency of the system got higher as the aperture of the needle valve got larger. This phenomenon occurs because

Table 5.1: Measured Pressures from the External Loss Tests

p_o (psia)	aperture setting	Re(p'_E) (Pa)	Im(p'_E) (Pa)	Re(p'_V) (Pa)	Im(p'_V) (Pa)
12	1/3	30.5	1.25	-0.150	-1.31
12	2/3	24.9	-0.197	-1.50	-3.32
12	full	22.8	0.028	-3.31	-4.40
50	1/12	69.5	0.314	-0.038	-0.310
50	1/6	60.7	0.470	-0.362	-1.21
50	1/3	43.0	0.157	-1.66	-3.66
50	2/3	34.0	0.392	-6.49	-4.94
100	1/12	49.9	0.562	-0.053	-0.579
100	1/6	42.2	0.070	-0.752	-2.35
100	1/3	34.5	0.157	-1.67	-1.46
100	2/3	30.9	0.351	-10.1	-4.51

in damped resonant systems, the damped resonant frequency goes as

$$\omega_d \propto \sqrt{1 - R \times \mathrm{K}}, \tag{5.10}$$

where K is a constant and R is the resistive term. When the aperture is open, the resistance to the load is lowered, thus increasing the resonant frequency of the system.

To detect nonlinear effects, the pressure signals were monitored for any irregularities, and the input to the tweeter was varied. In the case of $p_o = 100$ psia, the input to the tweeter was lowered to 1.27 V_{peak} because the acoustic wave showed signs of nonlinearities at the higher amplitudes. Pressure traces of the signal from the pressure transducer in the load show a nicely developed sine wave depicting linear behavior at the different aperture settings.

5.3 Summary

Looking at Table 5.2, an excellent agreement between the total measured energy dissipation, $\dot{E}_{tot}$, and the sum of the individually measured load and resonator dissipation, $\dot{W}_{ex}$

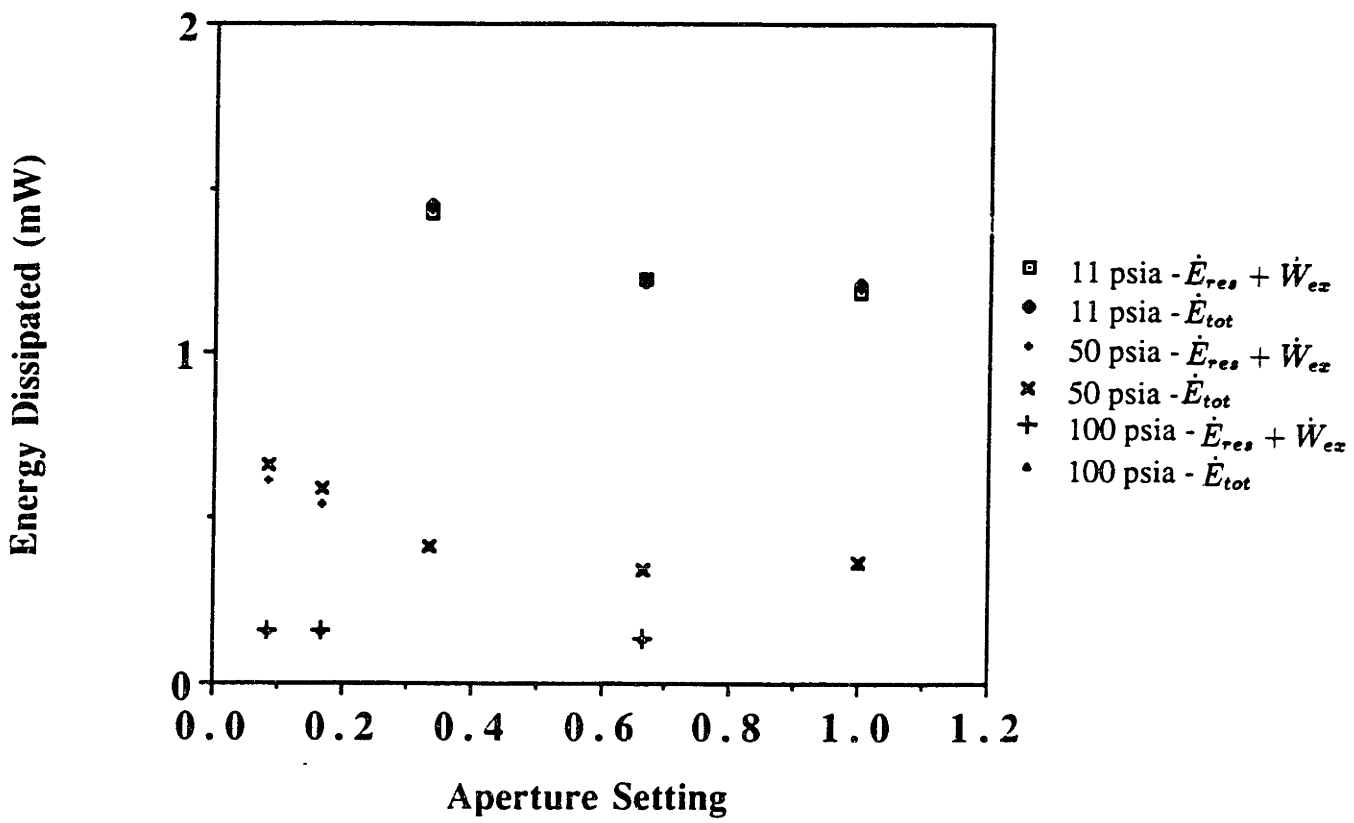

Figure 5-2: Energy dissipation versus mean pressure for the various valve settings, using the five inch diameter resonator.

Table 5.2: Results from External Load Measurements

p_o (psia)	aperture setting	Q_{tot}	f_{res} (Hz)	$\dot{E}_{res}$ (mW)	$\dot{W}_{ex}$ (mW)	$\dot{E}_{res} + \dot{W}_{ex}$ (mW)	$\dot{E}_{tot}$ (mW)
12	1/3	48.7	137.0	1.23	0.199	1.43	1.45
12	2/3	38.5	137.2	0.818	0.418	1.23	1.22
12	full	32.8	137.7	0.690	0.509	1.19	1.21
50	1/12	108.4	138.7	0.592	0.0246	0.617	0.662
50	1/6	95.0	138.8	0.460	0.0845	0.544	0.587
50	1/3	67.8	138.9	0.231	0.182	0.413	0.412
50	2/3	51.6	139.8	0.145	0.195	0.340	0.342
100	1/12	134.6	138.6	0.146	0.0167	0.163	0.161
100	1/6	96.0	138.6	0.104	0.0559	0.160	0.162
100	1/3	69.8	138.2	0.0617	0.0750	0.137	0.147
100	2/3	61.7	140.1	0.0567	0.0794	0.136	0.137

and $\dot{E}_{res}$, can be seen. A few conclusions can be made about this particular set of external loading measurements. First, the losses in the resonator can be measured accurately by measuring the sharpness of the resonance curve, Q. From these internal dissipation measurements, losses in an external load can be determined by measuring the Q of an externally loaded resonator and subtracting the measured internal losses, $\dot{E}_{res}$, from the total measurement, $\dot{E}_{tot}$. However, the major accomplishment of this exercise lies in the fact that losses induced by the dissipative volume attached to the resonator were also accurately measured using pressure readings from transducers inside of the volume and at the end of the resonator. Since the theoretical values of Q will be needed to compare to the two microphone method, the method of measuring $\dot{W}_{ex}$ and adding it to $\dot{E}_{res}$ will prove to be a useful comparison to the two microphone method when external loading is involved.

Chapter 6

The Two Microphone Method

The final step in this study of experimentally measuring energy losses in an acoustic resonator is to examine the method of detecting energy dissipation from pressure measurements at two points along the half wavelength resonator. The theory behind the two microphone method can now be discussed, using the background information provided in Chapter 2. Chapters 4 and 5 provide reliable methods of measuring internal and external energy dissipation to which the two microphone method can be compared. The experiments conducted in this chapter will yield results which will indicate whether or not the two microphone method is a useful tool in measuring energy dissipation in standing wave acoustic resonators.

6.1 Theoretical Analysis

With the basis of resonator theory with losses discussed, methods for measuring losses from within the resonator can be developed theoretically. The two microphone method involves measuring the pressure at different points along the length of the resonator and comparing the pressure amplitude drop and change of phase between those points due to energy dissipation. The energy dissipated from the midpoint of the locations of measurement in the resonator to the nondriven end of the resonator (including any

external loads) can be determined in this fashion.

To solve equation (2.48), the pressure amplitudes at the two points, A and B, shown in Figure 6.1, must be determined. The coordinates need to be redefined so $z = 0$ at the midpoint of A and B. Solving for $p'(z)$ at the two points, the amplitude can be found

$$p'(\frac{-\Delta z}{2}) = p'_A = Ae^{-ik\Delta z/2} + Be^{ik\Delta z/2}, \tag{6.1}$$

$$p'(\frac{\Delta z}{2}) = p'_B = Ae^{ik\Delta z/2} + Be^{-ik\Delta z/2}, \tag{6.2}$$

where Δz is the distance between the points of measurement. The constants A and B can be found by solving for the acoustic pressure amplitude, $p'(z)$, and its first derivative, $\frac{dp'(x)}{dz}$, at the midpoint, $z = 0$, giving

$$p'(z = 0) = A + B = (p'_A + p'_B)\frac{\sin(k\Delta z/2)}{\sin(k\Delta z)}, \tag{6.3}$$

and

$$\frac{dp'(z = 0)}{dz} = ik(A - B) = \frac{k(p'_B - p'_A)\cos(k\Delta z/2)}{\sin(k\Delta z)}. \tag{6.4}$$

Substituting equations (6.3) and (6.4) into equation (2.48), the energy dissipation becomes

$$\dot{E}_{2sen} = \frac{-\pi {r_o}^2}{2\omega\rho_o}\mathrm{Im}\left[(\tilde{p}'_A + \tilde{p}'_B)\frac{\sin(\tilde{k}\Delta z/2)}{\sin(\tilde{k}\Delta z)}k(p'_B - p'_A)\frac{\cos(k\Delta z/2)}{\sin(k\Delta z)}(1 - f_\nu)\right]. \tag{6.5}$$

When the pressure amplitudes are multiplied out in equation (6.5), the resulting factor is $|p'_B|^2 - |p'_A|^2 + 2i\mathrm{Im}(\tilde{p}'_A p'_B)$, where $|p'_A|^2$ and $|p'_B|^2$ are called the auto spectra of the total pressure at points A and B, and $\mathrm{Im}(\tilde{p}'_A p'_B)$ is the imaginary part of the cross spectrum between the total acoustic pressure at these points[5].

The expression derived in equation (2.68) can be approximated as follows

$$k \simeq \frac{\omega}{a}\Big(1 + \frac{(\gamma - 1)f_\kappa}{2} + \frac{f_\nu}{2}\Big), \tag{6.6}$$

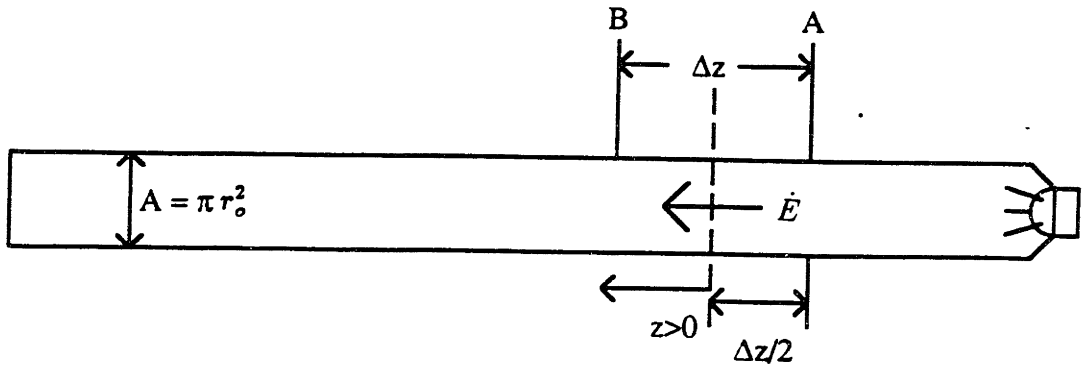

Figure 6-1: Measurement of the intensity of the standing wave from two points within the resonator.

which reduces to

$$\mathrm{k} \simeq \frac{\omega}{a}\left[1+\frac{(1-i)}{2}\left(1+\frac{\gamma-1}{\sqrt{\mathrm{Pr}}}\right)\frac{\delta_\nu}{r_o}\right], \tag{6.7}$$

where Pr is the Prandtl Number and $\mathrm{Pr} = \nu/\alpha$. By substituting equation (6.7) into equation (6.5) and doing a considerable amount of math, the dissipated power reduces to a function of the pressures and known constants

$$\begin{aligned}\dot{E}_{2sen} = \frac{-\pi {r_o}^2}{2\rho_o a \sin(\omega\Delta z/a)}\Big[&\mathrm{Im}(\tilde{p}'_A p'_B) - \frac{\delta_\nu}{2r_o}\big[\mathrm{Im}(\tilde{p}'_A p'_B)\big(1-\tfrac{\gamma-1}{\sqrt{\mathrm{Pr}}}+(1+\tfrac{\gamma-1}{\sqrt{\mathrm{Pr}}})\tfrac{\omega\Delta z}{a}\cot(\tfrac{\omega\Delta z}{a})\big)\\ &+\tfrac{1}{2}(|p'_A|^2-|p'_B|^2)\big(1-\tfrac{\gamma-1}{\sqrt{\mathrm{Pr}}}+(1+\tfrac{\gamma-1}{\sqrt{\mathrm{Pr}}})\tfrac{\omega\Delta z}{a}\csc(\tfrac{\omega\Delta z}{a})\big)\big]\Big].\end{aligned} \tag{6.8}$$

In most cases the terms $\frac{\omega\Delta z}{a}\cot(\frac{\omega\Delta z}{a}) \simeq 1$ and $\frac{\omega\Delta z}{a}\csc(\frac{\omega\Delta z}{a}) \simeq 1$, so equation (6.8) reduces to

$$\dot{E}_{2sen} = \frac{-\pi {r_o}^2}{2\rho_o a \sin(\frac{\omega\Delta z}{a})}\Big[\mathrm{Im}(\tilde{p}'_A p'_B)(1-\frac{\delta_\nu}{r_o}) + \frac{\delta_\nu}{2r_o}(|p'_B|^2-|p'_A|^2)\Big]. \tag{6.9}$$

Through some mathematical manipulations, the term $\mathrm{Im}(\tilde{p}'_A p'_B)$ can be shown to be equal

to $|p'_A||p'_B|\sin\phi$, where ϕ is the phase angle between p'_A and p'_B. This relation shows the dependence on the phase angle and will prove to be helpful later on. This method of determining the energy dissipation of the system accounts for losses incurred by external loading and internal dissipative losses for $z > 0$ in the resonator itself, if the load occurs at $z > 0$.

To check the accuracy of the two microphone method, the method of calculating internal energy dissipation, $\dot{E}_{res}$, with some Q and pressure amplitude, p'_E, will be used, similar to what is described in Chapter 4. Since the energy measured by the two microphone method does not account for the entire length of the resonator, as described earlier, $\dot{E}_{res}$ can only account for the same length of the resonator. So the integration carried out in equations (4.13) and (4.26) becomes more complicated since the trigonometric terms are not zero. The energy, $\dot{E}_{res}$, is thus

$$\dot{E}_{res} = \frac{(p'_E)^2\omega\pi r_o^2 L}{4\rho_o a^2}\Big[\frac{\delta_\kappa}{r_o}(\gamma-1)(1+\frac{\sin 2kL}{2kL}+\frac{r_o}{L})+\frac{\delta_\nu}{r_o}(1-\frac{\sin 2kL}{2kL})\Big], \qquad (6.10)$$

where L is the length from $z = 0$ to the nondriven end of the resonator.

6.2 Experimental Procedures

The two microphone method was tested in several ways. Information concerning the placement of the pressure sensors was needed to insure accurate readings, and these procedures are described in this section. The two microphone method measured only the internal losses in one set of tests and a combination of internal and external losses in a separate set of tests. This section also explains some of the problems and trade-offs encountered while conducting the two microphone tests.

6.2.1 Resonator Sizing

In the following set of experiments, the two microphone method will be used in both the five inch and one inch diameter resonators. The one inch resonator was used because higher internal losses were desired so measurements with the two microphone method would be easy to make and more reliable. Since the energy dissipated in a resonator is inversely proportional to Q, the Q of the resonance had to be lowered, and by looking at equation (4.27), $Q \propto r_o$

$$Q_{theory} = \frac{r_o}{\delta_\nu + \delta_\kappa(\gamma - 1)(1 + \frac{2r_o}{L})}. \tag{4.27}$$

Situations resulting in low Q's were desired for this study because the pressure sensing equipment was not very sensitive and lowered the accuracy of the measurements. To remedy the problem the one inch diameter resonator was used.

6.2.2 Predicting the Quality Factor

Since the two microphone method only accounts for losses incurred from the midpoint of the microphones to the nondriven end of the resonator, measuring the effective Q of the resonance could not be conducted as described in Section 4.2.1 since the driven end contained a tweeter which lowered the quality factor because the tweeter did not act like a perfectly rigid end plate. The two microphone method could not detect losses caused by the driver, since the driver was positioned before the midpoint of the pressure transducers, so the quality factor had to be predicted through the method of calculating an effective quality factor, Q_{eff}, and measuring Q_{misc}, as described and performed in Section 4.2.3. The quality factor used for calculating energy dissipation as a comparison to the two microphone method is a combination of Q_{eff} and Q_{misc}.

The term Q_{eff} can be extracted from the term in parentheses in equation (6.10)

$$\frac{1}{Q_{eff}} = \frac{\delta_\kappa}{r_o}(\gamma - 1)(1 + \frac{\sin 2kL}{2kL} + \frac{r_o}{L}) + \frac{\delta_\nu}{r_o}(1 - \frac{\sin 2kL}{2kL}). \tag{6.11}$$

The effective Q only accounts for losses for $z > 0$. Now the quality factor resulting from geometric imperfections in the resonator can be added in to describe the total effect of the resonator on internal losses,

$$\frac{1}{Q} = \frac{1}{Q_{eff}} + \frac{1}{Q_{misc}}, \tag{6.12}$$

which can be incorporated into equation (6.10). The assumption that the geometric imperfections are distributed evenly along the length of the resonator was made, since Q_{misc} does not play a major role in internal energy dissipation.

6.2.3 Measurement of Phase and Magnitude

By looking at equation (6.9), it can be seen that the two terms which determine the energy dissipation are $\mathrm{Im}(\tilde{p}'_A p'_B)$ and $|p'_B|^2 - |p'_A|^2$. $\mathrm{Im}(\tilde{p}'_A p'_B)$ will always be dominant, since it is always multiplied by a larger constant, but $|p'_B|^2 - |p'_A|^2$ can be important depending on where along the acoustic standing wave the pressure measurements are made. When measurements are taken straddling the quarter wavelength mark, $|p'_B|^2 - |p'_A|^2$ will be small since the amplitudes at those points are about the same. The phase angles at points straddling the quarter wavelength mark will add together, making $\mathrm{Im}(\tilde{p}'_A p'_B)$ large. On the other hand, $|p'_B|^2 - |p'_A|^2$ can be made more significant by taking measurements on one end of the quarter wavelength point at points which are a large distance apart.

To demonstrate the significance of $\mathrm{Im}(\tilde{p}'_A p'_B)$ and $|p'_B|^2 - |p'_A|^2$, tests were run on the one inch diameter resonator using three different sets of microphone coordinates, D, E, and M, at a mean pressure of 100 psia. The resonator configuration can be seen in Figure 6.2, and Table 6.1 tells which pressure transducers were used at the different points. To check the reliability of the two microphone method, the dissipated energy in the resonator was calculated and measured in the same fashion as described in Section 4.2.3. As explained earlier, the combination of Q_{eff} and Q_{misc} was used in equation (6.10) because of the undetectable effects of the tweeter. Readings from the pressure transducers used in the two microphone setup were separated into real and imaginary

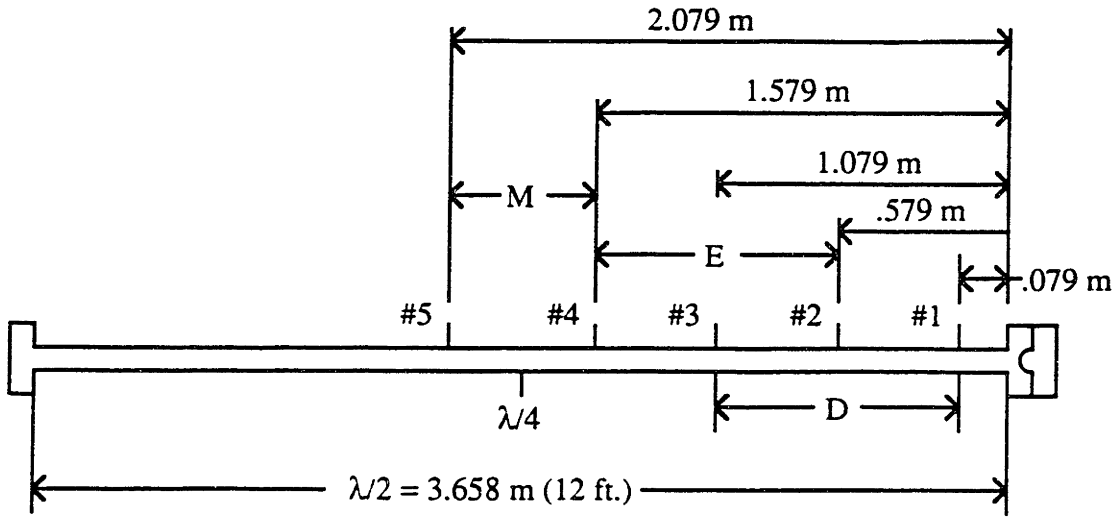

Figure 6-2: Placement of the pressure transducers for the phase angle measurements.

parts by the Lockin Amplifier. For consistency, the imaginary component of the reading from the pressure transducer closest to the nondriven end of the resonator in the two microphone tests will always be set as close as possible to zero. After this measurement was complete, the real and imaginary parts of the reading from the other transducer were recorded, and then the readings from the first were repeated, not setting the imaginary part to zero th time. By setting the imaginary part as close as possible to zero, the phase angle can be known more accurately since the Lockin Amplifier can multiply $\mathrm{Im}(p'(z))$ by 10 or 100 if $\mathrm{Im}(p'(z))$ is small. Two readings from the first pressure transducer were taken because the components from the first transducer could be averaged to gain a more accurate reading with respect to the second transducer, since the phase may have a tendency to drift as the temperature fluctuates. By finding the real and imaginary parts of each signal the phase angle, o, between the two points, the magnitudes at the points, and $|p'_B|^2 - |p'_A|^2$ and $\mathrm{Im}(\tilde{p}'_A p'_B)$ can be determined.

Table 6.1: Pressure Transducer Placement

Position	Pressure Transducer	Set
1	#6754	D
2	#6754	E
3	#6755	D
4	#6755	E, M
5	#7044	M

6.2.4 Internal Loss Measurements

The amount of energy dissipated in an acoustic resonator can be affected by the mean pressure of the working fluid. Much in the same way as changing the radius of the resonator, the Q can be affected because δ_ν and δ_κ vary inversely with mean pressure. So a higher mean pressure results in lower boundary layer thicknesses, higher Q's, and lower ϕ's, making energy dissipation more difficult to measure accurately. On the other hand, when the losses get too high at the lower pressures, the signal to noise ratio will be rather low, also making measurements difficult.

The procedure for these tests was quite simple. Both resonators were used. The one inch resonator was tested at mean pressures of 12, 20, 40, 60, 80, 100, 200, and 300 psia, while the five inch resonator was filled to 12, 20, 40, 60, 80, and 100 psia. Measurements from the two microphones were taken in the same fashion as described in the last section. Once again, the combination of Q_{eff} and Q_{misc} was used to check the energy dissipation measured by the two microphone method.

6.2.5 External Loss Measurements

Measurements of external dissipation were used as a second check of the reliability of the two microphone method. The object of these tests was to insure the accuracy of the measurements of the two microphone method against the measurements described in Chapter 5, and to see if there are any differences between measuring external and

internal energy dissipation.

The procedures for these tests have already been used in the preceding experiments, so there is no need for a detailed description. Again, both resonators were used. Tests using the one inch resonator used mean pressures of 12, 50, and 100 psia, and the tests using the five inch resonator used mean pressures of 12 and 50 psia. Due to differences in the types of needle valves leading to the external loading volume, tests on the one inch resonator were made at valve settings of 1/4, 1/2, and the full open position, while on the five inch resonator the settings were 1/12, 1/6, 1/3, 2/3, and full open. The driver was run so a strong sinusoidal standing wave was produced.

6.3 Experimental Results

The most difficult measurements made in these exercises are the two microphone measurements. The signals at the two points of measurement were difficult to decipher because they were extremely similar and the phase angles between the two points were small. This section states the results of the two microphone tests for measuring internal and external energy dissipation and compares these results to the results yielded from the methods discussed in Chapters 4 and 5. The first topic, however, concerns questions about the phase angles and proper microphone placement.

6.3.1 Phase Angle Measurement Results

The phase angles depend heavily on the placement of the two microphones. The phase angles can be predicted from the formula giving $\dot{E}_{2sen}$, equation (6.9). A high phase angle is desired because large phase angles are easier to measure than small phase differences between points. It becomes obvious after looking at equation (5.9) that the larger phase angles occur when the measurements are made on opposing sides of one quarter wavelength, since the individual angles at each point add due to the change in sign of the angle past the quarter wavelength spot.

Table 6.2: Results from the Phase Angle Measurement Experiment

Position	ϕ_{meas}	ϕ_{theory}	Re(p'_A) (Pa)	Im(p'_A) (Pa)	Re(p'_B) (Pa)	Im(p'_B) (Pa)	$\lvert p'_E \rvert$ (Pa)	$\dot{E}_{2sen}$ (mW)	$\dot{E}_{tot}$ (mW)
D	2.51°	2.94°	213	8.84	122	-0.285	227	0.416	0.449
E	6.85°	6.99°	203	22.9	42.7	-0.309	252	0.409	0.466
M	13.4°	14.4°	41.2	-10.0	-57.3	0.288	251	0.327	0.320

To determine the best locations from which to measure in the following tests, the phase angles from three sets of pressure transducers, D, E, and M, were measured following the procedure outlined earlier. The resulting experimental and theoretical phase angles and power dissipation are shown in Table 6.2, and Figure 6.3 illustrates how the different parts of equation (6.9) were significant (T_o = 22°C). Although agreement between the experimental data and the theoretical data is not perfect, the measurements from the middle set of pressure transducers gave the highest phase angle from both calculations and the most accurate measurement of energy dissipation, and thus were used for the remainder of the study.

6.3.2 Internal Loss Results

The next step in testing the reliability of the two microphone method was to measure internal energy dissipation of both the one inch and five inch diameter resonators. As explained in Section 6.2, a wide range of mean pressures was used to see when the method breaks down. For reference, the dissipated energy was calculated using equation (6.10). The combination of the quality factors, Q_{eff} and Q_{misc} was used since the losses detected by the two microphone method do not account for losses caused by the driver. The results from the tests are given in Table 6.3, and Figures 6.4 and 6.5 show the plots of the dissipated energy vs. mean pressure for both sets of tests (T_o = 20°C). The measured complex pressures from these tests are displayed in Appendix F, Table F.1.

Results from the set of tests on the one inch resonator were excellent, yielding results

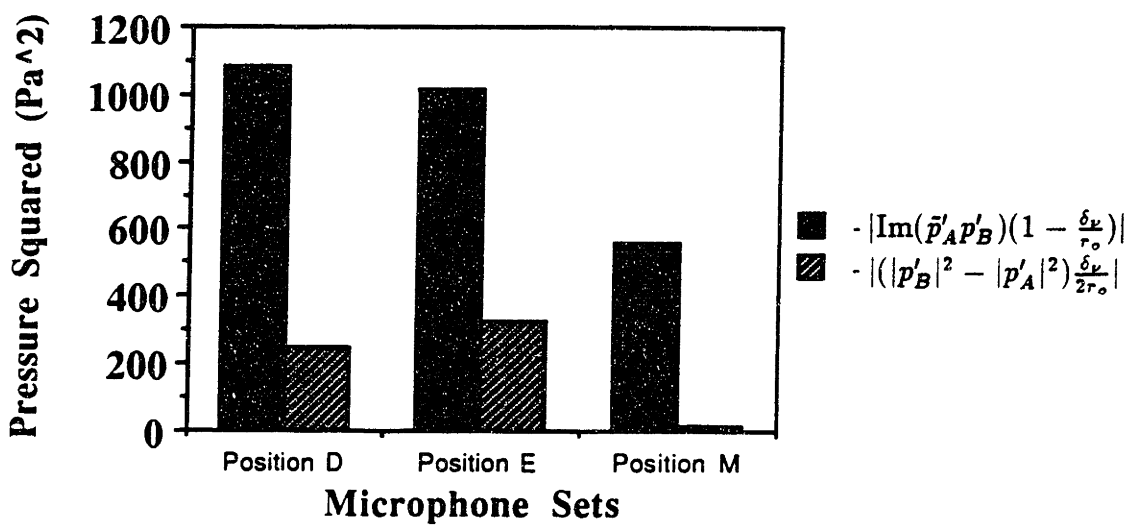

Figure 6-3: Values of the components of equation (6.9) for microphone sets D, E, and M.

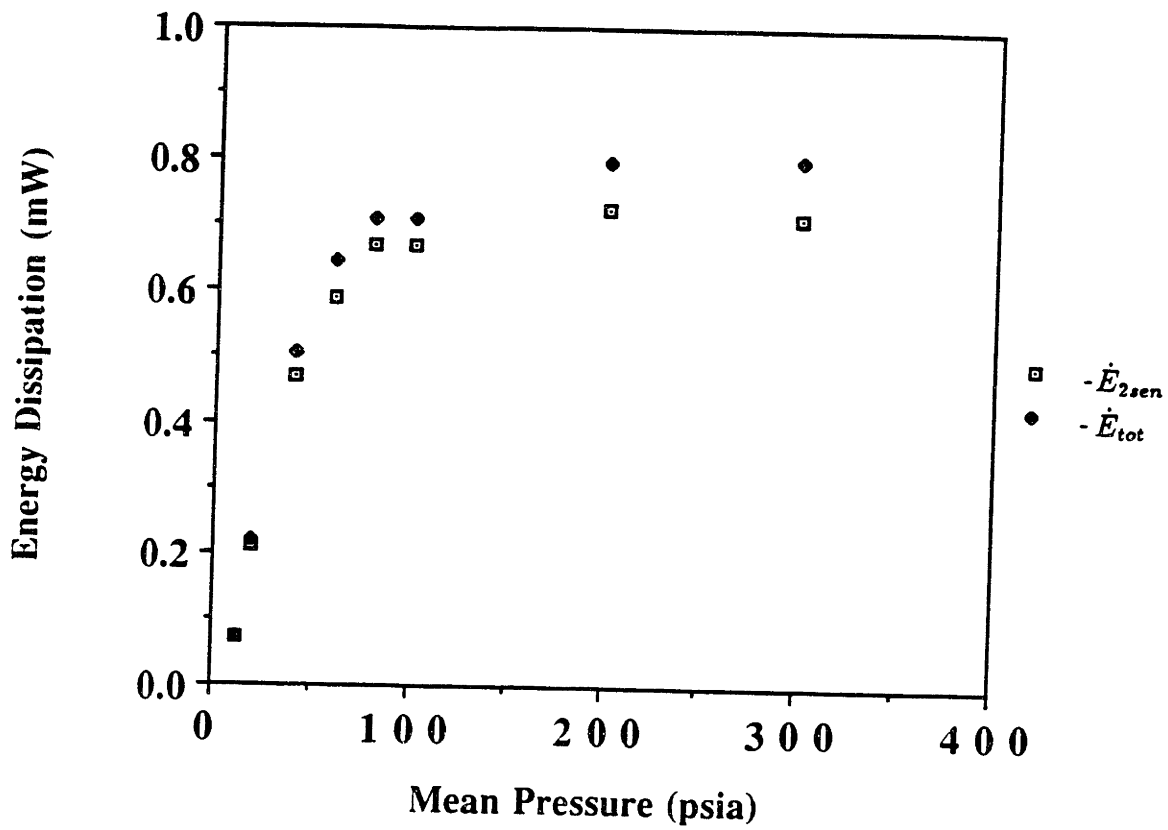

Figure 6-4: Energy dissipation versus mean pressure for two microphone tests on the one inch diameter resonator.

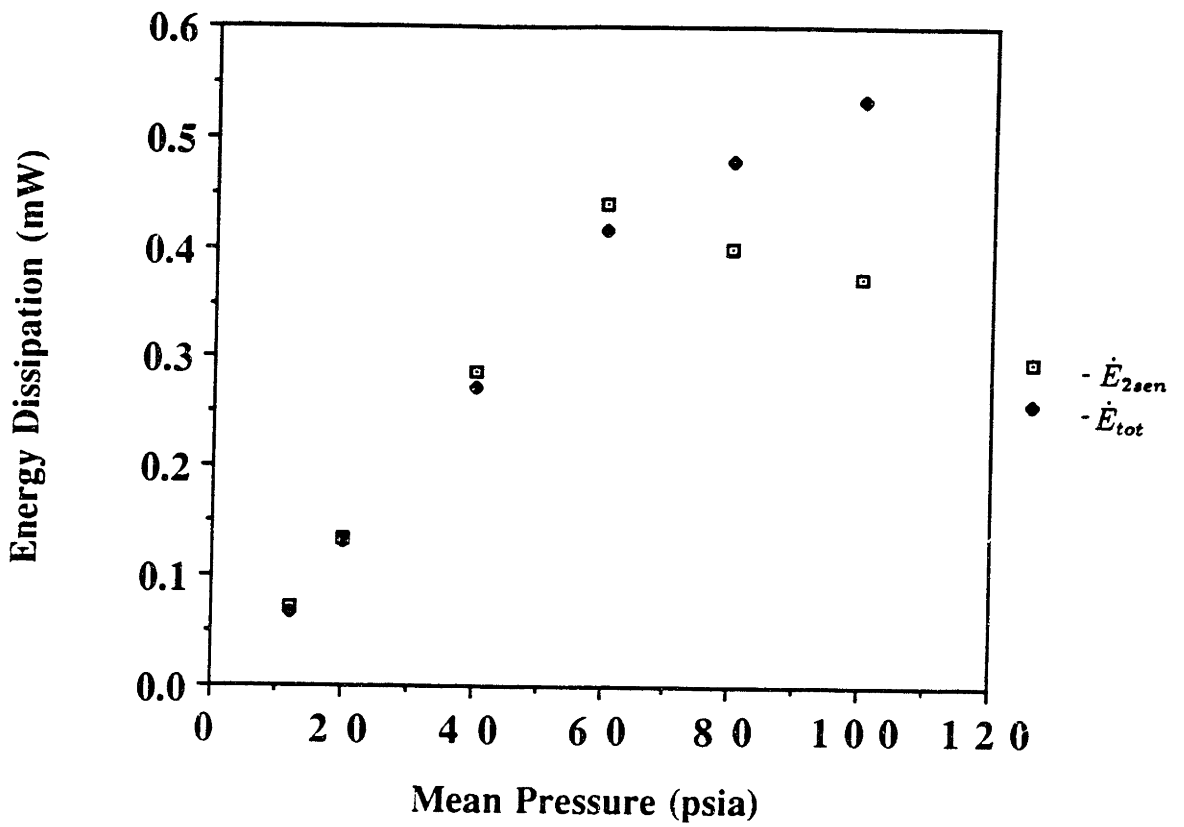

Figure 6-5: Energy dissipation versus mean pressure for two microphone tests on the five inch diameter resonator.

Table 6.3: Results from the Two Microphone Tests at Different Mean Pressures

	1 in. resonator			5 in. resonator		
p_o (psia)	$\dot{E}_{2sen}$ (mW)	$\dot{E}_{tot}$ (mW)	$\lvert p'_E \rvert$ (Pa)	$\dot{E}_{2sen}$ (mW)	$\dot{E}_{tot}$ (mW)	$\lvert p'_E \rvert$ (Pa)
12	0.0728	0.0718	24.6	0.0707	0.0680	7.95
20	0.210	0.218	63.0	0.135	0.131	16.3
40	0.470	0.506	150	0.286	0.272	39.2
60	0.591	0.645	243	0.439	0.417	63.3
80	0.671	0.710	315	0.399	0.479	86.4
100	0.668	0.709	379	0.372	0.533	108
200	0.725	0.796	667	—	—	—
300	0.715	0.801	903	—	—	—

within 10% of $\dot{E}_{tot}$. The measurements made on the five inch resonator were not as good. Reasonably accurate measurements were made up to a mean pressure of 60 psia. The cause for the break down of the two microphone method on the five inch diameter resonator can be attributed to the inability to measure the phase angle, ϕ, accurately due to a high quality factor. The phase angle was difficult to measure because the phase calibrations of the pressure transducers were not constant through a wide range of frequencies due to electrical and mechanical noise in the calibration system. In general, though, the two microphone method performed well in measuring the internal resonator losses.

6.3.3 External Loss Results

For a second test of the two microphone method, measurements were made of energy dissipation caused by a "dummy load" at the nondriven end of the resonator, as well as dissipation caused by internal losses. The values of $\dot{E}_{2sen}$ were compared to the measured values of $\dot{E}_{res} + \dot{W}_{ex}$. The quality factors Q_{eff} and Q_{misc} were used to determine $\dot{E}_{res}$.

Tests were run on both resonators at a variety of aperture settings to the external load and mean pressures, as described in Section 6.2.5. The results from these tests are

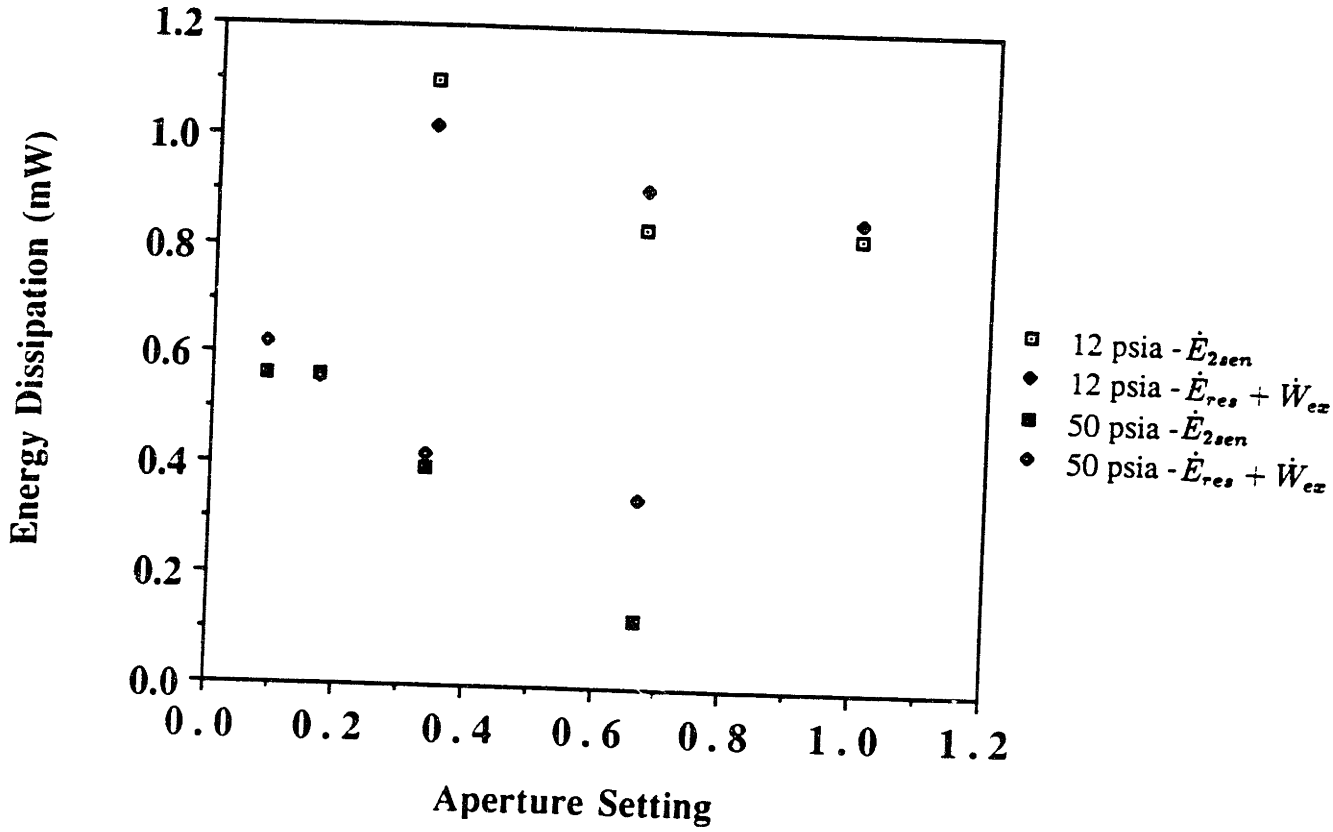

Figure 6-6: Energy dissipation versus mean pressure for different aperture settings using the five inch diameter resonator.

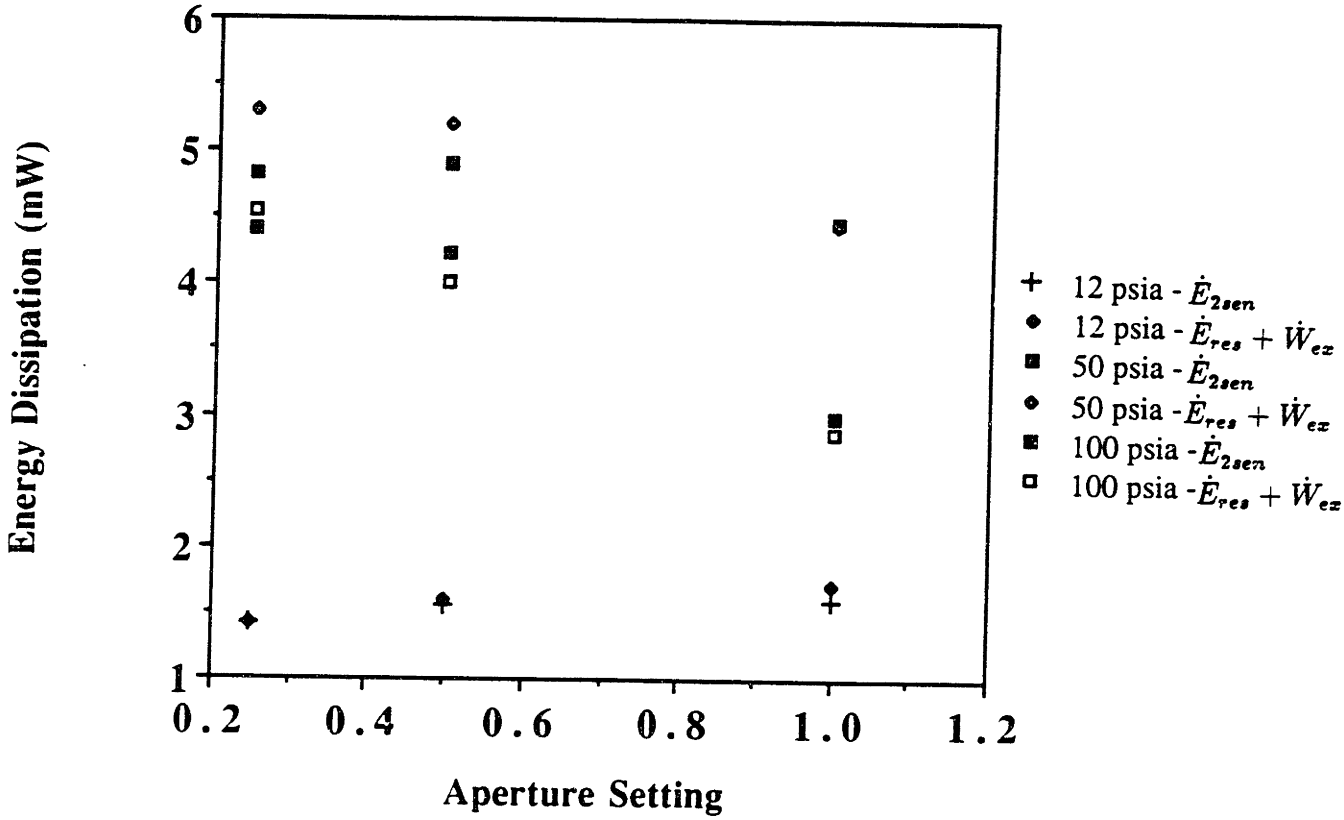

Figure 6-7: Energy dissipation versus mean pressure for different aperture settings using the one inch diameter resonator.

Table 6.4: External Loading Results on Five Inch Resonator (in W)

	valve setting	1/12	1/6	1/3	2/3	full
12 psia	$\dot{E}_{2sen}$	—	—	1.10×10^{-3}	8.37×10^{-4}	8.27×10^{-4}
	$\dot{W}_{ex} + \dot{E}_{res}$	—	—	1.02×10^{-3}	9.06×10^{-4}	8.55×10^{-4}
	$\dot{E}_{res}$	—	—	7.89×10^{-4}	5.21×10^{-4}	4.26×10^{-4}
	$\dot{W}_{ex}$	—	—	2.22×10^{-4}	3.86×10^{-4}	4.29×10^{-4}
50 psia	$\dot{E}_{2sen}$	5.62×10^{-4}	5.66×10^{-4}	3.99×10^{-4}	1.26×10^{-4}	—
	$\dot{W}_{ex} + \dot{E}_{res}$	6.22×10^{-4}	5.57×10^{-4}	4.19×10^{-4}	3.42×10^{-4}	—
	$\dot{E}_{res}$	5.98×10^{-4}	4.73×10^{-4}	2.37×10^{-4}	1.47×10^{-4}	—
	$\dot{W}_{ex}$	2.46×10^{-5}	8.44×10^{-5}	1.82×10^{-4}	1.95×10^{-4}	—

shown in Tables 6.4 and 6.5, and the plots of these results are shown in Figures 6.6 and 6.7 ($T_o = 21°C$). Appendix F shows the measured complex pressures from these tests in Tables F.2 and F.3. Similar to the tests run with no external load in the previous section, tests on the one inch resonator went well, giving agreement between both methods of measurement to within 10% of each other. The two microphone method performed well at low pressures on the five inch resonator, but once again the higher quality factor and the smaller phase angles at the higher pressures made the measurements difficult and inaccurate.

6.4 High Amplitude Tests

The final step in the evaluation of the two microphone method aims to expose the method to conditions identical to those in thermoacoustic engines. The only factor lacking from the previous tests is that the acoustic amplitudes measured are not as large as those found in thermoacoustic engines. This section describes two sets of tests which provide high pressure amplitudes. The first experiment discussed uses a larger speaker as a driver coupled to the one inch diameter resonator, and the second experiment uses an actual thermoacoustic engine.

Table 6.5: External Loading Results from the One Inch Resonator (in W)

	valve setting	1/4	1/2	Full
12 psia	$\dot{E}_{2sen}$	1.41×10^{-3}	1.56×10^{-3}	1.59×10^{-3}
	$\dot{W}_{ex} + \dot{E}_{res}$	1.41×10^{-3}	1.60×10^{-3}	1.72×10^{-3}
	$\dot{W}_{ex}$	6.93×10^{-7}	6.99×10^{-6}	1.34×10^{-4}
	$\dot{E}_{res}$	1.41×10^{-3}	1.59×10^{-3}	1.59×10^{-3}
50 psia	$\dot{E}_{2sen}$	4.82×10^{-3}	4.91×10^{-3}	4.46×10^{-3}
	$\dot{W}_{ex} + \dot{E}_{res}$	5.30×10^{-3}	5.21×10^{-3}	4.45×10^{-3}
	$\dot{W}_{ex}$	1.94×10^{-4}	1.38×10^{-3}	2.69×10^{-3}
	$\dot{E}_{res}$	5.11×10^{-3}	3.82×10^{-3}	1.76×10^{-3}
100 psia	$\dot{E}_{2sen}$	4.41×10^{-3}	4.23×10^{-3}	2.99×10^{-3}
	$\dot{W}_{ex} + \dot{E}_{res}$	4.54×10^{-3}	4.01×10^{-3}	2.87×10^{-3}
	$\dot{W}_{ex}$	1.05×10^{-3}	2.24×10^{-3}	2.24×10^{-3}
	$\dot{E}_{res}$	3.49×10^{-3}	1.77×10^{-3}	6.34×10^{-4}

6.4.1 Measurements with the High Amplitude Speaker

The 4.5 inch diameter speaker, described in Section 3.1, was used to produce an acoustic wave in the one inch diameter resonator. To simulate actual thermoacoustic engine conditions, the mean pressure was kept at 100 psia ($T_o = 18°C$). One set of tests measured only internal energy dissipation, with the valve to the dummy load closed. A second set of tests measured energy dissipation with the needle valve to the load opened half way. For both sets of tests, the speaker was driven by peak inputs of 2.5 V, 4.8 V, and 12.3 V. The pressure amplitudes and phase angles were measured using the Lockin Detector, as described earlier.

The two sets of tests yielded results similar to the results produced by the one inch tweeter. The geometry of the large speaker lowered the quality factor of the resonance, Q_{tot}, to about 7. One by-product of the losses induced by the driver was a lowering of the resonant frequency to 105 Hz. For both sets of tests, $\dot{E}_{2sen}$ matched the quantities predicted by $\dot{E}_{res}$ and $\dot{E}_{res} + \dot{W}_{ex}$ well, using equation (6.10) and Q_{eff} and Q_{misc}. With the maximum input of 12.3 V, the speaker was able to drive the acoustic wave to an amplitude of 5.93 kPa. Table 6.6 shows the results from the high amplitude tests on

Table 6.6: Energy Dissipation Measurements Using the High Amplitude Speaker (in W)

input	valve setting	closed	1/2
2.5 V	f_o	104.53 Hz	104.28 Hz
	$\dot{E}_{res}$	9.04×10^{-3}	6.93×10^{-3}
	$\dot{W}_{ex}$	—	5.89×10^{-3}
	$\dot{W}_{ex} + \dot{E}_{res}$	9.04×10^{-3}	1.28×10^{-2}
	$\dot{E}_{2sen}$	8.78×10^{-3}	1.36×10^{-2}
4.8 V	f_o	104.78 Hz	104.78 Hz
	$\dot{E}_{res}$	3.17×10^{-2}	2.59×10^{-2}
	$\dot{W}_{ex}$	—	1.86×10^{-2}
	$\dot{W}_{ex} + \dot{E}_{res}$	3.17×10^{-2}	4.45×10^{-2}
	$\dot{E}_{2sen}$	3.28×10^{-2}	4.72×10^{-2}
12.3 V	f_o	105.78 Hz	105.78 Hz
	$\dot{E}_{res}$	1.48×10^{-1}	1.28×10^{-1}
	$\dot{W}_{ex}$	—	7.04×10^{-2}
	$\dot{W}_{ex} + \dot{E}_{res}$	1.48×10^{-1}	1.99×10^{-1}
	$\dot{E}_{2sen}$	1.55×10^{-1}	2.19×10^{-1}

the one inch resonator, and Figure 6.8 plots the energy dissipation vs. acoustic pressure amplitude. Table F.4 has the measured complex pressures from the tests.

6.4.2 Measuring Losses in a Thermoacoustic Engine

The final test of the two microphone method involved using a thermoacoustic driver (TAD) on the five inch resonator. Using the TAD required some different experimentation techniques. First, two different pressure transducer mounting holes were made to produce a larger phase angle which could be measured more easily. The coordinates of these holes are shown in Figure 3.4 along with a layout of the entire apparatus. The effects from the heat exchangers in the TAD caused uncontrollable temperature swings in the helium, making phase measurements with the Lockin Detector impossible. As an alternative method of measuring the phase, the Dynamic Signal Analyzer was used. The analyzer could simultaneously measure the amplitudes of two pressure signals and calculate the phase between the two pressure transducers. To get the most accurate readings, the

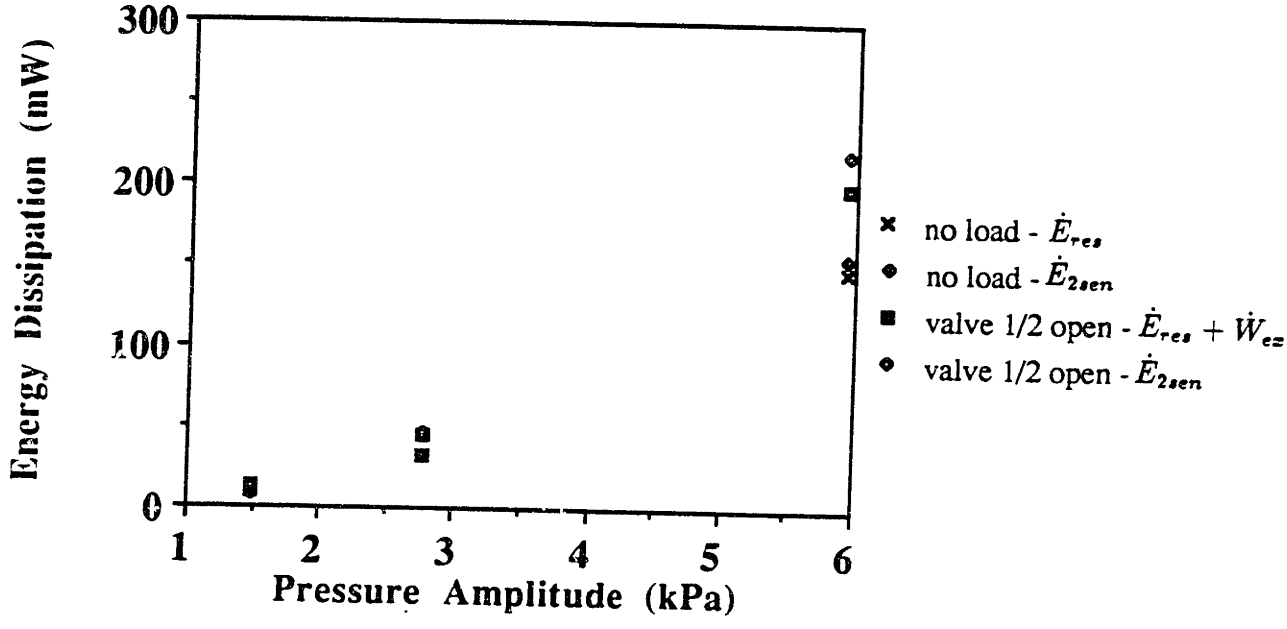

Figure 6-8: Energy dissipation versus acoustic pressure amplitude using the high amplitude speaker.

analyzer was set to average the signals over a period of 50 seconds.

Since only two pressure signals could be processed simultaneously, amplitude and phase drift needed to be accounted for. To compensate, the amplitudes and phases of p'_E and p'_V were read first (or in the case of a closed needle valve, just p'_E was read), then the amplitudes and phases of p'_A and p'_B were read, and once again readings from the end and load were made. Using this method, the dummy load and end readings could be averaged to improve agreement with p'_A and p'_B.

Six sets of tests were run. Three sets measured energy dissipation at $p_o = 100$ psia, while the other three were run at $p_o = 150$ psia. For each mean pressure, measurements were made with the needle valve closed and opened to 1/3 and 2/3 settings. The TAD was driven with several temperature gradients corresponding to heater input voltages of 75 V, 90 V, 100 V, 110 V, 120 V, 130 V, 140 V, and 150 V.

The energy measured by the two microphone method matched $\dot{E}_{res}$ and $\dot{E}_{res} + \dot{W}_{ex}$ well in all cases. All of the methods of measurement were within 10% agreement of each other. The maximum peak pressure amplitude got as high as 8 psi with a 130 V heater input and a mean pressure of 150 psia. The results from these tests are shown in Tables 6.7 through 6.9, and Figures 6.9 and 6.10 show the energy dissipation vs. acoustic pressure amplitude ($T_o = 23°C$). Appendix F shows the measured pressures and phase angles from these tests in Tables F.5 - F.7.

An interesting note about these sets of data is that turbulent conditions existed during all of the tests. According to Merkli and Thomann[11], the Reynold's Number for the flow in resonant tubes can be defined as

$$A_{\mathrm{Re}} = \frac{2v_z}{(\nu\omega)^{1/2}}. \tag{6.13}$$

Merkli and Thomann state that a transition to turbulence occurs at about $A_{\mathrm{Re}} = 300$. In these tests A_{Re} got as high as 670. So, the energy dissipation measured by each of the methods stayed consistent with each other under the turbulent conditions.

To get the ratio of measured external dissipation to measured internal losses higher,

Table 6.7: Energy Dissipation Measurements Using the TAD (in W), $p_o = 100$ psia

Heater Input	valve setting	closed	1/3	2/3
75 V	f_o	118.4 Hz	118.9 Hz	119.2 Hz
	E_{res}	18.3	19.0	21.9
	W_{ex}	—	6.1	10.9
	$W_{ex} + E_{res}$	18.3	25.0	32.8
	E_{2sen}	16.8	25.2	30.3
90 V	f_o	118.8 Hz	119.1 Hz	119.4 Hz
	E_{res}	32.4	27.4	32.5
	W_{ex}	—	8.1	14.8
	$W_{ex} + E_{res}$	32.4	35.5	47.3
	E_{2sen}	30.9	37.4	44.4
100 V	f_o	119.0 Hz	119.3 Hz	119.6 Hz
	E_{res}	37.2	34.8	40.1
	W_{ex}	—	9.7	17.2
	$W_{ex} + E_{res}$	37 2	44.5	57.3
	E_{2sen}	35.7	45.9	54.2
110 V	f_o	119.3 Hz	119.6 Hz	119.9 Hz
	E_{res}	43.2	40.7	49.8
	W_{ex}	—	11.1	20.4
	$W_{ex} + E_{res}$	43.2	51.8	70.2
	E_{2sen}	42.8	53.7	67.5

Table 6.8: Energy Dissipation Measurements Using the TAD (in W), p_o = 100 psia, cont'd

Heater Input	valve setting	closed	1/3	2/3
120 V	f_o	119.6 Hz	119.9 Hz	120.0 Hz
	$\dot{E}_{res}$	49.3	49.0	56.8
	$\dot{W}_{ex}$	—	12.9	22.5
	$\dot{W}_{ex} + \dot{E}_{res}$	49.3	61.9	79.3
	$\dot{E}_{2sen}$	51.1	64.0	75.9
130 V	f_o	120.1 Hz	120.4 Hz	120.3 Hz
	$\dot{E}_{res}$	60.3	58.3	65.3
	$\dot{W}_{ex}$	—	14.8	25.5
	$\dot{W}_{ex} + \dot{E}_{res}$	60.3	73.1	91.8
	$\dot{E}_{2sen}$	62.9	76.0	88.0
140 V	f_o	120.3 Hz	120.7 Hz	120.6 Hz
	$\dot{E}_{res}$	68.7	66.4	75.9
	$\dot{W}_{ex}$	—	15.8	28.3
	$\dot{W}_{ex} + \dot{E}_{res}$	68.7	82.2	104.2
	$\dot{E}_{2sen}$	72.9	87.8	100.9
150 V	f_o	120.6 Hz	121.0 Hz	120.9 Hz
	$\dot{E}_{res}$	77.8	76.2	86.1
	$\dot{W}_{ex}$	—	17.4	30.9
	$\dot{W}_{ex} + \dot{E}_{res}$	77.8	93.6	117.0
	$\dot{E}_{2sen}$	84.5	99.7	116.1

Table 6.9: Energy Dissipation Measurements Using the TAD (in W), p_o = 150 psia

Heater Input	valve setting	closed	1/3	2/3
75 V	f_o	117.9 Hz	118.0 Hz	118.1 Hz
	E_{res}	22.2	21.0	19.2
	W_{ex}	—	7.8	13.1
	$W_{ex} + E_{res}$	22.2	28.8	32.3
	E_{2sen}	20.5	26.7	31.5
90 V	f_o	118.3 Hz	118.4 Hz	118.5 Hz
	E_{res}	33.6	31.0	29.8
	W_{ex}	—	10.6	18.5
	$W_{ex} + E_{res}$	33.6	41.6	48.3
	E_{2sen}	31.5	39.0	44.8
100 V	f_o	118.7 Hz	118.8 Hz	118.9 Hz
	E_{res}	41.9	38.0	38.2
	W_{ex}	—	12.4	22.8
	$W_{ex} + E_{res}$	41.9	50.4	61.0
	E_{2sen}	39.2	45.7	56.7
110 V	f_o	119.0 Hz	119.1 Hz	119.3 Hz
	E_{res}	50.3	47.1	44.8
	W_{ex}	—	14.7	25.1
	$W_{ex} + E_{res}$	50.3	61.7	69.9
	E_{2sen}	46.4	57.4	66.9
120 V	f_o	119.4 Hz	119.5 Hz	119.7 Hz
	E_{res}	59.4	55.2	54.2
	W_{ex}	—	17.0	29.3
	$W_{ex} + E_{res}$	59.4	72.2	83.5
	E_{2sen}	55.2	71.6	78.8
130 V	f_o	119.7 Hz	119.8 Hz	119.9 Hz
	E_{res}	71.3	66.5	64.7
	W_{ex}	—	19.9	34.7
	$W_{ex} + E_{res}$	71.3	86.4	99.4
	E_{2sen}	67.5	82.6	94.1

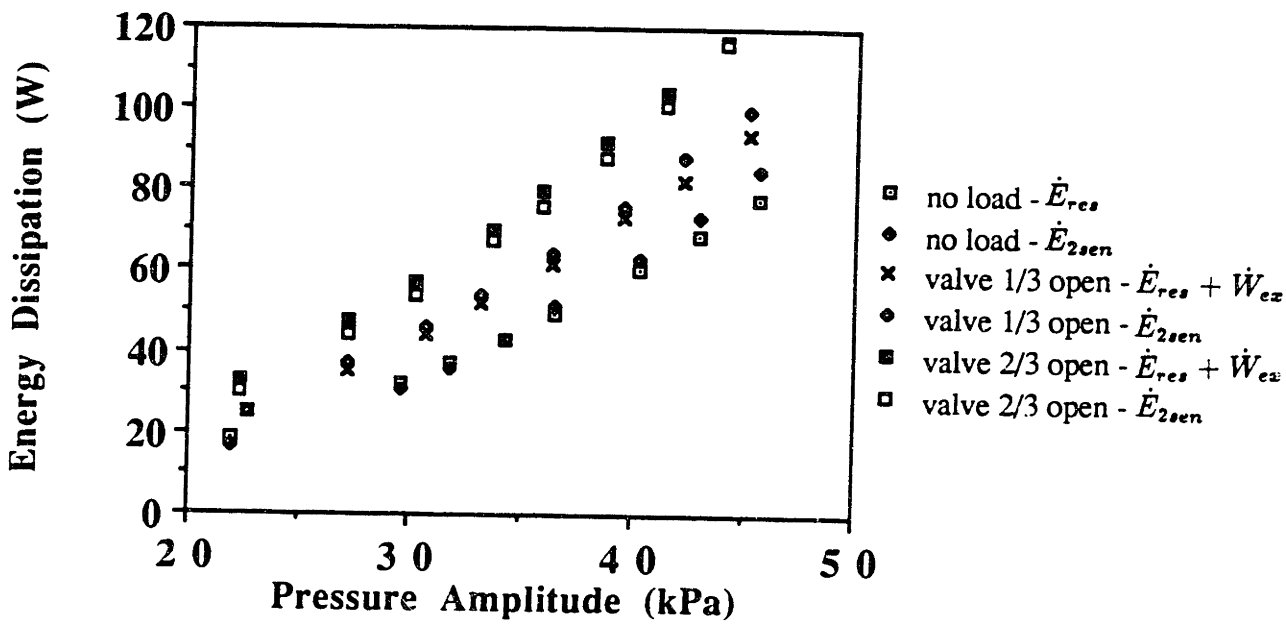

Figure 6-9: Energy dissipation versus acoustic pressure amplitude for the TAD, with a mean pressure of 100 psia.

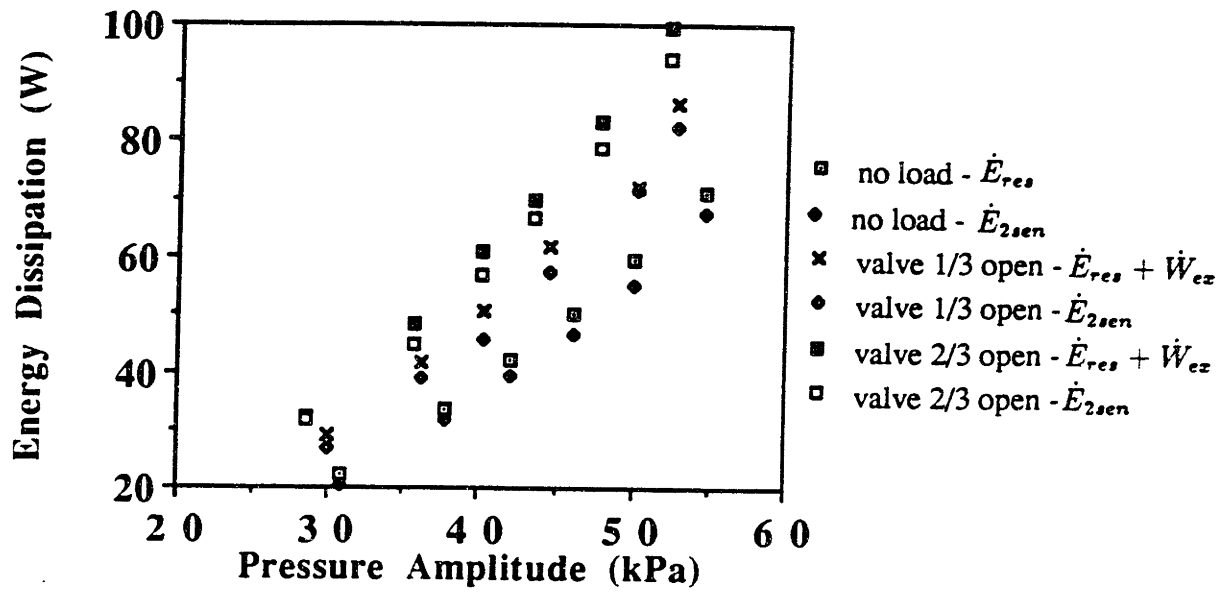

Figure 6-10: Energy dissipation versus acoustic pressure amplitude for the TAD, with a mean pressure of 150 psia.

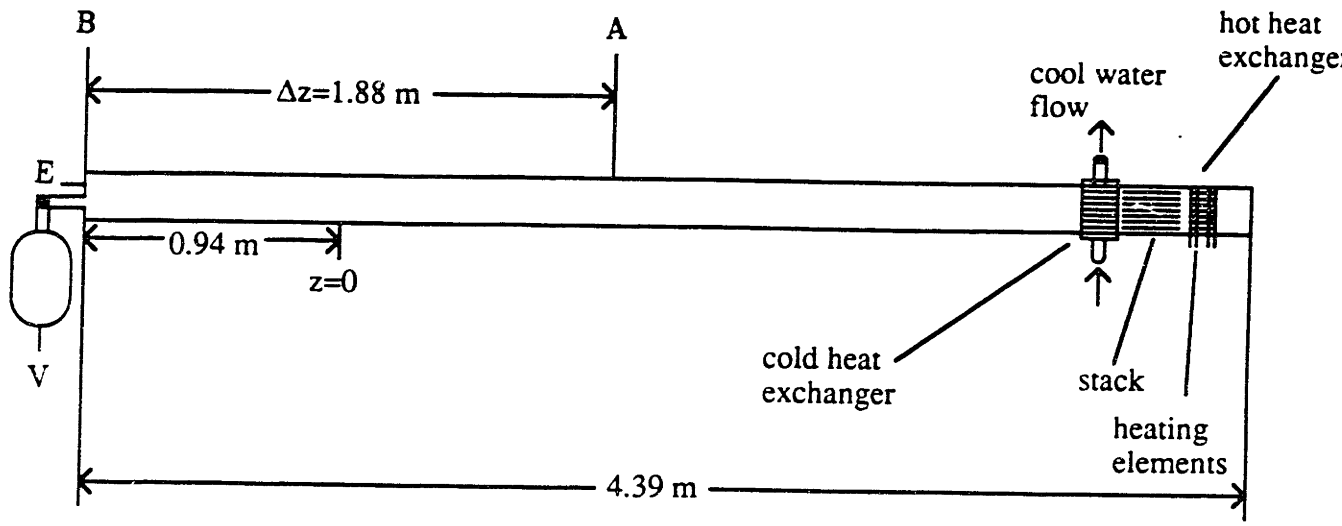

Figure 6-11: The two microphone configuration for external load enhancement.

another set of data was taken at a mean pressure of 150 psia ($T_o = 22°C$). This time the needle valve to the dummy load was fully opened, and points A and B used in the two microphone method were changed, as shown in Figure 6.11. As shown, point B occurs at the same spot where p'_E is measured, so measurements for p'_E were used to calculate $\dot{E}_{2sen}$, $\dot{W}_{ex}$, and $\dot{E}_{res}$. The data was recorded using the Dynamic Signal Analyzer, as before, and the inputs to the heaters were 90 V, 100 V, 110 V, 120 V, 130 V, and 140 V.

The results from this set of tests showed agreement between $\dot{E}_{res} + \dot{W}_{ex}$ and $\dot{E}_{2sen}$ to within 9%. With the new microphone placements and the valve to the volume fully opened, $\dot{W}_{ex}$ constituted about 72% of the total measured losses, demonstrating that $\dot{E}_{2sen}$ agrees as well with $\dot{W}_{ex}$ as with $\dot{E}_{res}$. The results from this set of data are given in Table 6.10, and Figure 6.12 plots the energy dissipation vs. pressure amplitude. Table F.8 contains the measured pressures and phases.

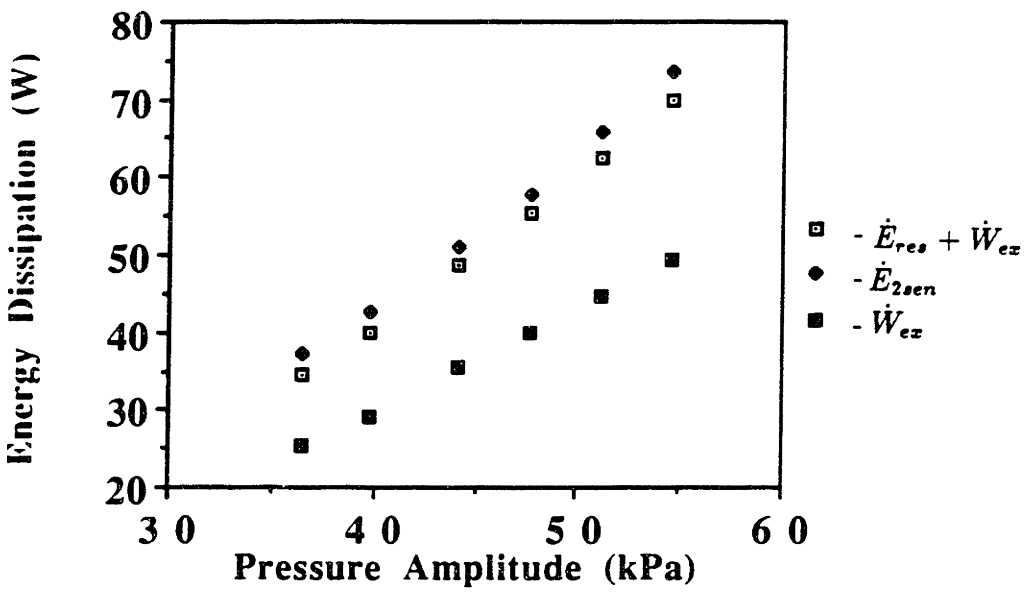

Figure 6-12: Energy dissipation versus acoustic pressure amplitude for the TAD, with measured external losses dominating.

Table 6.10: Energy Dissipation Measurements with External Load Enhancement (in W)

Heater Input			Heater Input		
90 V	f_o	118.9 Hz	120 V	f_o	119.5 Hz
	$\bar{E}_{res}$	9.0		$\bar{E}_{res}$	15.5
	$\bar{W}_{ex}$	25.4		$\bar{W}_{ex}$	40.0
	$\bar{W}_{ex} + \bar{E}_{res}$	34.4		$\bar{W}_{ex} + \bar{E}_{res}$	55.5
	$\bar{E}_{2sen}$	37.3		$\bar{E}_{2sen}$	57.9
100 V	f_o	119.1 Hz	130 V	f_o	119.7 Hz
	$\bar{E}_{res}$	10.7		$\bar{E}_{res}$	17.9
	$\bar{W}_{ex}$	29.1		$\bar{W}_{ex}$	44.6
	$\bar{W}_{ex} + \bar{E}_{res}$	39.8		$\bar{W}_{ex} + \bar{E}_{res}$	62.5
	$\bar{E}_{2sen}$	42.7		$\bar{E}_{2sen}$	66.0
110 V	f_o	119.2 Hz	110 V	f_o	119.9 Hz
	$\bar{E}_{res}$	13.3		$\bar{E}_{res}$	20.4
	$\bar{W}_{ex}$	35.4		$\bar{W}_{ex}$	49.4
	$\bar{W}_{ex} + \bar{E}_{res}$	48.7		$\bar{W}_{ex} + \bar{E}_{res}$	69.8
	$\bar{E}_{2sen}$	50.9		$\bar{E}_{2sen}$	73.5

Chapter 7

Conclusions and Suggestions

The progression of the experiments in this study began with the examination of the sources of internal energy dissipation, expanded into simulating and measuring external loading, and culminated in the testing of the two microphone method of measuring both internal and external energy losses. Predicting the proper internal losses through the calculation of the quality factor proved essential in knowing what losses were relevant to the two microphone method. The two microphone method was also subjected to different loading situations, a variety of mean pressures, and a wide range of peak pressure amplitudes.

7.1 Summary

Chapter 4 described the major factors involved in internal energy dissipation. As expected, viscous and thermal effects played a major role in energy dissipation, depending on mean pressure and resonator size. The most important discoveries in Chapter 4 which pertain to the two microphone method dealt with substantial losses caused by the drivers and geometric irregularities in the resonators. The losses caused by the drivers were quite substantial, and these effects must be omitted from any energy dissipation comparison to the two microphone method since the effects of the drivers were not detectable with the

two microphone method. On the other hand, the energy dissipation caused by geometric irregularities can be responsible for up to 5% of the internal resonator losses, so they must be considered.

Modeling external loads was discussed in Chapter 5. The method of measuring losses in the dummy load proved to be easy and quite reliable, through comparison to measuring Q_{tot} and $\dot{E}_{tot}$. While the empty volumes provided losses which were easy to measure, the only drawback to the simulations was that the external loads only got as high as 40% larger than the internal losses, and even appeared to be insignificant compared to $\dot{E}_{res}$ in some instances. The simulated load did, however, provide significant losses in most cases, which aided in the tests of the two microphone method.

Chapter 6 combined the methods of measurement and simulation developed in Chapters 4 and 5, and compared them to measurements produced by the two microphone method. While a large majority of the comparisons fell within 10% of each other, the two microphone method appeared to have some limitations at the low pressure amplitudes. At high Q resonances, as losses diminished, the measurement procedures and the instrumentation hampered measurements because of a lack of resolution and the time required to make a pressure measurement on the Lockin Detector at point A and switch to the signal at point B to make a measurement there. The phase angle was particularly difficult to capture, especially in the five inch resonator. Drifting phase angles due to temperature fluctuations over the time period required for the measurements (averaging about five minutes each) and small phase angles caused these difficulties. In most of the low amplitude cases, though, relatively large phase angles were obtained, through design.

Conditions similar to actual thermoacoustic engines were reached, and the measurements made by the two microphone method under these conditions appeared to be reliable. One reason why the higher amplitude tests were successful was because the phase angle between the points, A and B, was increased by changing the pressure transducer placement. Also, a more accurate method of measuring the phase was discovered through the use of the Dynamic Signal Analyzer. Since the analyzer measured the two complex

signals simultaneously, the phase angles could be pinpointed since there was no time lapse in between the measurement of the two signals. The results from Section 6.4 demonstrate that the two microphone method can accurately measure internal and total energy dissipation in thermoacoustic engines.

7.2 Suggestions

Further testing of the two microphone method in standing wave resonators still needs to be conducted, especially in the areas of loading and larger amounts of energy dissipation. Larger external to internal load ratios need to be tested to simulate actual operating conditions. External loading measurements must move into actual loading situations, such as refrigerators or generators, where the two microphone method can be compared to some measured or predicted dissipation of the load. The magnitude of the total energy dissipation must be increased also. A study of the method should be made in the kilowatt and possibly the megawatt range. Questions to be addressed when dealing with such large amounts of dissipation deal with the method's accuracy when extreme nonlinearities and turbulent conditions in the boundary layers are present.

As far as optimizing the two microphone method, a few things should be done. Measuring the phase difference between measurement points poses the biggest problem. The problem can be treated in a few ways. Proper pressure transducer placement helps to increase the angle, as was done in Section 6.3.1. More sensitive pressure transducers could help, especially if the transducers have tuned phase agreement with each other, and their internal phase shift remains small and constant through a broad range of frequencies. Since mechanical and electrical noise is a problem in the phase calibrations of the pressure transducers, a better way of calibrating the phase is needed, which reduces system noise. Simultaneous readings of the complex pressure amplitudes also improve the accuracy of the measurements, as was done in Section 6.4. Since the magnitudes of p'_A and p'_B are relatively easy to capture, an accurate phase measurement should make

the method extremely reliable.

Appendix A

Calculation of Dissipative Volume Size

The volume of the external load, or "dummy load", can be determined with accuracy by using order of magnitude, thermodynamic relations. The object is to pick a volume that is not too large, where external losses will dominate, while being sure the pressure variations in the volume are large enough to read accurately.

To start with, a thermodynamic relation for the oscillating pressure is used,

$$V = \frac{p_o \gamma \Delta V}{p'_V}, \tag{A.1}$$

where ΔV is the volume of the gas that enters the dummy load in a cycle, and p'_V is the pressure amplitude in the volume. By setting the pressure in the volume, $p'_V = 0.1 p'_E$ (where p'_E is the pressure amplitude of the acoustic wave at the nondriven end of the resonator), the signal in the volume can be easily measured, while keeping the dissipated energy in a reasonable range. The volume of the gas entering the bottle can be determined by knowing the work required to move it,

$$\dot{W} = \omega p'_E \Delta V, \tag{A.2}$$

The energy dissipation rate, $\dot{W}$, can be estimated by equating the work required to move ΔV in and out of the load to be about the same as the energy dissipated by the resonator. The resulting volume of the dummy load turns out to be

$$V = \frac{10\gamma p_o \dot{W}}{\omega (p'_E)^2}. \tag{A.3}$$

For the five inch diameter resonator, the following estimations were made: $p_o = 50$ psia, $\gamma = 1.67$, $\dot{W} = 10^{-3}$ W, and $p'_E = 150$ Pa. The estimated volume was 1860 cc, so a 1500 cc volume was deemed close enough to yield the desired results from the tests.

The following estimations were made for the one inch diameter resonator: $p_o = 50$ psia, $\gamma = 1.67$, $\dot{W} = 10^{-4}$ W, and $p'_E = 200$ Pa. The resulting volume estimated was 104 cc, so a 75 cc volume was used, due to a limited selection, but it was close enough to give reasonable results.

Appendix B

Pressure Transducer Calibration

B.1 Pressure Transducers

To assure accurate pressure readings, the pressure transducers must be calibrated. Relative differences in magnitude and phase need to be included in all calculations. Described in this appendix is the method used to determine any difference in sensitivity and phase, and the results from the calibration procedure.

The transducers used in all of the experiments were PCB Piezotronics, Inc. model #102A05, serial #6599, #6600, #6754, #6755, and #7044. This particular model is a general purpose, high frequency pressure transducer. The specifications are given in Table B.1.

B.2 Sensitivity Calibrations

To measure the relative sensitivities of the transducers, two types of measurements were made. First, a qualitative measurement was made by exposing a set of pressure transducers to the same acoustic wave at the same location. Using the five inch resonator, an acoustic wave was produced in atmospheric air. A coupling block coupled four transducers and was located at the end of the resonator. The magnitudes generated by each of

Table B.1: Specifications for PCB Model #102A05 Pressure Transducers

RANGE (5 V OUTPUT)	psi	100
USEFUL OVERRANGE	psi	200
MAXIMUM PRESSURE	psi	1000
RESOLUTION	psi	.002
SENSITIVITY	mV/psi	50 $\pm$10
RESONANT FREQUENCY	kHz	250
RISE TIME	μSec	2
DISCHARGE TIME CONST (2)	Sec	$\geq$1
LOW FREQ RESPONSE -5%	Hz	.50
LINEARITY (1)	% FS	1
POLARITY		POSITIVE
OUTPUT IMPEDANCE	ohm	<100
OUTPUT BIAS	-volt	8 to 14
OVERLOAD RECOVERY	μSec	10
ACCELERATION SENS	psi/G	.002
TEMP COEFFICIENT	%/^{o}F	$\leq$.03
TEMPERATURE RANGE	^{o}F	-100 to +275
MAXIMUM FLASH TEMP	^{o}F	3000
VIBRATION/SHOCK	G's peak	2000/20000
SEALING		EPOXY
CASE/DIAPHRAGM MAT'L		17-4/INVAR
WEIGHT	gm	11
CONNECTOR (micro)	coaxial	10-32
EXCITATION	-VDC/mA	24-27/2-20

(2) AT ROOM TEMPERATURE

(1) ZERO BASED BEST STRAIGHT LINE.

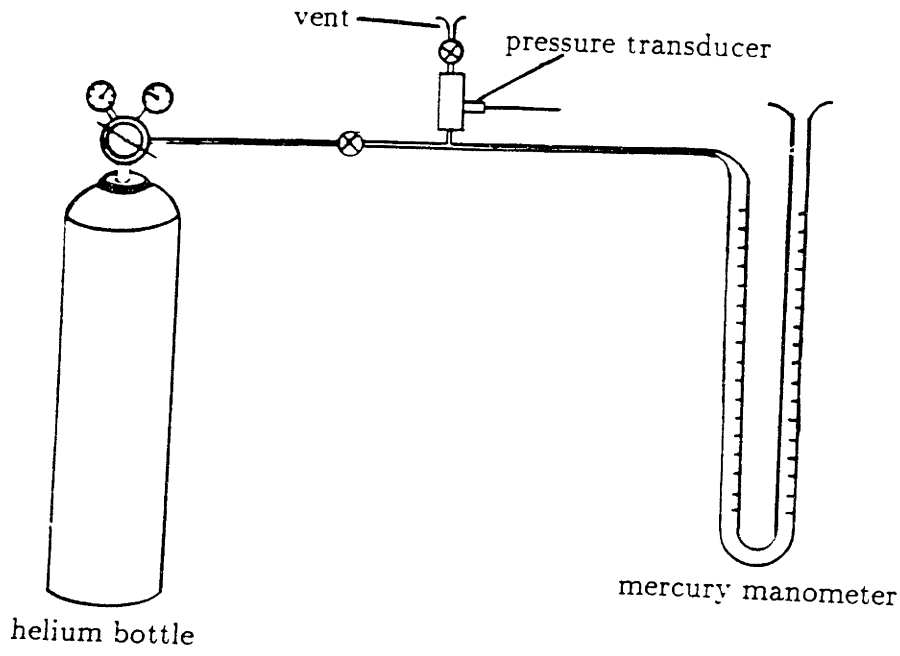

Figure B-1: Quantitative calibration configuration.

the transducers were then recorded by the Lockin Amplifier for acoustic waves driven at several amplitudes.

The pressure transducer exhibiting a high sensitivity with a reasonable amount of consistency was chosen for reference, to be used in the quantitative calibration. This transducer was #6755. The quantitative calibration involved pressurizing a tube coupling the transducer to a mercury manometer (shown in Figure B.1). After pressurization, the system was vented rapidly to atmospheric pressure, and the voltage drop from the transducer was compared to the pressure drop measured by the manometer. The results from the quantitative calibration are shown in Table B.2. The resulting sensitivity for #6755 was 49.1 mV/psi. The data from the qualitative calibration and resulting

Table B.2: Quantitative Calibration Results

PCB	#6755
Δh (cm Hg)	60.0
Δp (psi)	11.6
ΔV (mV)	568
S ($\frac{\text{mV}}{\text{psi}}$)	49.1

Table B.3: Qualitative Calibration Results and Sensitivities

		Calculated Sensitivity (mV/psi)			
Trial #	p' (psi) re: #6755	$S_{\#6754}$	$S_{\#6600}$	$S_{\#6599}$	$S_{\#7044}$
1	0.0097	48.5	45.7	43.9	49.1
2	0.0224	48.4	45.8	44.0	49.3
3	0.0375	48.6	45.9	44.0	49.2
4	0.0529	48.4	46.0	44.1	49.1
avg.		48.5	45.9	44.0	49.2

sensitivities are shown in Table B.3.

B.3 Phase Calibrations

Calibrating the phases of the pressure transducers is crucial to the measurements of resonator losses, since a discrepancy of one tenth of a degree in phase can offset the experimental results considerably. To check the relative phase angles in the pressure transducers, the same multiple transducer coupler used in the qualitative sensitivity calibration was used. Performing the phase calibration using the five inch diameter resonator posed a problem because of uncontrollable temperature shifts in the gas in the resonator.

To imitate actual testing conditions, helium was used, and the system was driven at 138 Hz. In the following calculations the change in phase angle with respect to the

change in temperature is found. The speed of sound in the helium is

$$a^2 = \frac{\gamma RT}{M}, \tag{B.1}$$

where R is the gas constant and M is the molecular weight, which can be related to the resonant frequency of the resonator

$$f \propto \sqrt{\frac{\gamma RT}{M}}. \tag{B.2}$$

Now a differential relation can be made,

$$\frac{df}{f} = \frac{1}{2}\frac{dT}{T}. \tag{B.3}$$

Through the chain rule $\frac{d\phi}{dT}$ can be found,

$$\frac{d\phi}{dT} = \frac{d\phi}{df}\frac{df}{dT} = \frac{180°Q}{f_o}\left(\frac{1}{2}\right)\frac{f_o}{T_o} = \frac{90°Q}{T_o}. \tag{B.4}$$

Since Q can get as high as 150 and $T_o \simeq 300K$, the phase dependence on temperature, $\frac{d\phi}{dt}$, can be as high as 45° per Kelvin. Not only did the temperature dependence ruin the phase calibrations in the five inch resonator, but the fluctuating temperature made the two microphone measurements difficult too.

To solve the temperature problem, the driver was bolted directly to the end plate, serving the purpose of making the phase calibration. Once again the driver was run at several amplitudes, at 138 Hz (which is the resonant frequency under normal conditions). To measure the phase, the signals from the transducers were separated into real and imaginary parts using the Lockin Amplifier. A phase angle measured by each transducer could be found by

$$\phi = \tan^{-1}\left(\frac{\mathrm{Im}(p')}{\mathrm{Re}(p')}\right). \tag{B.5}$$

The phase angles were then compared, and relative phase differences between the pressure

Table B.4: Phase Calibration Results

Phase Relation	ϕ_{12}
$\phi_{\#6599} = \phi_{12} + \phi_{\#6600}$	0.52^o
$\phi_{\#7044} = \phi_{12} + \phi_{\#6755}$	0.08^o
$\phi_{\#6754} = \phi_{12} + \phi_{\#6755}$	0.11^o

transducers could be found. The results of the phase calibrations are given in Table B.4. System noise (electrical and mechanical) in the manufacturer's calibrations and the calibrations discussed here limited the phase calibrations to only two digits.

Appendix C

Helium Properties

The values for ρ were obtained from the ideal gas law, and the values for a were derived from a combination of the ideal gas law and thermodynamic relations. The dynamic viscosity, μ, and the thermal conductivity, K, were calculated from the following expressions,

$$\mu = (5.131 \times 10^{-7}) \times T^{0.6441} \text{kg/ms}, \tag{C.1}$$

and

$$K = (4.4 \times 10^{-3}) \times T^{0.618} \text{W/mK}. \tag{C.2}$$

The remaining quantities are either constant in the relevant ranges or can be calculated from the other quantities. The constant quantities through the relevant temperature and pressure ranges are: $\gamma = 1.67$, $\text{Pr} = 0.703$, and $c_p = 5200 \frac{J}{kgK}$.

Table C.1: $T_o = 290$ K $(17°C)$, $f = 138$ Hz

$p_o[psi]$	12	20	40	50	60	80	100	200	300
$\rho[\frac{kg}{m^3}]$	0.137	0.229	0.458	0.572	0.686	0.915	1.144	2.288	3.432
$\delta_\nu[mm]$	0.576	0.447	0.311	0.282	0.258	0.223	0.200	0.141	0.115
$\delta_\kappa[mm]$	0.687	0.533	0.377	0.337	0.307	0.266	0.238	0.168	0.137

Table C.2: $T_o = 295$ K $(22°C)$, $f = 138$ Hz

$p_o[psi]$	12	20	40	50	60	80	100	200	300
$\rho[\frac{kg}{m^3}]$	0.135	0.225	0.450	0.562	0.675	0.900	1.125	2.249	3.374
$\delta_\nu[mm]$	0.585	0.453	0.320	0.286	0.261	0.226	0.203	0.143	0.117
$\delta_\kappa[mm]$	0.697	0.540	0.382	0.341	0.312	0.270	0.241	0.171	0.139

Table C.3: $T_o = 300$ K $(27°C)$, $f = 138$ Hz

$p_o[psi]$	12	20	40	50	60	80	100	200	300
$\rho[\frac{kg}{m^3}]$	0.133	0.221	0.442	0.553	0.664	0.885	1.106	2.212	3.318
$\delta_\nu[mm]$	0.593	0.459	0.325	0.290	0.265	0.230	0.205	0.145	0.119
$\delta_\kappa[mm]$	0.707	0.547	0.387	0.346	0.316	0.274	0.245	0.173	0.141

Table C.4: Quantities Constant in the Given Pressure Ranges ($f = 138$ Hz)

$T_o[K]$	290	295	300
$\mu \times 10^{-5}[\frac{kg}{ms}]$	1.98	2.00	2.02
$k[\frac{W}{mK}]$	0.1463	0.1478	0.1494
$a[\frac{m}{s}]$	1002.3	1011.0	1019.5

Appendix D

Power Spectrum Curves

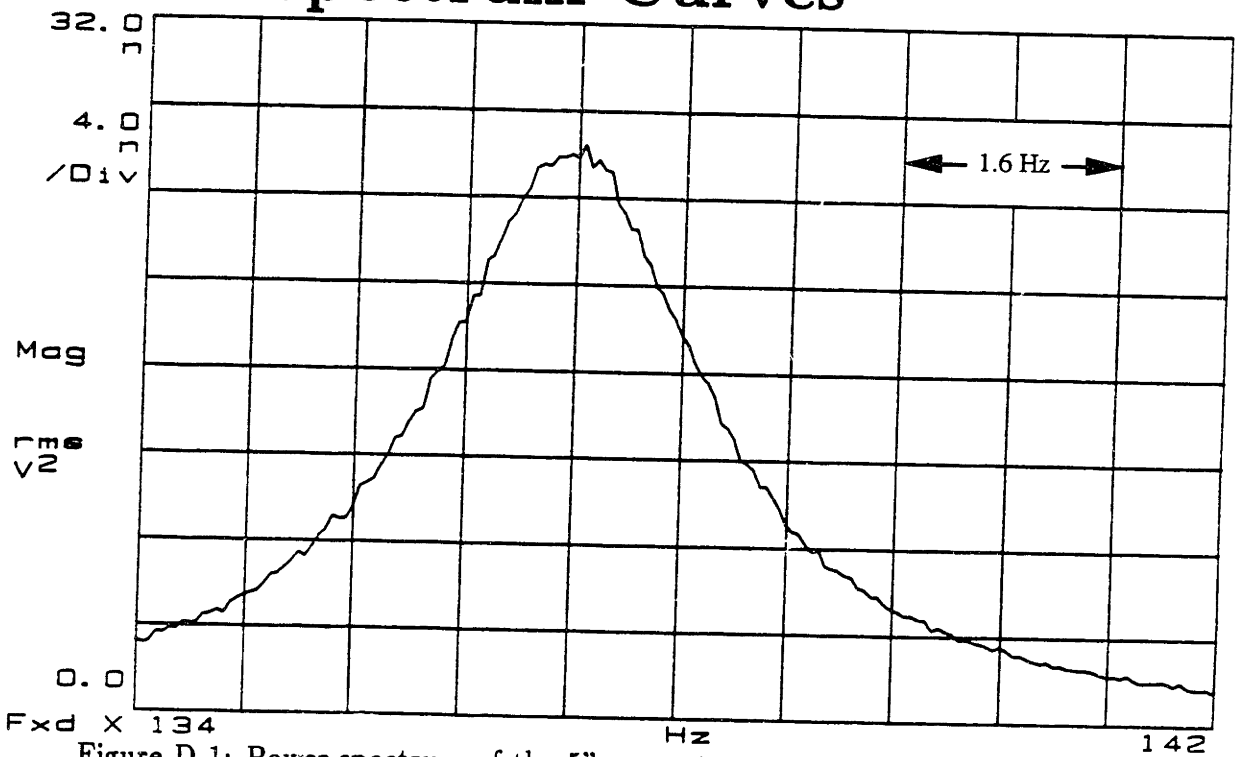

Figure D-1: Power spectrum of the 5" resonator at a mean pressure of 12 psia.

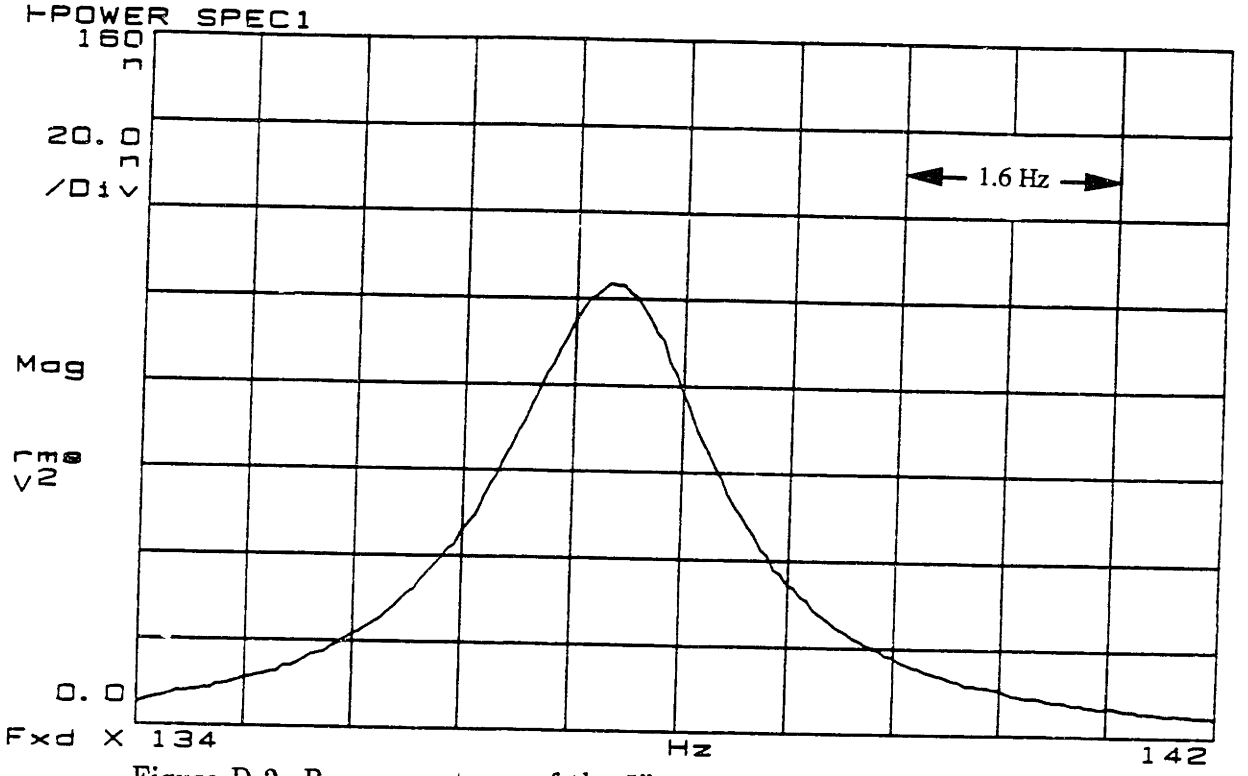

Figure D-2: Power spectrum of the 5" resonator at a mean pressure of 20 psia.

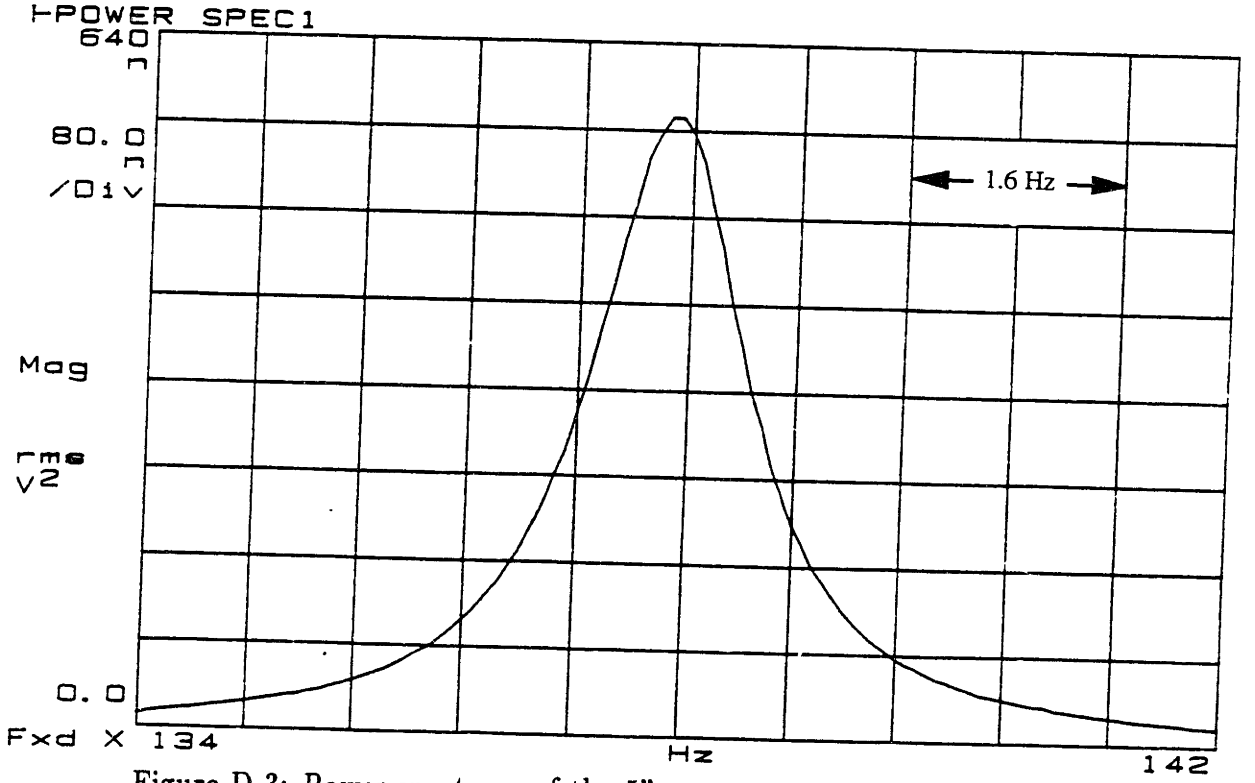

Figure D-3: Power spectrum of the 5" resonator at a mean pressure of 40 psia.

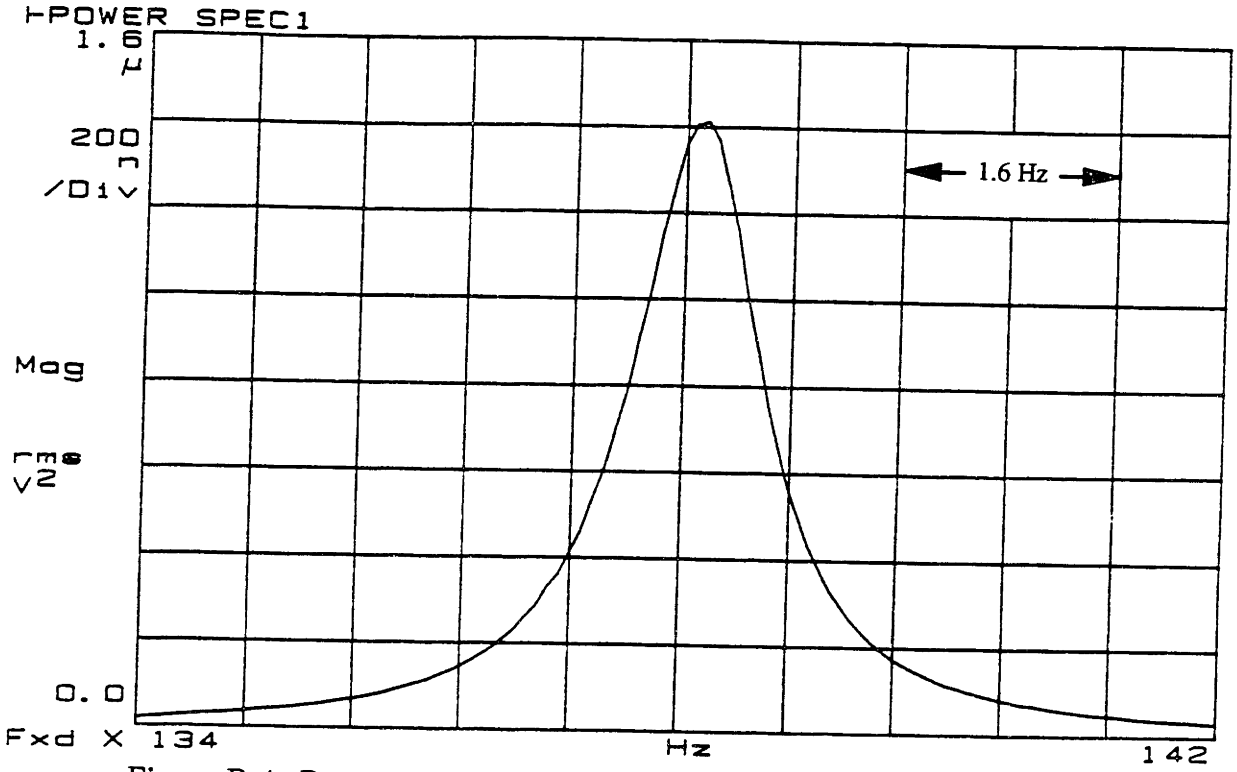

Figure D-4: Power spectrum of the 5" resonator at a mean pressure of 60 psia.

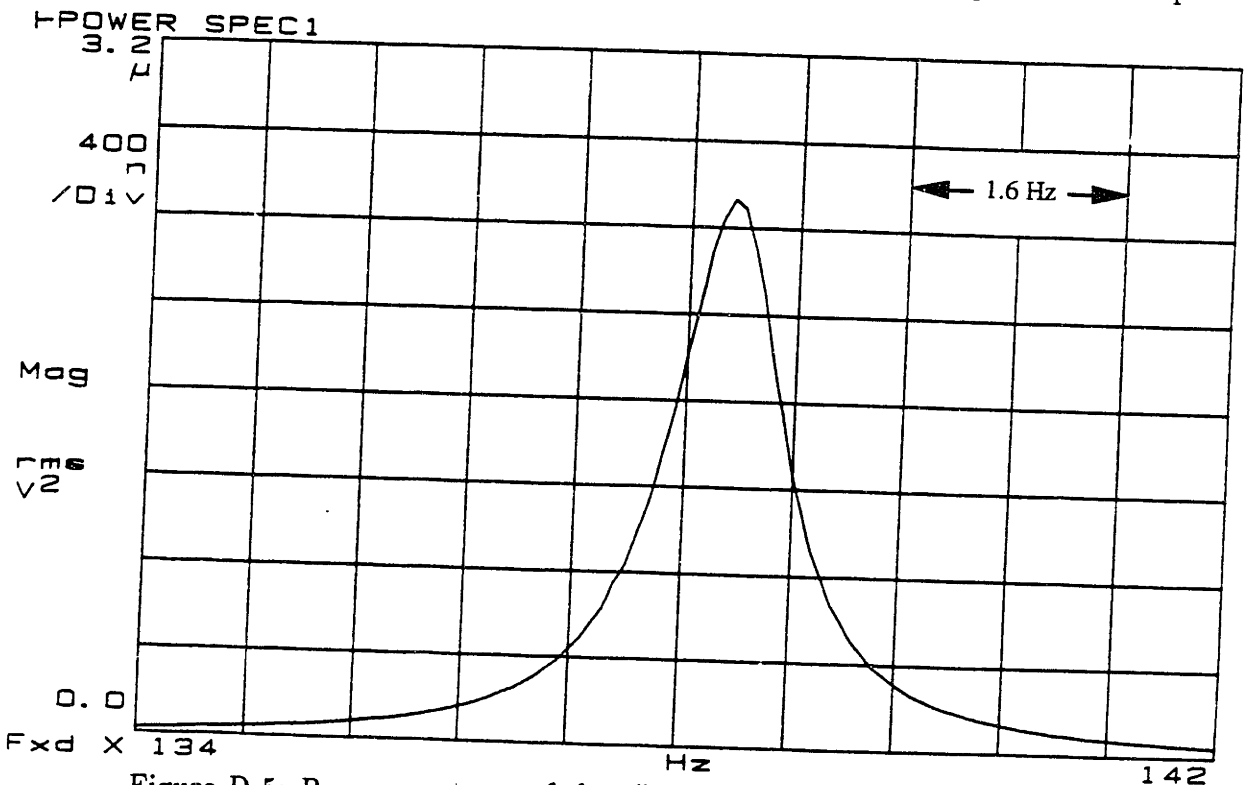

Figure D-5: Power spectrum of the 5" resonator at a mean pressure of 80 psia.

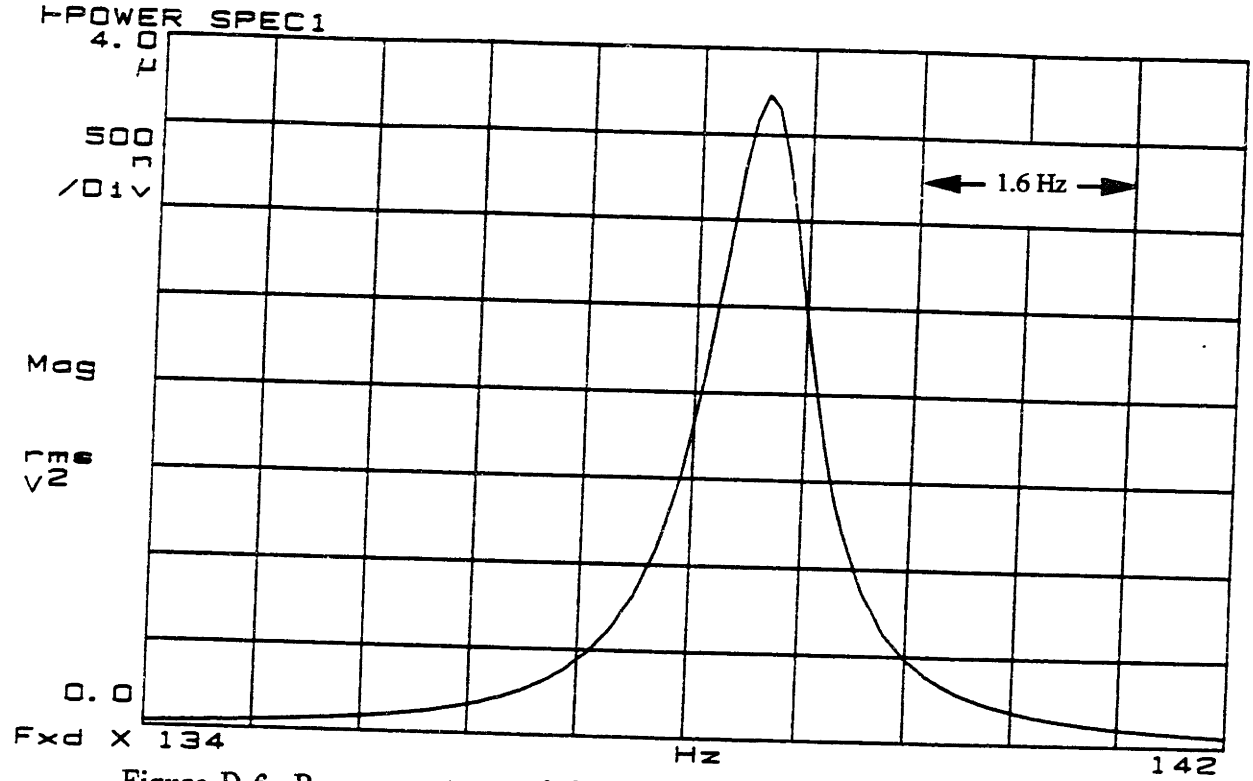

Figure D-6: Power spectrum of the 5" resonator at a mean pressure of 100 psia.

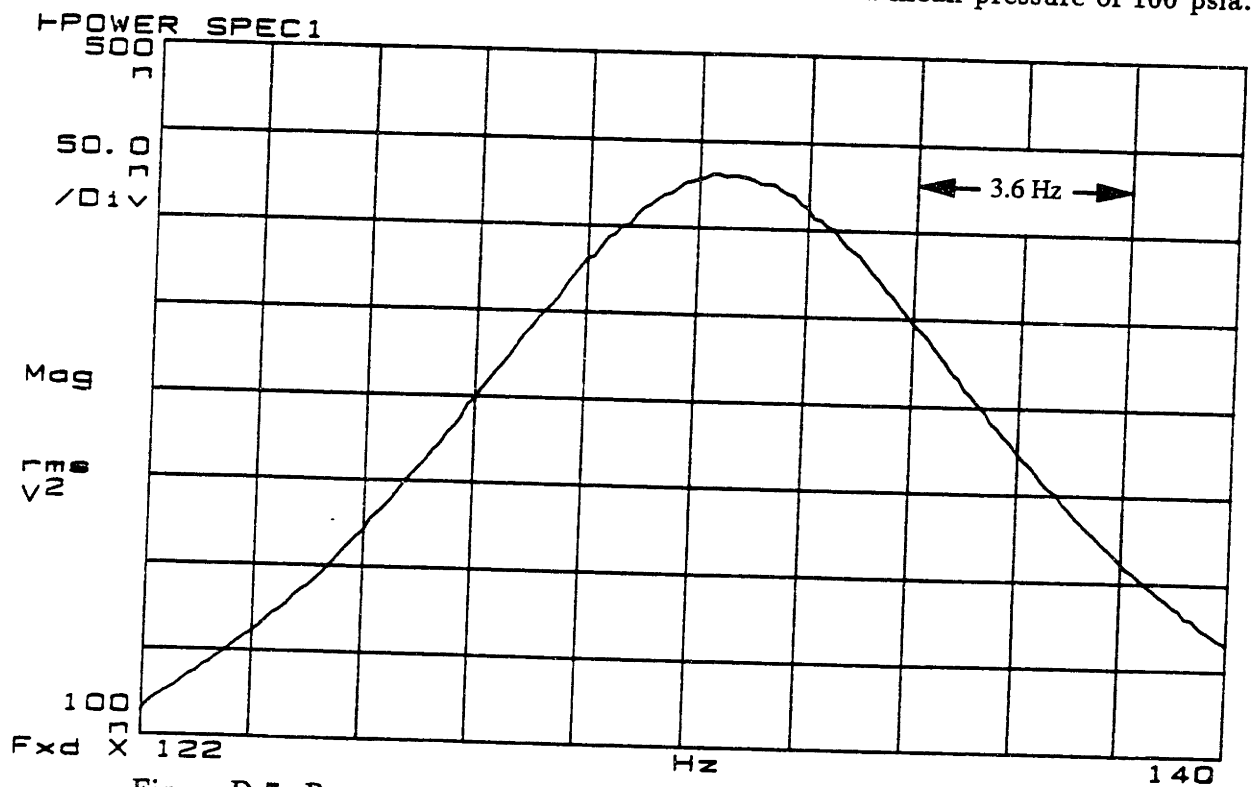

Figure D-7: Power spectrum of the 1" resonator at a mean pressure of 12 psia.

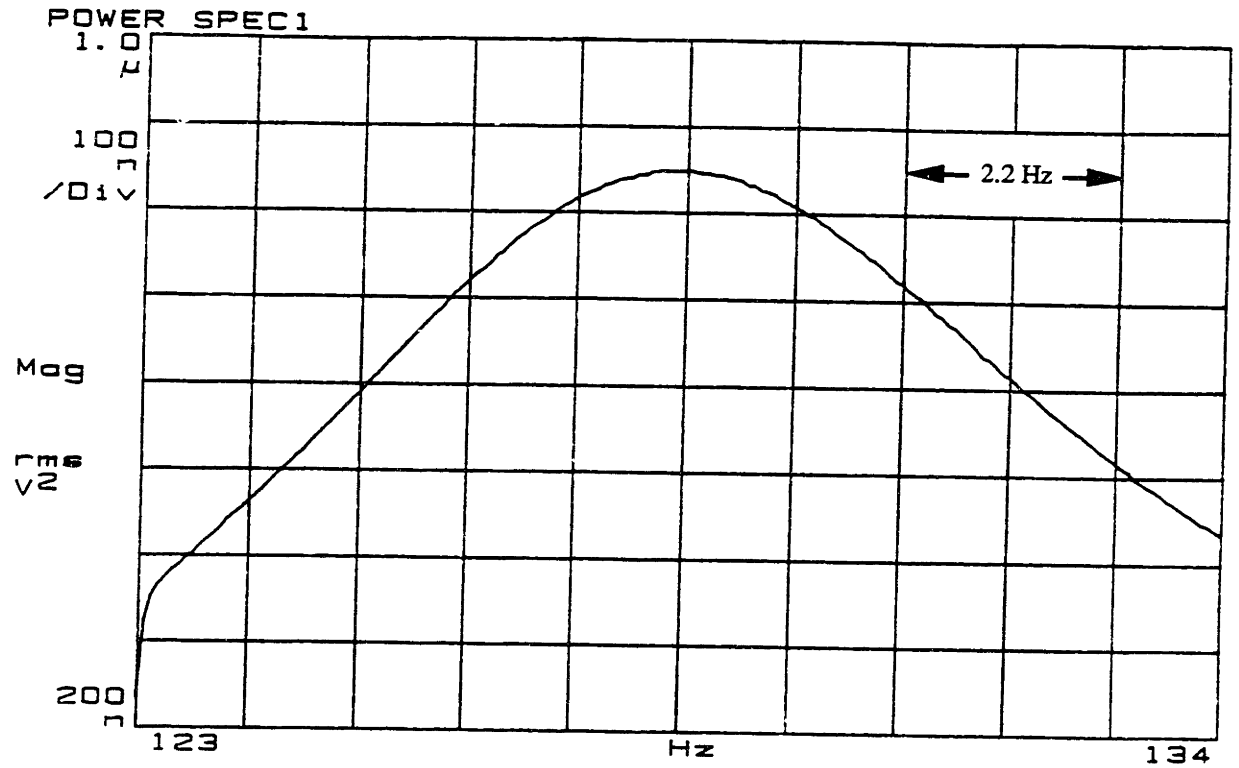

Figure D-8: Power spectrum of the 1" resonator at a mean pressure of 20 psia.

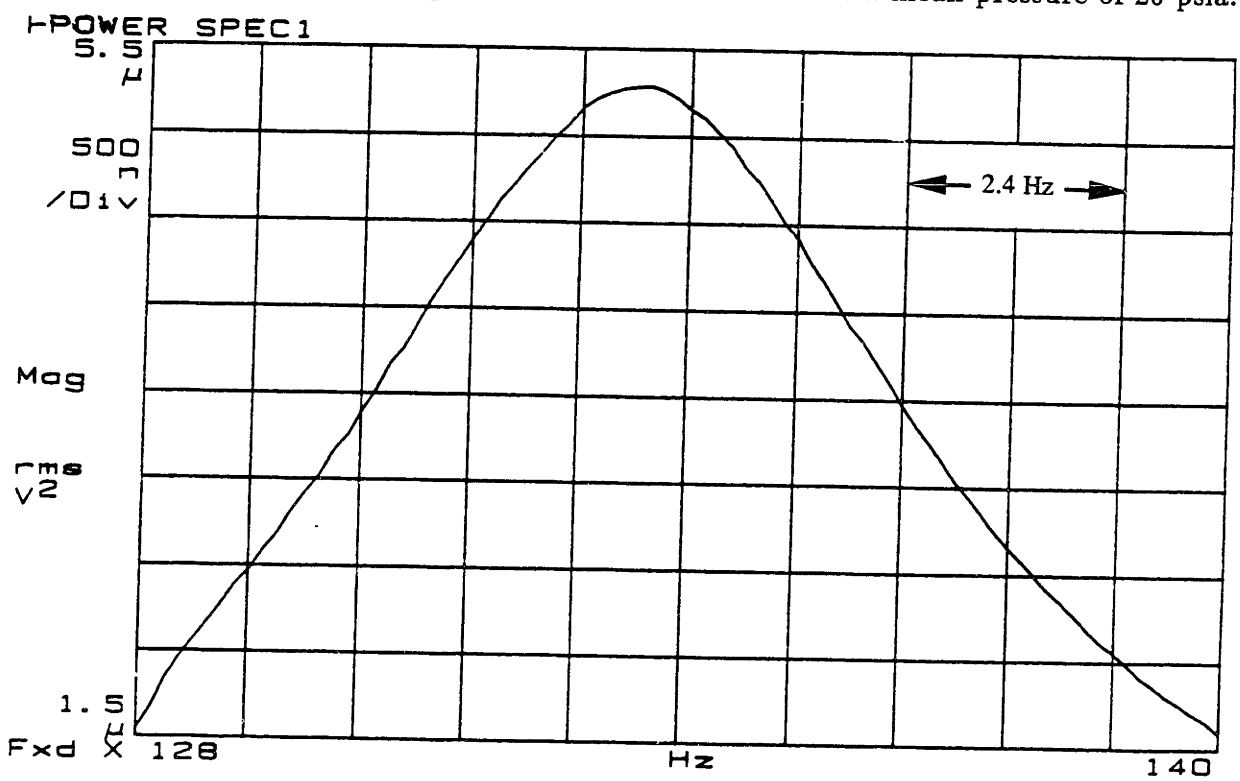

Figure D-9: Power spectrum of the 1" resonator at a mean pressure of 40 psia.

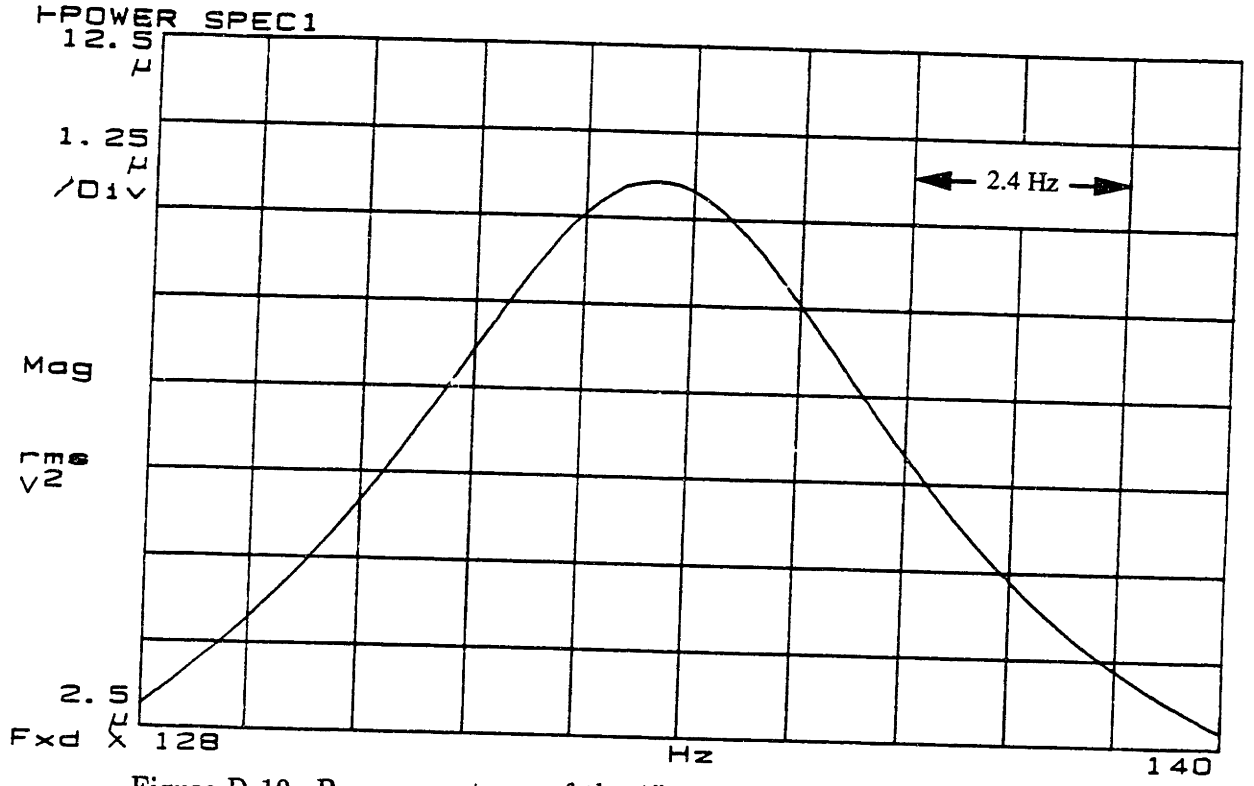

Figure D-10: Power spectrum of the 1" resonator at a mean pressure of 60 psia.

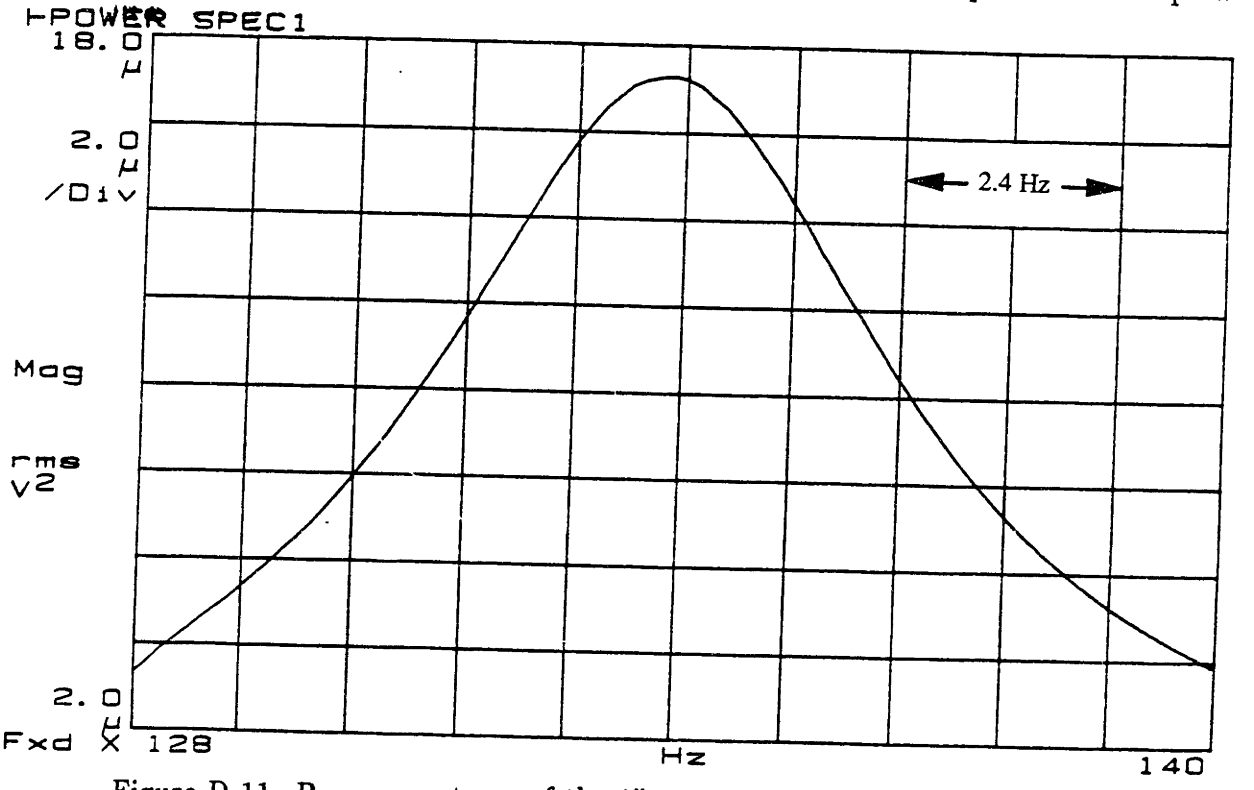

Figure D-11: Power spectrum of the 1" resonator at a mean pressure of 80 psia.

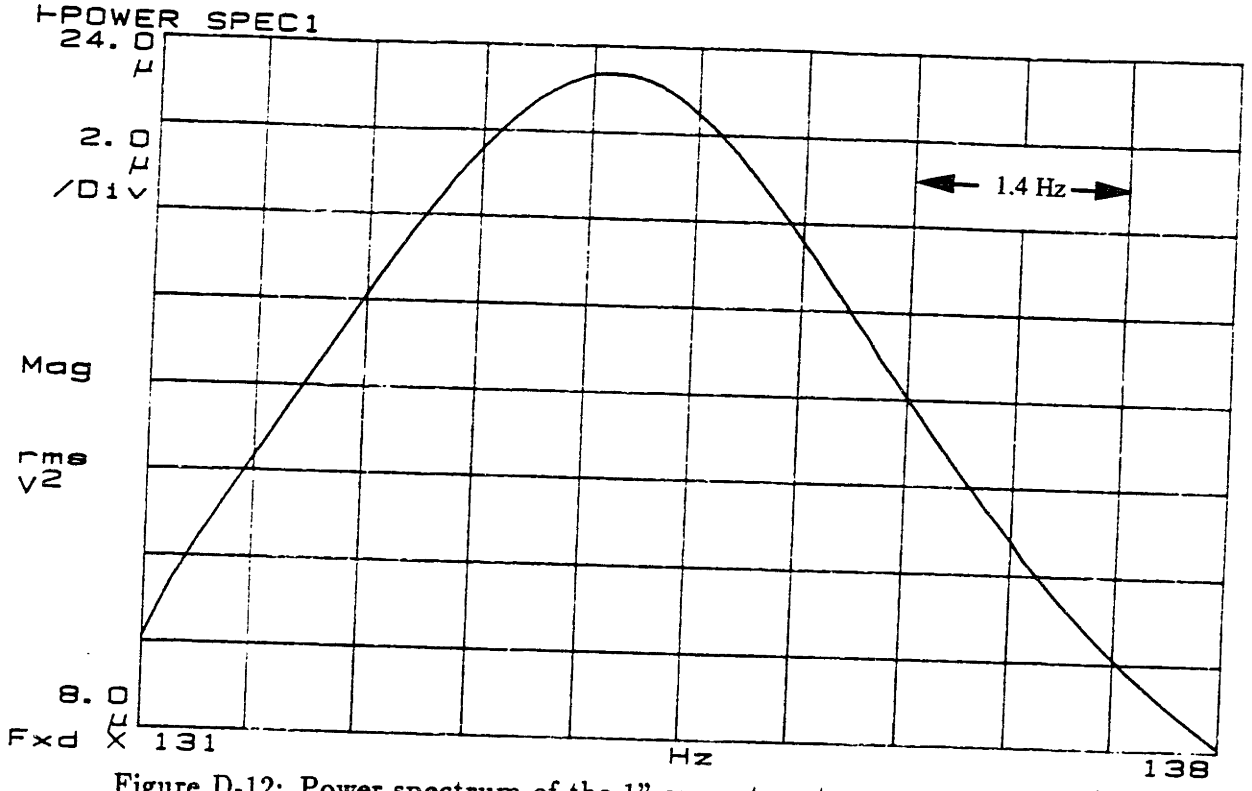

Figure D-12: Power spectrum of the 1" resonator at a mean pressure of 100 psia.

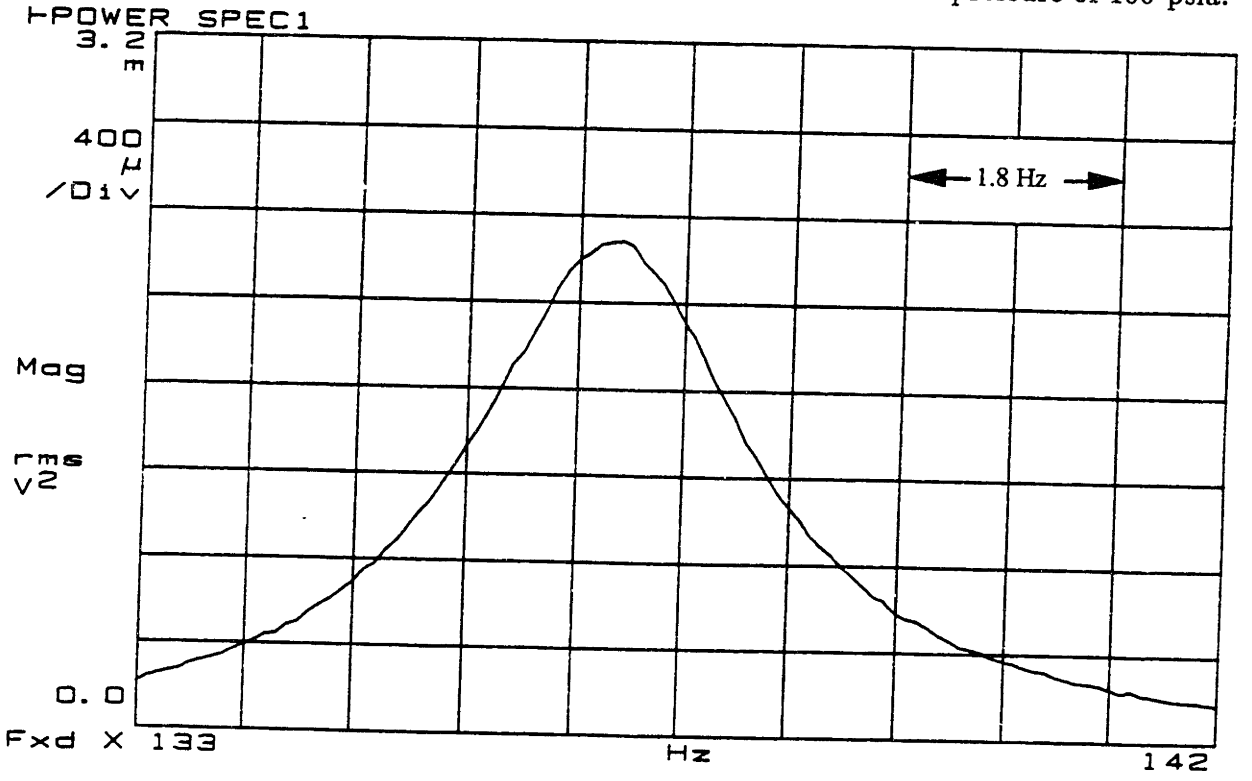

Figure D-13: Power spectrum of the 5" resonator at a mean pressure of 12 psia and an aperture setting of 1/3 to the external load.

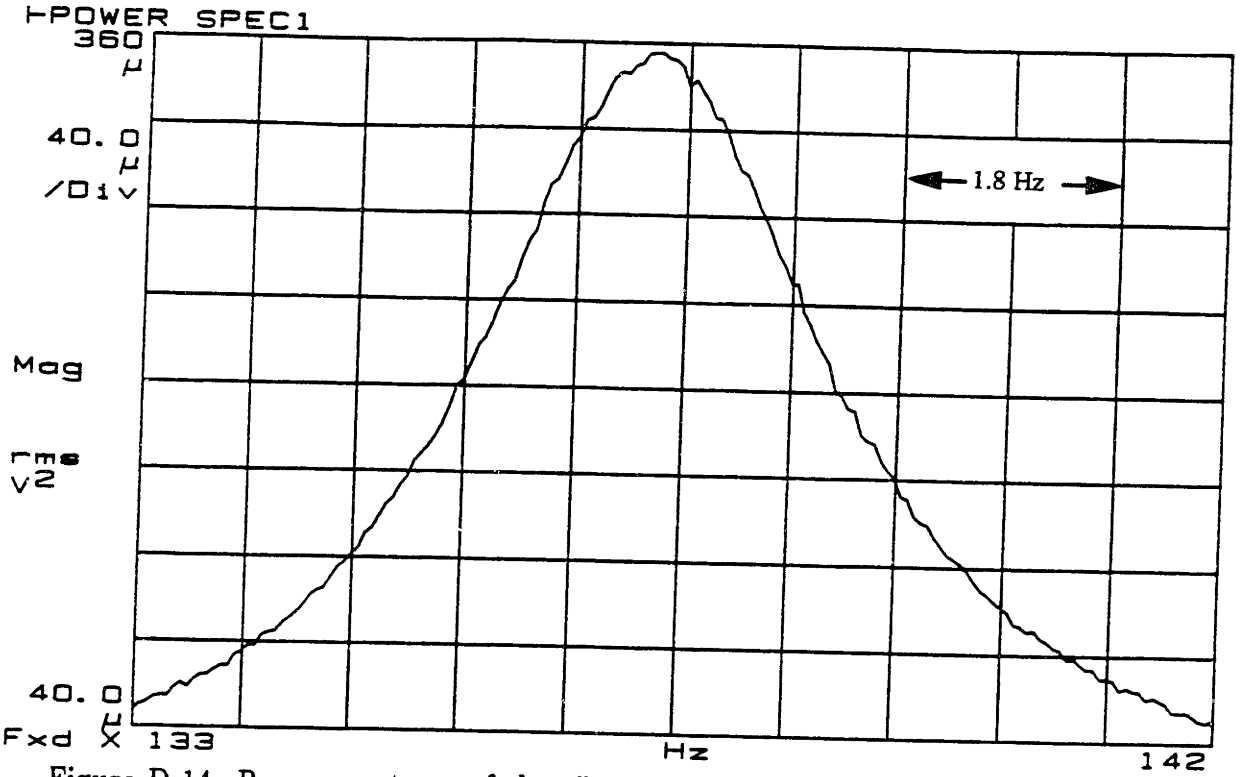

Figure D-14: Power spectrum of the 5" resonator at a mean pressure of 12 psia and an aperture setting of 2/3 to the external load.

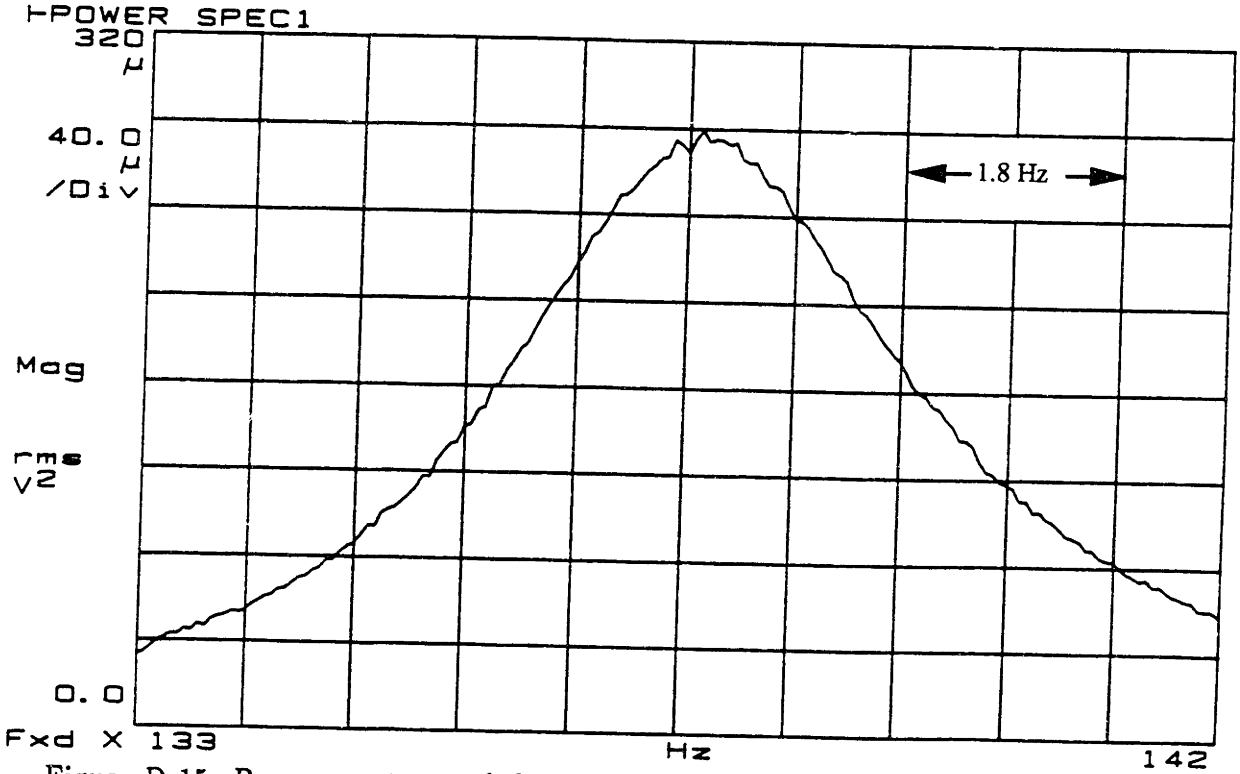

Figure D-15: Power spectrum of the 5" resonator at a mean pressure of 12 psia and an aperture setting fully opened to the external load.

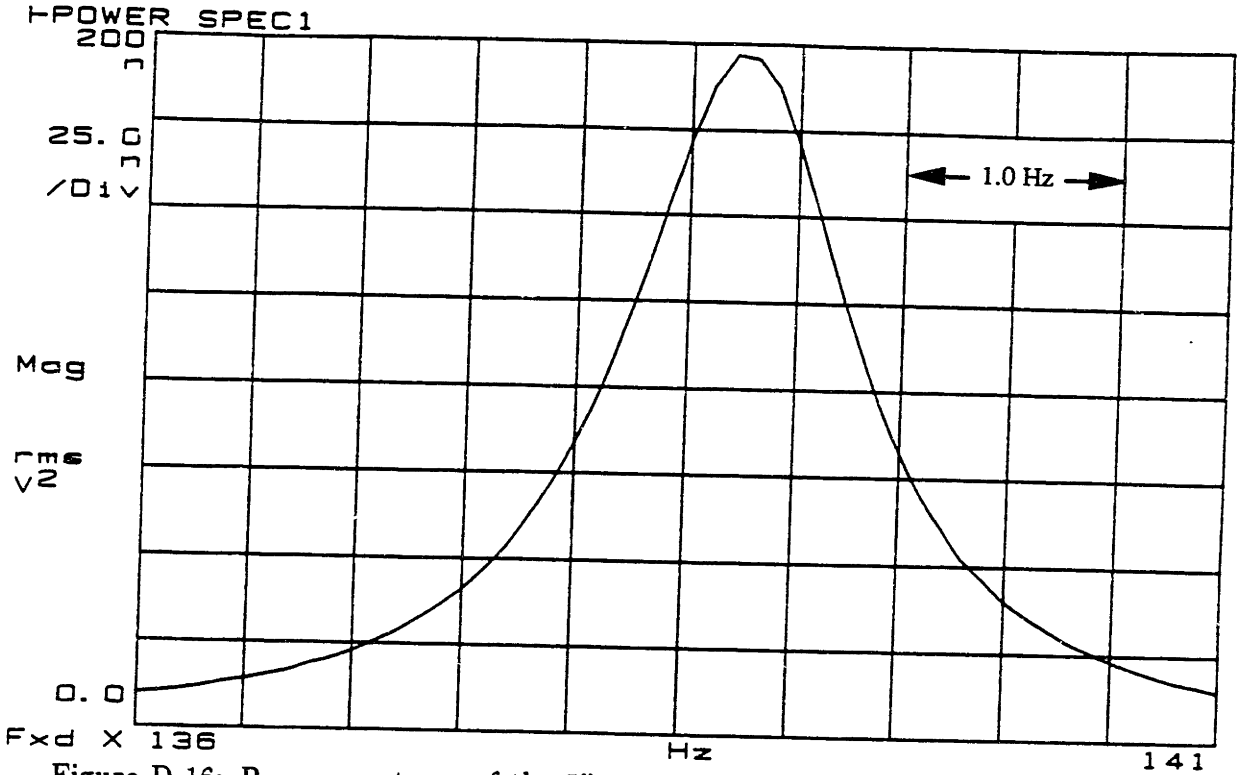

Figure D-16: Power spectrum of the 5" resonator at a mean pressure of 50 psia and an aperture setting of 1/12 to the external load.

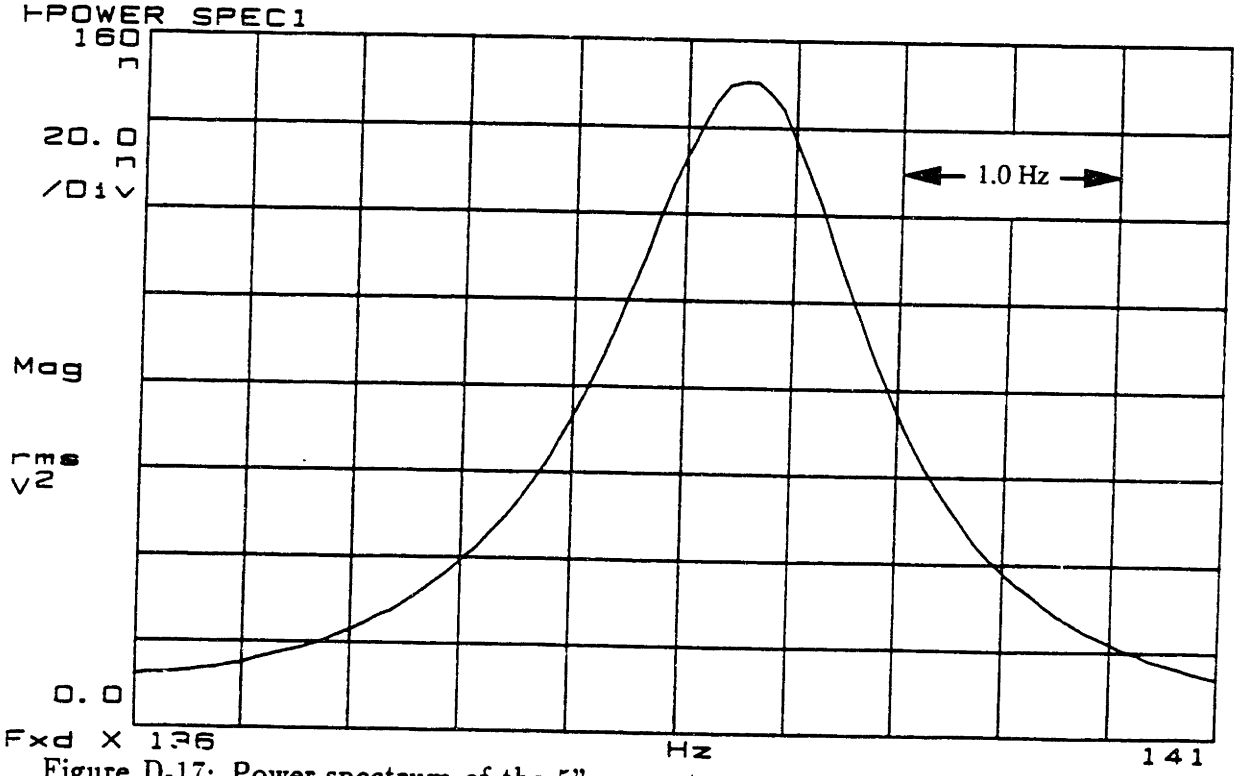

Figure D-17: Power spectrum of the 5" resonator at a mean pressure of 50 psia and an aperture setting of 1/6 to the external load.

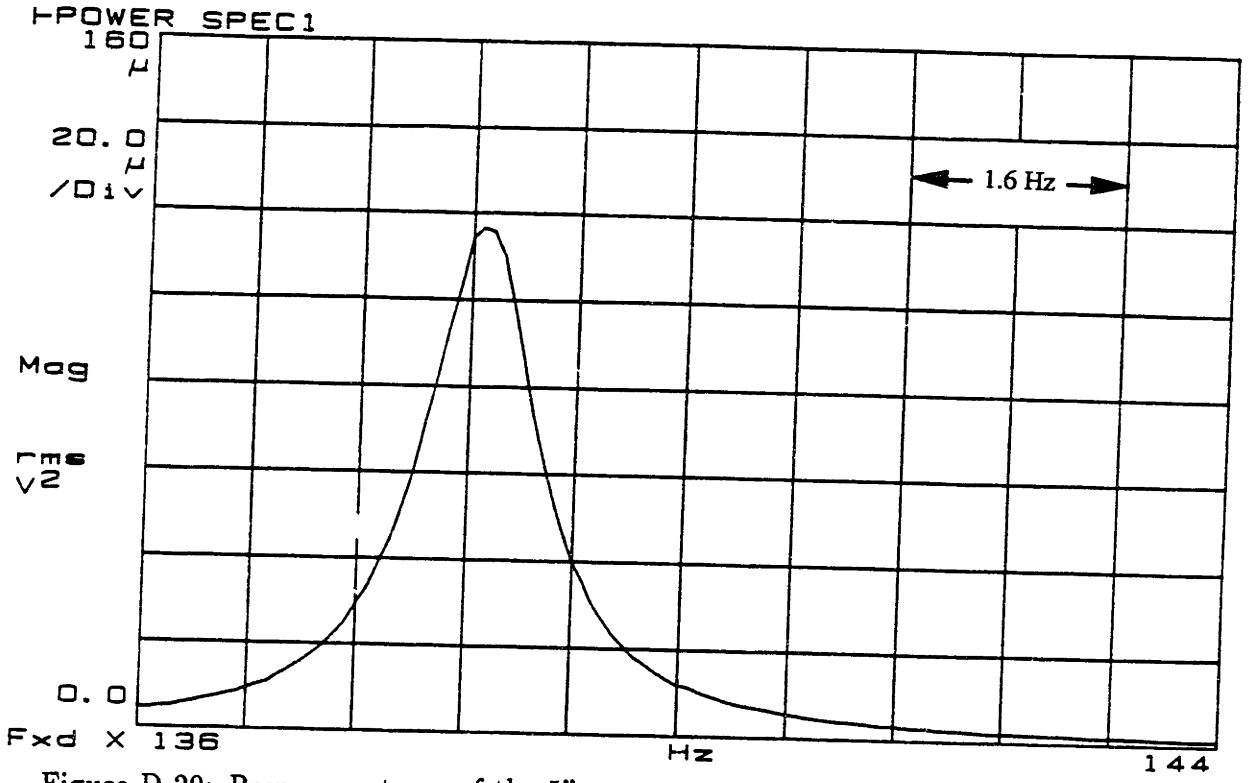

Figure D-20: Power spectrum of the 5" resonator at a mean pressure of 100 psia and an aperture setting of 1/12 to the external load.

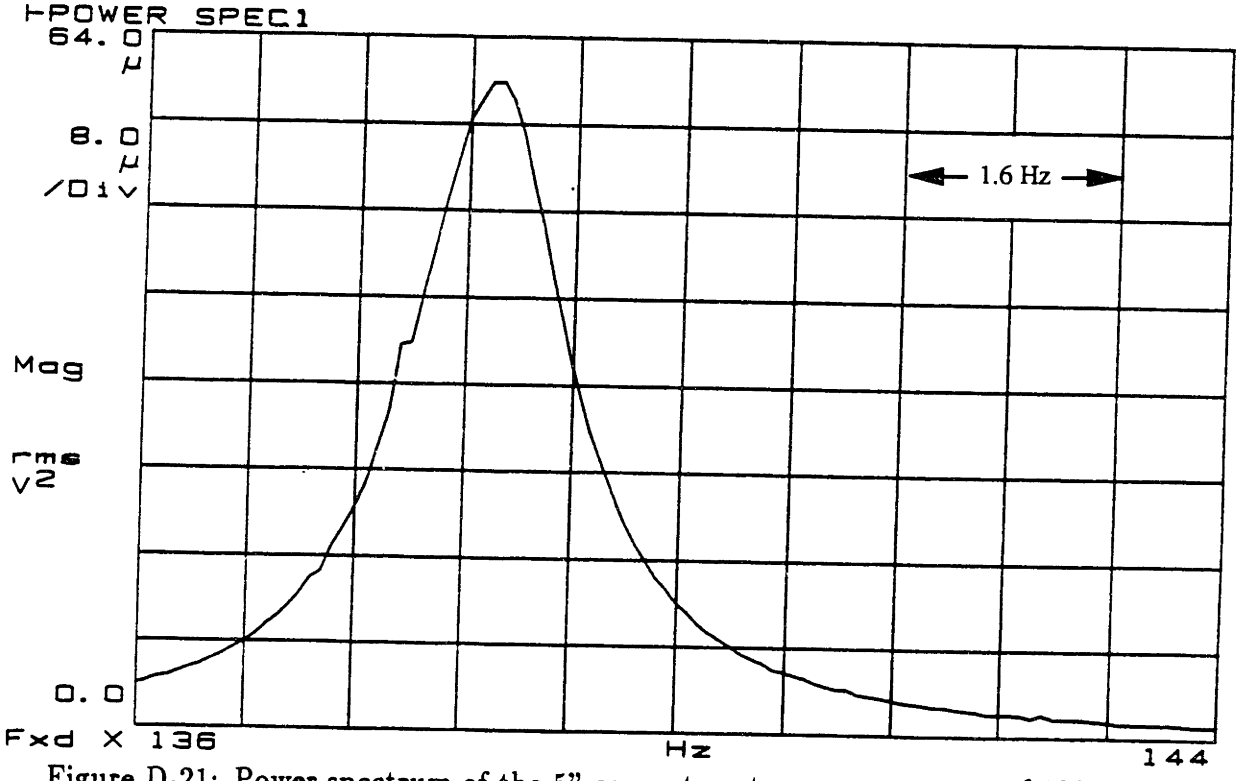

Figure D-21: Power spectrum of the 5" resonator at a mean pressure of 100 psia and an aperture setting of 1/6 to the external load.

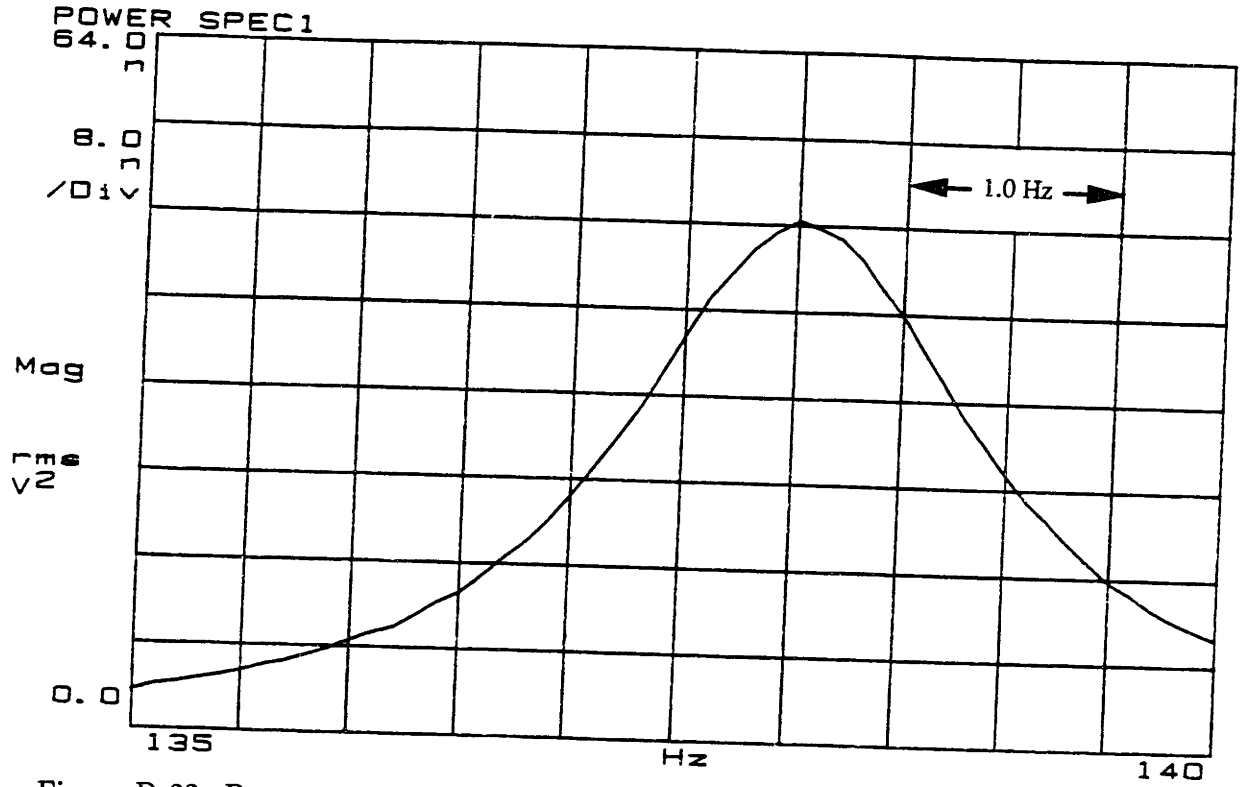

Figure D-22: Power spectrum of the 5" resonator at a mean pressure of 100 psia and an aperture setting of 1/3 to the external load.

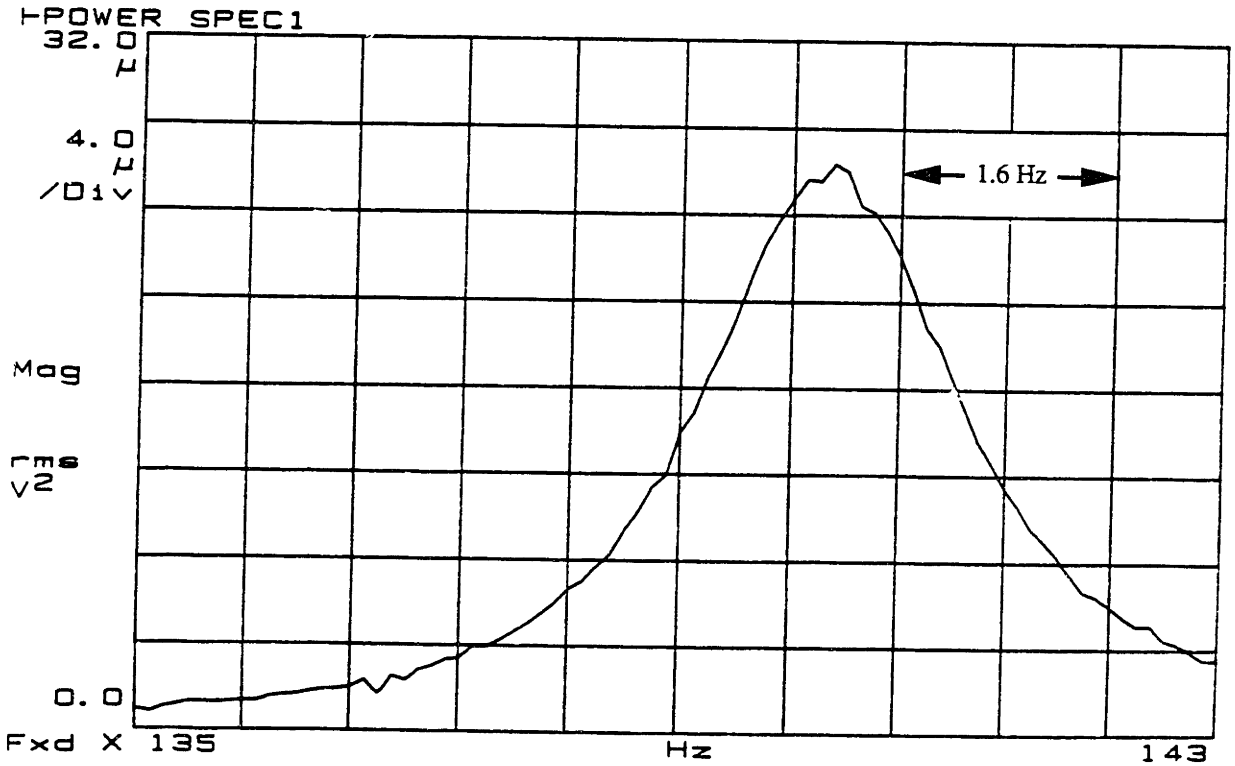

Figure D-23: Power spectrum of the 5" resonator at a mean pressure of 100 psia and an aperture setting of 2/3 to the external load.

Appendix E

Derivation of Compressive Energy Losses in an Acoustic Load

In a system where the volume flow oscillates, as in the case of the load described in Section 5.1, compressive energy at the walls of the volume is dissipated through thermal relaxation into the walls. This thermal relaxation in the volume all occurs within the thermal boundary layer, which is shown in Figure E.1. The temperature of the fluid changes with the pressure swings, and with respect to the distance from the walls. To begin the derivation of the oscillating temperature, the general equation of heat transfer, equation (2.38), must be used. Simplifying equation (2.38) to first order, and neglecting the velocity term because the velocity of the fluid at the walls of the volume is quite small, the equation becomes

$$\rho_o T_o(i\omega s') = K\frac{\partial^2 T'}{\partial y^2}, \tag{E.1}$$

where the first order entropy per unit mass, s', is

$$s' = \frac{c_p}{T_o}T' - \frac{\beta}{\rho_o}p'_V. \tag{E.2}$$

Substituting equation (E.2) into equation (E.1), the resulting expression is

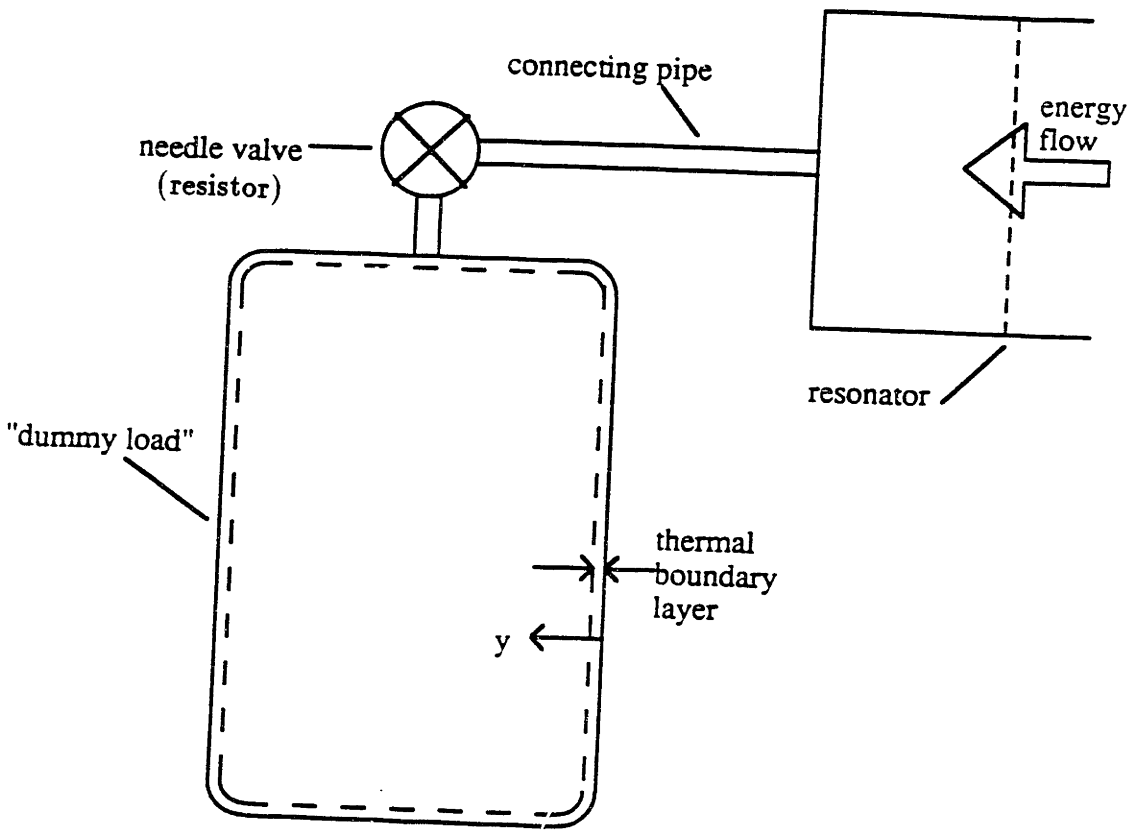

Figure E-1: Compressive energy dissipation in an external load.

$$\rho_o c_p T' - p'_V = K\frac{\partial^2 T'}{\partial y^2}, \tag{E.3}$$

for an ideal gas. By solving the differential equation, the first order temperature expression becomes

$$T' = \frac{p'_V}{\rho_o c_p}\left[1 - e^{-(1+i)y/\delta_\kappa}\right]. \tag{E.4}$$

To arrive at the volume velocity of the gas entering and leaving the tank, the oscillating velocity must be found. Using the conservation of mass, equation (2.17), the velocity can be derived, but an expression for the oscillating density must be obtained. By using equation (2.56), and substituting in equation (E.4) for T', the oscillating density is

$$\rho' = \frac{p'_V}{a^2}\left[1 + (\gamma - 1)e^{-(1+i)y/\delta_\kappa}\right]. \tag{E.5}$$

Considering the conservation of mass, the reciprocating velocity can be derived by integrating from 0 to y, giving

$$v(y) = \frac{-i\omega p'_V}{\rho_o a^2}\left[y + (\gamma - 1)\frac{\delta_\kappa}{(1+i)}(1 - e^{-(1+i)y/\delta_\kappa})\right], \tag{E.6}$$

and assuming y is large compared to δ_κ,

$$v(y) \simeq \frac{-1}{\rho_o a^2}\frac{dp'_V}{dt}\left[y - i\frac{\gamma - 1}{2}\delta_\kappa\right]. \tag{E.7}$$

Using the thermodynamic relation, $\frac{1}{\gamma p_o} = \frac{1}{\rho_o a^2}$, the velocity becomes

$$v(y) = \frac{-1}{\gamma p_o}\frac{dp'_V}{dt}\left[y - i\frac{\gamma - 1}{2}\delta_\kappa\right]. \tag{E.8}$$

To get the correct volume velocity, $v(y)$ must be multiplied by an area, but the terms in the velocity equation must be multiplied by different areas. The first term, $\frac{-1}{\gamma p_o}\frac{dp'_V}{dt}y$, accounts for the one-dimensional gas flow in and out of the volume, so it is multiplied by

the cross-sectional area of the tank (which is a cylinder). By letting y equal the height of the tank, the volume of the tank, V, results. The second term, $\frac{i}{\gamma p_o}\frac{dp'_V}{dt}\frac{\gamma-1}{2}\delta_\kappa$, accounts for the compressive losses at the walls of the volume. The second term should be multiplied by the entire internal surface area of the tank, A, instead of the cross-sectional area so the losses at the walls can be determined. Also, the expression derived for $v(y)$ accounts for the velocity of the fluid leaving the tank, but the volume velocity required in Chapter 5 refers to the fluid entering the tank, so the equation must be multiplied by -1 to be correct. The resulting volume velocity is

$$\dot{V} = \frac{1}{\gamma p_o}\frac{dp'_V}{dt}\left[V - i\frac{\gamma-1}{2}\delta_\kappa A\right], \tag{E.9}$$

shown in equation (5.3).

Appendix F

Measured Pressures from the Two Microphone Method Tests

Table F.1: Two Microphone Pressures Using the Low Amplitude Driver at Different Mean Pressures

	1 in. resonator				5 in. resonator			
p_o (psia)	Re(p'_A) (Pa)	Im(p'_A) (Pa)	Re(p'_B) (Pa)	Im(p'_B) (Pa)	Re(p'_A) (Pa)	Im(p'_A) (Pa)	Re(p'_B) (Pa)	Im(p'_B) (Pa)
12	4.19	-2.94	-5.87	-0.018	7.53	0.133	4.78	-0.0541
20	10.2	-5.49	-14.4	0.080	-15.5	-0.288	-9.74	0.0641
40	26.3	-9.70	-36.3	0.092	-37.5	-2.52	-23.8	-0.897
60	41.9	-12.2	-54.6	0.134	-60.3	-0.607	-37.7	0.010
80	53.1	-13.8	-71.3	0.336	82.4	1.25	51.5	0.342
100	62.5	-14.9	-86.5	0.754	-103	-0.117	-64.1	0.073
200	-111	18.8	151	-0.967	—	—	—	—
300	-150	20.9	204	-1.52	—	—	—	—

Table F.2: External Loading Pressures for the Five Inch Resonator (in Pa)

	valve setting	1/12	1/6	1/3	2/3	full
12 psia	$\mathrm{Re}(p'_A)$	—	—	36.7	27.4	24.7
	$\mathrm{Im}(p'_A)$	—	—	1.19	1.14	1.34
	$\mathrm{Re}(p'_B)$	—	—	22.7	16.9	15.0
	$\mathrm{Im}(p'_B)$	—	—	0.128	0.0567	0.0993
	$\mathrm{Re}(p'_V)$	—	—	0.257	1.91	4.02
	$\mathrm{Im}(p'_V)$	—	—	1.76	4.09	5.01
	$\lvert p'_E \rvert$	—	—	38.4	28.7	26.0
50 psia	$\mathrm{Re}(p'_A)$	65.9	57.8	40.9	34.6	—
	$\mathrm{Im}(p'_A)$	1.15	0.815	0.96	0.365	—
	$\mathrm{Re}(p'_B)$	41.6	36.4	26.0	21.4	—
	$\mathrm{Im}(p'_B)$	0.249	-0.074	0.016	0.070	—
	$\mathrm{Re}(p'_V)$	0.0375	0.362	1.66	9.97	—
	$\mathrm{Im}(p'_V)$	0.310	1.21	3.66	4.65	—
	$\lvert p'_E \rvert$	68.8	60.7	43.0	36.2	—

Table F.3: External Loading Pressures for the One Inch Resonator (in Pa)

	valve setting	1/4	1/2	Full
12 psia	$\mathrm{Re}(p'_A)$	-20.8	-21.1	-19.0
	$\mathrm{Im}(p'_A)$	12.8	13.4	13.6
	$\mathrm{Re}(p'_B)$	24.8	26.4	26.8
	$\mathrm{Im}(p'_B)$	-0.0313	-0.0285	-0.120
	$\mathrm{Re}(p'_V)$	-0.0301	-0.0459	0.246
	$\mathrm{Im}(p'_V)$	-0.0286	-0.271	-5.21
	$\lvert p'_E \rvert$	108	115	116
50 psia	$\mathrm{Re}(p'_A)$	-97.4	-81.1	-46.0
	$\mathrm{Im}(p'_A)$	33.2	38.7	50.6
	$\mathrm{Re}(p'_B)$	139	121	82.2
	$\mathrm{Im}(p'_B)$	-0.270	-0.249	-0.0370
	$\mathrm{Re}(p'_V)$	0.355	3.86	33.6
	$\mathrm{Im}(p'_V)$	-5.98	-49.0	-141
	$\lvert p'_E \rvert$	601	520	353
100 psia	$\mathrm{Re}(p'_A)$	-135	-89.3	-33.5
	$\mathrm{Im}(p'_A)$	42.3	55.5	66.1
	$\mathrm{Re}(p'_B)$	191	137	80.5
	$\mathrm{Im}(p'_B)$	-0.712	-0.369	-0.145
	$\mathrm{Re}(p'_V)$	3.02	21.1	106
	$\mathrm{Im}(p'_V)$	-46.7	-139	-240
	$\lvert p'_E \rvert$	826	588	354

Table F.4: Measured Pressures Using the High Amplitude Speaker (in Pa)

input	valve setting	closed	1/2
2.5 V	$\mathrm{Re}(p'_A)$	266	236
	$\mathrm{Im}(p'_A)$	23.9	37.2
	$\mathrm{Re}(p'_B)$	698	616
	$\mathrm{Im}(p'_B)$	0.327	0.996
	$\mathrm{Re}(p'_V)$	—	21.1
	$\mathrm{Im}(p'_V)$	—	-212
	$\lvert p'_E \rvert$	1480	1290
4.8 V	$\mathrm{Re}(p'_A)$	493	445
	$\mathrm{Im}(p'_A)$	45.5	69.3
	$\mathrm{Re}(p'_B)$	1308	1160
	$\mathrm{Im}(p'_B)$	3.17	3.33
	$\mathrm{Re}(p'_V)$	—	39.2
	$\mathrm{Im}(p'_V)$	—	-347
	$\lvert p'_E \rvert$	2760	2490
12.3 V	$\mathrm{Re}(p'_A)$	984	927
	$\mathrm{Im}(p'_A)$	105	145
	$\mathrm{Re}(p'_B)$	2750	2590
	$\mathrm{Im}(p'_B)$	3.43	3.78
	$\mathrm{Re}(p'_V)$	—	55.7
	$\mathrm{Im}(p'_V)$	—	-582
	$\lvert p'_E \rvert$	5930	5520

Table F.5: Measured Pressures Using the TAD (in Pa), $p_o = 100$ psia

Heater Input	valve setting	closed	1/3	2/3
75 V	$\|p'_A\|$	16600	17410	17320
	$\|p'_B\|$	3860	4050	4080
	ϕ_{AB}	2.06°	2.94°	3.66°
	$\|p'_E\|$	21940	22730	22350
	$\|p'_V\|$	—	545	990
	ϕ_{EV}	—	85.1°	85.0°
90 V	$\|p'_A\|$	22330	21390	21100
	$\|p'_B\|$	5090	4830	4900
	ϕ_{AB}	2.14°	2.97°	3.64°
	$\|p'_E\|$	29640	27240	27230
	$\|p'_V\|$	—	600	1100
	ϕ_{EV}	—	86.1°	85.4°
100 V	$\|p'_A\|$	24000	23570	23400
	$\|p'_B\|$	5420	5350	5400
	ϕ_{AB}	2.23°	2.99°	3.64°
	$\|p'_E\|$	31790	30700	30200
	$\|p'_V\|$	—	640	1150
	ϕ_{EV}	—	84.0°	84.5°
110 V	$\|p'_A\|$	25730	25480	26200
	$\|p'_B\|$	5730	5700	6000
	ϕ_{AB}	2.30°	3.04°	3.64°
	$\|p'_E\|$	34240	33180	33600
	$\|p'_V\|$	—	680	1220
	ϕ_{EV}	—	83.8°	85.7°

Table F.6: Measured Pressures Using the TAD (in Pa), $p_o = 100$ psia, cont'd

Heater Input	valve setting	closed	1/3	2/3
120 V	$\lvert p'_A \rvert$	27500	27550	27900
	$\lvert p'_B \rvert$	6050	6090	6270
	ϕ_{AB}	2.45°	3.14°	3.68°
	$\lvert p'_E \rvert$	36490	36300	35870
	$\lvert p'_V \rvert$	—	715	1260
	ϕ_{EV}	—	86.3°	85.8°
130 V	$\lvert p'_A \rvert$	30150	30160	29900
	$\lvert p'_B \rvert$	6500	6540	6640
	ϕ_{AB}	2.57°	3.17°	3.74°
	$\lvert p'_E \rvert$	40300	39540	38700
	$\lvert p'_V \rvert$	—	750	1320
	ϕ_{EV}	—	83.9°	85.9°
140 V	$\lvert p'_A \rvert$	32080	31980	32050
	$\lvert p'_B \rvert$	6840	6830	7020
	ϕ_{AB}	2.67°	3.32°	3.80°
	$\lvert p'_E \rvert$	42930	42160	41370
	$\lvert p'_V \rvert$	—	780	1370
	ϕ_{EV}	—	86.0°	85.9°
150 V	$\lvert p'_A \rvert$	34200	33770	34020
	$\lvert p'_B \rvert$	7200	7100	7350
	ϕ_{AB}	2.80°	2.44°	3.94°
	$\lvert p'_E \rvert$	45600	45070	44000
	$\lvert p'_V \rvert$	—	810	1400
	ϕ_{EV}	—	86.0°	85.9°

Table F.7: Measured Pressures Using the TAD (in Pa), p_o = 150 psia

Heater Input	valve setting	closed	1/3	2/3
75 V	$\|p'_A\|$	23500	22900	22000
	$\|p'_B\|$	5800	5600	5370
	ϕ_{AB}	1.84°	2.67°	3.50°
	$\|p'_E\|$	30820	29900	28550
	$\|p'_V\|$	—	800	1400
	ϕ_{EV}	—	85.6°	84.3°
90 V	$\|p'_A\|$	29000	27700	27000
	$\|p'_B\|$	7060	6720	6530
	ϕ_{AB}	1.89°	2.68°	3.33°
	$\|p'_E\|$	37800	36260	35600
	$\|p'_V\|$	—	890	1580
	ϕ_{EV}	—	85.8°	84.7°
100 V	$\|p'_A\|$	32100	30100	30600
	$\|p'_B\|$	7740	7230	7320
	ϕ_{AB}	1.94°	2.69°	3.30°
	$\|p'_E\|$	42100	40300	40160
	$\|p'_V\|$	—	940	1670
	ϕ_{EV}	—	85.9°	85.0°
110 V	$\|p'_A\|$	34840	33840	33410
	$\|p'_B\|$	8320	8060	7920
	ϕ_{AB}	1.98°	2.70°	3.30°
	$\|p'_E\|$	46070	44580	43460
	$\|p'_V\|$	—	1000	1750
	ϕ_{EV}	—	85.9°	85.1°
120 V	$\|p'_A\|$	37560	37400	36200
	$\|p'_B\|$	8890	8800	8510
	ϕ_{AB}	2.04°	2.79°	3.34°
	$\|p'_E\|$	50000	50200	47700
	$\|p'_V\|$	—	1070	1850
	ϕ_{EV}	—	85.8°	85.2°
130 V	$\|p'_A\|$	41110	40100	39500
	$\|p'_B\|$	9700	9440	9300
	ϕ_{AB}	2.10°	2.80°	3.34°
	$\|p'_E\|$	54700	52800	52100
	$\|p'_V\|$	—	1100	1940
	ϕ_{EV}	—	86.2°	85.4°

Table F.8: Measured Pressures with External Load Enhancement (in Pa)

Heater Input			Heater Input		
90 V	$\lvert p'_A \rvert$	36420	120 V	$\lvert p'_A \rvert$	47720
	$\lvert p'_B \rvert$	6740		$\lvert p'_B \rvert$	8600
	ϕ_{AB}	2.74°		ϕ_{AB}	2.59°
	$\lvert p'_E \rvert$	36420		$\lvert p'_E \rvert$	47720
	$\lvert p'_V \rvert$	2120		$\lvert p'_V \rvert$	2455
	ϕ_{EV}	84.3°		ϕ_{EV}	84.8°
100 V	$\lvert p'_A \rvert$	39730	130 V	$\lvert p'_A \rvert$	51120
	$\lvert p'_B \rvert$	7330		$\lvert p'_B \rvert$	9160
	ϕ_{AB}	2.66°		ϕ_{AB}	2.58°
	$\lvert p'_E \rvert$	39730		$\lvert p'_E \rvert$	51120
	$\lvert p'_V \rvert$	2220		$\lvert p'_V \rvert$	2550
	ϕ_{EV}	84.5°		ϕ_{EV}	84.9°
110 V	$\lvert p'_A \rvert$	44180	140 V	$\lvert p'_A \rvert$	54540
	$\lvert p'_B \rvert$	8030		$\lvert p'_B \rvert$	9640
	ϕ_{AB}	2.62°		ϕ_{AB}	2.57°
	$\lvert p'_E \rvert$	44180		$\lvert p'_E \rvert$	54540
	$\lvert p'_V \rvert$	2350		$\lvert p'_V \rvert$	2640
	ϕ_{EV}	84.7°		ϕ_{EV}	85.0°

Appendix G

Nomenclature

English Letters

A - area

A_{Re} - Reynold's Number in resonant tubes

a - speed of sound

C - electrical capacitance

c - specific heat

d - diameter

E - energy

$\dot{E}$ - power

e - energy density

$\dot{e}$ - energy dissipation rate per unit area

f - frequency or Rott function

h - height

I - electrical current

Im - imaginary part of

J_o, J_1 - Bessel functions

K - thermal conductivity

$\mathbf{k}$ - complex wavenumber

k - wavenumber

L - length

M - molecular weight

P - electric power

Pr - Prandtl Number

p - pressure

Q - quality factor

Re - real part of

r - radius or radial coordinate

S - sensitivity

s - entropy per unit mass

T - temperature

t - time

V - volume or voltage

$\dot{V}$ - volume velocity

V_m - specific volume

$\mathbf{v}$ - complex velocity

v - velocity

W - work

$\dot{W}$ - work flux or acoustic power

w - enthalpy per unit mass

z - z-axis coordinate

Greek Letters

α - thermal diffusivity

β - thermal expansion coefficient

ϵ - internal energy per unit mass

γ - ratio of specific heats

δ - boundary layer thickness

λ - wavelength

μ - dynamic viscosity

ν - kinematic viscosity

ζ - second viscosity

ρ - density

Φ - energy flux density

ϕ - phase angle

ω - angular frequency

Subscripts and Superscripts

A, B - amplitude or two microphone placements

AB - between points A and B

d - damped

$diss$ - dissipated

$driver$ - from driver

E - end of resonator

EV - between the end of the resonator and the dummy load

eff - effective

ex - external

$meas$ - measured quantity

p - constant pressure

$peak$ - peak to peak amplitude

r - radial direction

res - from resonator

s - standing wave or constant entropy

st - stored

T - tangential

$theory$ - theoretical quantity

tot - total

V - in "dummy load"

z - longitudinal direction

κ - thermal

ν - viscous

o - mean, resonant, or at resonator wall

$2sen$ - two microphone

$'$ - first order amplitude

Bibliography

[1] Gregory W. Swift. Thermoacoustic engines. *J. Acoust. Soc. Am.*, 84:1145–1178, 1988.

[2] A. Migliori and G.W. Swift. Liquid-sodium thermoacoustic engine. *Appl. Phys. Lett.*, 53:350, 1988.

[3] J.Y. Chung. Cross-spectral method of measuring acoustic intensity without error caused by phase mismatch. *J. Acoust. Soc. Am.*, 64:1613–1616, 1978.

[4] W.T. Chu. Extension of the two-microphone transfer function method for impedence tube measurements. *J. Acoust. Soc. Am.*, 80:347–348, 1986.

[5] A.F. Seybert. Two-sensor methods for the measurement of sound intensity and acoustic properties in ducts. *J. Acoust. Soc. Am.*, 83:2233–2239, 1988.

[6] Nikolaus Rott. Damped and thermally driven acoustic oscillations in wide and narrow tubes. *Z. Agnew. Math. Phys.*, 20:230–243, 1969.

[7] L.D. Landau and E.M. Lifshitz. *Fluid Mechanics.* Pergamon, Oxford, 1982.

[8] Asger Kjerbye Nielsen. Acoustic resonators of circular cross-section and with axial symmetry. *Trans. Danish Acad. Tech. Sci.*, 10:9–70, 1949.

[9] Lawrence E. Kinsler and Austin R. Frey. *Fundamentals of Acoustics.* John Wiley and Sons, Inc., New York, 1962.

[10] Allen D. Pierce. *Acoustics: An Introduction to Its Physical Principles and Applications.* McGraw Hill Book Co., New York, 1981.

[11] P. Merkli and H. Thomann. Transition to turbulence in oscillating pipe flow. *J. Fluid Mech.*, 68:567–575, 1975.